UC Berkeley
UC Berkeley Electronic Theses and Dissertations

Title
Hydrodynamic Modeling, Optimal Control, and Performance Evaluation of an Array of Ocean-Wave Energy Converters

Permalink
https://escholarship.org/uc/item/7x45766j

Author
Zhong, Qian

Publication Date
2018

Peer reviewed|Thesis/dissertation

eScholarship.org Powered by the California Digital Library
University of California

Hydrodynamic Modeling, Optimal Control, and Performance Evaluation of an Array of Ocean-Wave Energy Converters

by

Qian Zhong

A dissertation submitted in partial satisfaction of the

requirements for the degree of

Doctor of Philosophy

in

Engineering - Mechanical Engineering

in the

Graduate Division

of the

University of California, Berkeley

Committee in charge:

Professor Ronald W. Yeung, Chair
Professor Fai Ma
Professor Francesco Borrelli
Professor Per-Olof Persson

Fall 2018

Hydrodynamic Modeling, Optimal Control, and Performance Evaluation of an Array of Ocean-Wave Energy Converters

Copyright 2018
by
Qian Zhong

Abstract

Hydrodynamic Modeling, Optimal Control, and Performance Evaluation
of an Array of Ocean-Wave Energy Converters

by

Qian Zhong

Doctor of Philosophy in Engineering - Mechanical Engineering

University of California, Berkeley

Professor Ronald W. Yeung, Chair

The wave power resource along the U.S. shelf edge is enormous. It was estimated that in the U.S. the total recoverable wave resource, more than 40% of the total available wave power, could cover around 30% of the electricity used in the country each year. A large variety of wave-energy extraction technologies has been proposed, with relatively few designs reaching commercial scales. Wave farm, an array of wave-energy converters (WECs), has been proposed as a solution for commercializing the wave-energy extraction technology. However, wave-interaction effects among the WEC devices in the farm introduce uncertainties in the estimation of the power production from the wave farm and hence the levelized cost of energy (LCOE). This can present hurdles in promoting wave-energy extraction technology.

This dissertation focuses upon the realistic estimation of the optimal power generation for a wave farm. A semi-analytical method based on potential-flow theory is developed to efficiently obtain the hydrodynamic properties of the devices in a WEC array with the "exact" wave-interference effects taken into account. The newly-derived Haskind relation is applied to multiple floating bodies to obtain the diffraction properties of individual bodies based on the solution to the radiation problem. With the knowledge of the hydrodynamic properties of individual devices, maximal power production from the WEC array is computed for arrays of different configurations in waves of all frequencies and incident angles. However, physical constraints on the system are not able to be accounted for in this phase of modeling.

To investigate the optimal power production of a WEC array in constrained conditions, a constrained optimal control method using model-predictive control (MPC) is developed for an array of heaving point absorbers. Wave-interaction effects among the devices are included in the dynamic model. The cost function of the proposed optimization model for this WEC problem is developed to be convex, which enables the efficient computation of the optimal control outputs for multiple coordinated devices. The proposed MPC is demonstrated for real-time implementation on a single point absorber and applied to a point-absorber array. Results show that with constraints on the motion amplitudes of the devices and the power take-off forces considered, the array would produce less power than the case that they were

operated individually in isolation in the majority of wave conditions. Effects of the spacing among devices, wave-incidence angle, and array configurations on the power performance are discussed and compared to those predicted by the frequency-domain analysis where constraints were not applied.

Furthermore, a method is proposed to implement the optimal control force obtained by the MPC, using an in-house designed permanent magnetic linear generator (PMLG). The proposed MPC needs to use the PTO force as the optimizing variable to attain the convex formulation of the optimization problem, which results in reactive power defined as the power flowing from the PTO system to the absorber. This would require the PTO to be both a generator and a motor and would significantly complicate the PTO design. To resolve this issue, an additional constraint is added to the PTO force in the optimization problem such that the reactive power can be eliminated and the convexity of the problem can be retained. The optimal PTO force obtained by this modified MPC is then realized by using the PMLG with a time-varying damping. Simulation results are presented for a three-device array with the optimal PTO forces implemented by the PMLG, operated in irregular sea states at seven sites in the west coast of the U.S.

In conclusion, this dissertation developed a set of tools to reduce uncertainties in evaluating the annual power production of a WEC array. Results show that wave-interaction effects appear to be destructive for common sea states in the west coast of the U.S., with physical constraints of the systems considered. The loss of absorbed power caused by the wave-interference effects is less than 5% when the spacing among devices is larger than 3 body diameters. Considering the permitted area of occupancy, mooring-line arrangements, and reduction of production cost with the increase of the array size, we conclude that a relatively close-spacing wave farm consisting of more than 10 devices can be beneficial to the commercialization of the wave-energy extraction technology.

To my family.

Contents

Contents **ii**

List of Figures **iv**

List of Tables **vii**

1 Introduction **1**
1.1 Background 1
1.2 Scope and Objectives 4
1.3 Outline of the Dissertation 6

2 Hydrodynamics of a Wave-Energy Converter Array **8**
2.1 Overview 8
2.2 Modeling Analysis of a System of Bodies 10
2.3 Wave-Exciting Forces and Moments 17
2.4 Results of Hydrodynamic Study 19
2.5 Power Extraction from a WEC Array 25
2.6 Summary Remarks 31

3 MPC Control of a Single WEC **33**
3.1 Overview 33
3.2 State-space Model of a Point Absorber 35
3.3 Model-Predictive Control Formulation 36
3.4 Simulation Results in Regular Waves 40
3.5 Simulation Results in Irregular Waves 47
3.6 Summary remarks 50

4 MPC Control of a WEC Array **52**
4.1 Overview 52
4.2 Modeling an Array of Point Absorbers 53
4.3 Model-Predictive Control Formulation with Convexity 58
4.4 Performance of a Constrained WEC Array 62
4.5 Wave-Interaction Effects on Power Performance of a Constrained WEC Array 71

4.6 Effects of the Point-Absorber Approximation 74
4.7 Summary Remarks 74

5 Implementation of the control strategy on a WEC array 77
5.1 Overview 77
5.2 Eliminating the Reactive Power 79
5.3 Implementation of the MPC 81
5.4 Performance Evaluation of a Three-Device Array in the West Coast U.S. . . 84
5.5 Summary Remarks 88

6 Conclusions and Future Work 89
6.1 Conclusions 89
6.2 Future Work 91

A Appendix 93

Bibliography 96

List of Figures

1.1 Wave-energy converters of different categories: 1. Pelamis (Attenuator), 2. Energetech OWC (Terminator), 3. Wave Dragon (Overtopping), 4. WaveBob (Point absorber) . . . 2
1.2 Artist conception of a community of WEC working in consonance, in communication with a global controller or among one another (Artwork credit: Lu Wang, Ph.D.) . . . 4
1.3 Overview of the developed co-axial cylinder system. . . . 5

2.1 Illustration of a group of truncated vertical cylinders . . . 10
2.2 Decomposition of the fluid domain . . . 12
2.3 Illustration for Graf's Addition Theorem . . . 15
2.4 Configurations of arrays of cylinders . . . 19
2.5 Hydrodynamic forces on cylinder 1 induced by surge motion of cylinder 1 . . . 22
2.6 Hydrodynamic interaction forces (surge force on cylinder 1 induced by surge motion of cylinder 2) . . . 22
2.7 Wave-exciting surge force on cylinder 1 and 2 . . . 22
2.8 Surge hydrodynamic coefficients of a four-cylinder array . . . 23
2.9 Surge wave-exciting forces on a four-cylinder array . . . 23
2.10 Damping coefficients of the square arrays in heave and roll motion. . . . 24
2.11 Wave-exciting moments in heave and roll direction on the square arrays with the incident-wave angle $\beta = 0^o$ for heave and $\beta = 45^o$ for roll. . . . 24
2.12 Contour plots of q for arrays of two, three, and four cylinders . . . 27
2.13 Contour plots of q for two cylinders with the spacing being $L = 8a$ and $L = 10a$. 28
2.14 Contour plots of q for three cylinders with the cylinder 1 positioned off the centerline. 29
2.15 Illustration of multiple units of a three-cylinder array. . . . 30
2.16 The interaction factor for three units of a triangular array with the distance between the units $L = 10r$. . . . 30
2.17 The interaction factor for three units of a triangular array with the distance between the units $L = 20r$. . . . 31
2.18 Wave-interaction effects on eight units of a triangular array with the distance between the units $L = 20r$. . . . 32

3.1 Impulse response of the radiation subsystem and damping coefficients with respect to wave frequency. 41
3.2 Averaged absorbed power by an unconstrained point absorber plotted over the angular frequency. 42
3.3 Time histories of $\dot{\zeta}_3$ (blue), ζ_3 (black, dash-dotted), and f_e (red, dashed) on the left, and f_m (grey, dash-dotted) and f_e on the right, for the absorber in regular waves with amplitude of 1 m and period of 9 s. Constraints, if any, are shown by dashed lines, values of which are set to $\zeta_{3,\max} = 5$m, and $f_{m,\max} = 2$ MN. Simulated cases are (a) no constraints, (b) constraints on the heaving motion, (c) constraints on the machinery force, and (d) constraints on both of the heaving motion and the machinery force. 42
3.4 Schematic of the dual coaxial-cylinder system in [62]. 44
3.5 Comparisons of capture width by current method with those using NMPC. . . . 45
3.6 Comparisons of RAO by current method with those using NMPC. 45
3.7 The ratio of the reactive power to the power flowing from the absorber to the PTO unit (so-called "active power"). 47
3.8 Computational time for simulated cases of regular waves. 48
3.9 Time-averaged useful power in irregular waves. 49
3.10 The ratio of reactive power to "active power" in irregular waves. 49
3.11 Computational time for simulated cases of irregular waves. 50
3.12 Time histories of $\dot{\zeta}_3$, ζ_3, and f_e on the left, and f_m and f_e on the right, for the absorber in irregular waves of $T_p = 2.2$ s. 50

4.1 Birdseye view of the configuration of two to four identical WEC devices, separated by a distance of L as defined, with incident waves striking at an angle β. 63
4.2 Schematic of the heaving point absorber and the PTO system developed in [64]. 64
4.3 Impulse response of the radiation subsystems and the damping coefficient in heave for three cylinders with the spacing $L = 5a$. Coupling hydrodynamics is shown as superscript ^{12} and ^{13} 64
4.4 Nondimensional capture width of three WECs in regular waves with the spacing ratio $L/a = 5$ and $L/a = 10$. 65
4.5 Maximal RAO of three WECs in regular waves with the spacing ratio $L/a = 5$ and $L/a = 10$. 66
4.6 The ratio of the reactive power to the power flowing from the absorbers to the PTO units (so-called "active power") for a three-WEC array with the spacing ratio $L/a = 5$ and $L/a = 10$. 66
4.7 Time histories of the heaving velocity $\dot{\zeta}_3$, the wave-exciting force f_e, the instantaneous power P, and the machinery force f_m for a three-device array at two selected wave periods, showing rather different behavior ($L/a = 5$). 68
4.8 Averaged useful power for three WECs in irregular waves. 70
4.9 The ratio of reactive power to active power for three WECs in irregular waves. . 70

4.10 Box plot of the computational time for irregular-wave cases plotted over the number of cylinders. 71
4.11 The q factor for three devices with constrained MPC control and (unconstrained) complex-conjugate (CC) control in head seas ($\beta = 0$). 72
4.12 Power extracted by a two-device array: the upper plot shows the averaged capture width for the array and the lower ones show the capture width for individual devices. 73
4.13 Comparisons of the performance of a three-WEC array in irregular waves with the wave-interaction effect modeled by the PA approximation and an "exact" method ($L/a = 5$). 75
4.14 Comparisons of the performance of a three-WEC array in irregular waves with the wave-interaction effect modeled by the PA approximation and an "exact" method ($L/a = 10$). 75

5.1 Capture width based on the grid power obtained by a single point absorber. . . 78
5.2 Capture width based on the grid power for a three-WEC array MPC control with (blue markers) or without (red markers) reactive-power occurrence ($L/a = 10$, head-sea condition) 80
5.3 The ratio of the reactive power to the "active" power for the three-WEC array shown in Fig. 5.2. 80
5.4 Comparisons of the capture width of a single WEC under MPC control with and without constraints on the PTO damping. 82
5.5 Comparisons of the results for a three-WEC array under MPC control with and without constraints on the PTO damping ($L/a = 10$, head-sea condition). 83
5.6 Comparisons of the results for a three-WEC array in irregular waves under MPC with damping control and force control ($L/a = 10$, head-sea condition). 83
5.7 CaPex (left) and OpEx (right) contributions to LCOE (cents/kWh) per deployment scale [49]. 87

List of Tables

1.1 Main specifications of the WECs shown in Fig. 1.1 3

2.1 Convergence behavior: relative error (%) of hydrodynamic coefficients of two truncated columns with $L/a = 5$, $d/a = 0.5$, $h/a = 10$, $k_0a = 1.0$ 21
2.2 Properties of the array with the maximal interaction factor 26

5.1 Full-Scale Properties of the Unidirectional Sea States used to calculate $ACCW$. 84
5.2 Weighting factors used to calculate the $ACCW$ and the full-scale average annual wave energy flux for the seven sites in the west coast of U.S. [9] 85
5.3 Specifications of the Controller 86
5.4 Capture width ratio η_1 (%) of a three-WEC array ($L/a = 5$) with different controller settings in sea states of seven sites in the West Coast of the U.S. . . . 86
5.5 Mean value of the interaction factor q over the seven sites obtained with different controllers 87

Acknowledgments

I wish to express my sincere gratitude to Professor Ronald W. Yeung for his guidance and assistance throughout this academic course. His pursuit of perfection, attention to details, passion for this field of naval architecture and ocean engineering, and dedication to education are all things to admire. I am especially thankful for his invaluable insights in guiding the direction of this research and for providing the fexibility for us to explore our own research interests.

I would like to thank Professor Fai Ma and Professor Francisco Borrelli, who served on both my qualifying exam (QE) and dissertation committee, Professor Per-Olof Persson for being my dissertation committee member, and Professor Ming Gu on my QE committee. Special thanks to Prof. Ma for serving as the chair of my QE and the inspiring discussion. Many thanks to Prof. Borrelli for his constant support to my exploration of the control field. I thank Prof. Persson for his kind support and his crystal teaching style that I have benefited a lot from.

This work would not have been possible without support from faculty and students in the Department of Mechanical Engineering. In particular, I wish to thank Nathan Tom, Daewoong Son, and Farshad Madhi for their pioneering work on the development of the point-absorber system. Many thanks to Samuel Kanner, Mohamed Hariri Nokob, and Lu Wang for their insightful opinions during our discussion. Heartfelt thanks to Qiuchen Guo and Dongchi Yu for their support as reliable teammates and genuine friends. The support provided by administrative and technical staff of the Department has also been valuable and greatly appreciated.

During the Ph.D. program, I had opportunities teaching and assisting various courses at UC Berkeley. For this, I would also like to thank Dr. Kourosh Youssefi, Dr. Gabriel Gomes, Professor Roberto Horowitz, Professor Alexandre Bayen, and Professor Vera Serganova for their encouragement and guidance in teaching.

Furthermore, I am wholeheartedly grateful for the friendship I had throughout the years. Thank you, Peihan, Yu, Haokun, Xuexin, and many many others, for your understanding, encouragement, and friendship along the way. Lastly, I wish to give my deepest thanks to my parents, Hong Zhong and Yiping Lu. Without their unconditional love and unwavering faith in me, I would not be where I am today.

Partial support in the form of Ocean-Technology Fellowship provided by the American Bureau of Shipping (ABS), the block grant provided by the Mechanical Engineering Department at UC Berkeley, and the Outreach Award provided by the ASME-Ocean, Offshore & Arctic Engineering Division are gratefully acknowledged.

Chapter 1

Introduction

A transition of the energy infrastructure is happening worldwide to tackle the increasing seriousness of the air-pollution, climate, and energy-security problems. Wave power was brought to researchers' attention by Stephen Salter's paper published in *Nature* [54] in 1970s. Ocean waves, generated by the influence of wind on the ocean surface, have high power density and can be accurately predicted more than 48 hours in advance, which make this energy source especially attractive for electricity generation compared to other renewable energy such as solar and wind.

1.1 Background

Wave Energy Technology

With 70% of the earth covered by the ocean, the potential for wave power as the energy resource is very promising, especially on west-facing coasts in either hemisphere with latitudes between 40^o and 60^o. In Europe, Denmark, Ireland, Norway, Portugual, Sweden and the United Kingdom have been actively engaged in wave energy utilization under government support for more than three decades [13]. In the U.S., the Electric Power Research Institute (EPRI) conducted rigorous estimations of the wave energy resource along the U.S. coastline in 2004 and 2011. According to the 2011 report [34], the total available wave energy resource along the U.S. continental shelf edge is estimated to be $2,640$ terawatt-hours per year (TWh/yr), which is roughly half of U.S. electricity consumption. California, in particular, has more than $1,200$ km of useable coastline, and the annual deep water average power flux is over 300 TWh/yr, according to California Energy Commission's report in 2007 [56]. It is technically possible to meet about 23% of California's electricity needs with ocean wave energy.

Over the past 50 years, there are more than 1000 patents filed for wave power converters (WECs). A number of devices have been proved to have technical and commercial potential. Conventionally, WECs can be classified based on the installation location or the type of

operation. Detailed descriptions of different categories of WECs can be found in literature reviews [2, 17, 60]. In general, the WECs are classified into four categories: attenuator, terminator, overtopping, and point absorbers. Attenuator is aligned in parallel to the wave direction. Terminator has a principal axis perpendicular to the wave incident direction to intercept waves. Overtopping device has a reservoir above the sea level. The water captured in the reservoir from waves is released into the ocean through a low-head hydraulic turbine, which generates electrical power. The point absorber is defined to have a small dimension relative to the wave length ($< 1/20$) and generate electricity from motions excited by waves. Fig. 1.1 shows a few well-known devices with mature development status with their categories described in the caption. A summary of critical dimensions and power capacity of the devices [56] is provided in Table. 1.1. A database for existing WEC designs and estimated performance was presented in [3].

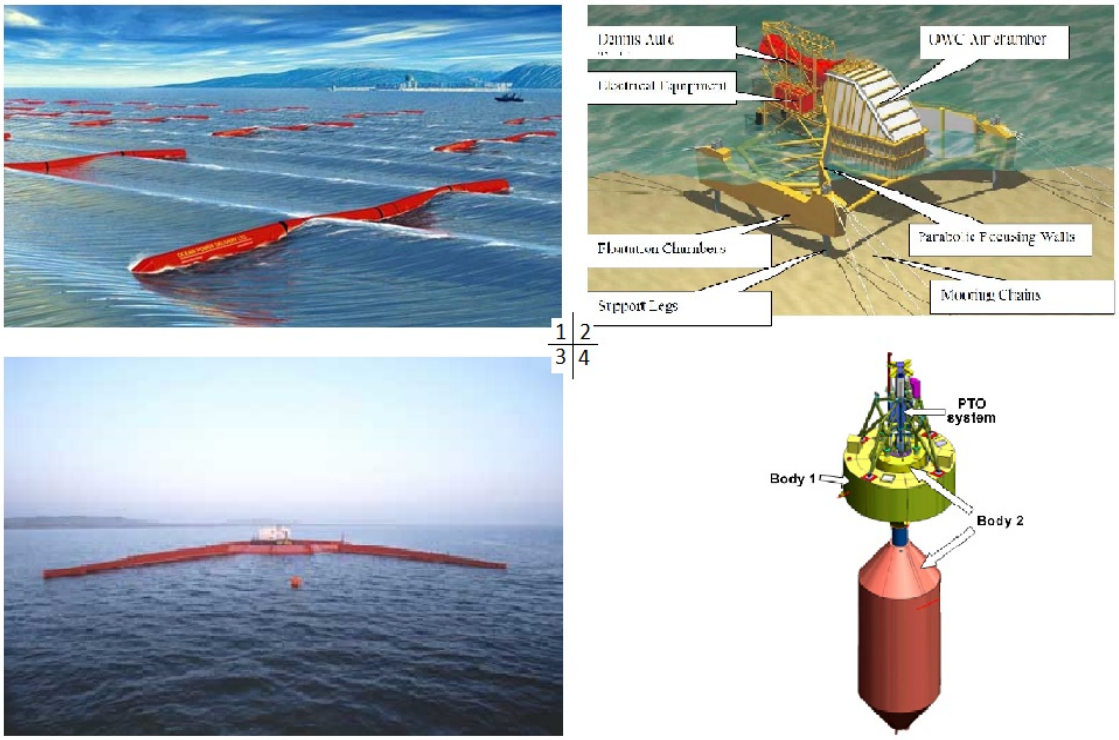

Figure 1.1: Wave-energy converters of different categories: 1. Pelamis (Attenuator), 2. Energetech OWC (Terminator), 3. Wave Dragon (Overtopping), 4. WaveBob (Point absorber)

Relative to the large number of WEC designs, few devices achieve the stage of commercial-scale deployment. Traditionally, investment in marine energy has been assessed in terms of LCOE, or levelised cost of electricity. A report from Sandia National Laboratory [49] in 2014 presented a LCOE study for different types of marine energy devices, where the LCOE estimated for a heaving point absorber, referred to as RM3, is $\$1.45/kWh$, which is much higher than other alternative energy sources, for example, offshore wind with mean LCOE

Table 1.1: Main specifications of the WECs shown in Fig. 1.1

Device	Width (m)	Length (m)	Annual Production (MWh)
Pelamis	3.5	120	1337
Energetech OWC	35	18	2275
Wave Dragon	260	150	12,000
WaveBob	15	15	1147

being €$0.152/kWh$ [16]. It was pointed out in [49] that the lack of experiences and tools available for developing the wave energy technology is the primary reason for the high LCOE.

To encourage the design of techno-economical WEC devices, Department of Energy (DOE) sponsored in 2015 the the Wave Energy Prize [52] (the Prize), an 18-month public design-build-test competition with the goal to double the energy captured from ocean waves compared to the current designs and ultimately reduce the cost of wave energy. The first placed team, AquaHarmonics, built a point absorber with latching/declutching control and surpassed the goal with a fourfold increase in the captured energy compared to the reference device RM3.

Wave Farm Development

The point absorber (PA) is considered one of the most promising WEC design because its power performance is independent of the wave direction and its small size is favored from the viewpoint of the development cost. However, the small size also limits the power production capability of the PA. Taking into account the PTO capacity and the WEC's maximum swept volume to set the upper bounds for absorbed power in the 'Budal diagram', Falnes and Hals concluded in [26] that for a PA, a power capacity of only about 0.3MW matches well to a typical offshore wave climate. As reported in [27], the average production for WECs in the most common sea states is usually around 1/10 of the installed generator capacity, which means the generated power will be below 100kW even for large point absorbers with diameters of 15 20 meters. Hence, for a sizeable wave-power plant, an array consisting of a number of WECs, so-called wave farm as shown in Fig. 1.2, is in great needs.

In the meantime, development of the technology and tools for designing a wave farm is still in a preliminary stage. For a wave farm, wave interactions among the units can have significant effects on the power production of the array, compared to the one produced by multiple isolated devices, in particular when the devices are closely spaced. Avoiding such effects requires the WECs placed farther apart, which can increase the cost of production and maintenance. Hence, to optimize the design of a WEC array, wave-interaction effects need to be considered to provide a practical estimate of the power generated from an array.

Furthermore, control strategy plays an essential role in making the WECs economically viable. The majority of existing control strategies are developed for a single device. Few studies have discussed how control strategies would affect the power absorption when it comes

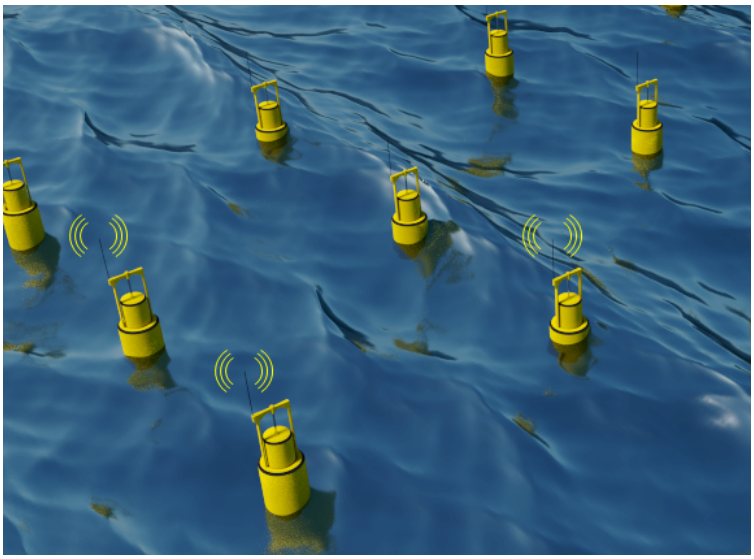

Figure 1.2: Artist conception of a community of WEC working in consonance, in communication with a global controller or among one another (Artwork credit: Lu Wang, Ph.D.)

to a wave farm. What is the condition for a WEC array to generate the maximal power as a whole in a given wave environment? How would the wave-interaction effects affect the power production of the array, particularly when physical constraints on the devices, including motion amplitudes and PTO capability, were taken into account? Would there be any difference in the power production from the array if the devices were doing the best for the group and if they are doing the best for their individual selves? Would it be possible to construct an array configuration such that the array can produce more power than isolated devices with the help of interacting waves among the array, as predicted by the frequency-domain hydrodynamic study for the array? How is the energy extraction distributed among different devices in the array? All the questions are left open. There are hence lots of uncertainties remain in the process of assessing the performance of a wave farm, which essentially increases the LCOE for a wave farm and impact the competitiveness of the wave technology to other forms of alternative energy. In this work, we will formulate a complete scheme to efficiently account for the exact wave-interaction effects on a wave farm and develop an optimal control strategy applicable to a constrained WEC array with guaranteed computation efficiency.

1.2 Scope and Objectives

The Berkeley Marine Mechanics Lab has been devoting to the development of a heaving point absorber since 2010, including the analysis, design, and geometry optimization of the floater, in-house PTO design, advanced controller design, manufacture, and model test for the integrated system [63, 64, 65]. Fig. 1.3 shows the illustration of the optimized

design, a co-axial cylinder point absorber. The power take-off (PTO) system is an in-house designed permanent magnetic linear generator (PMLG), which consists of an array of magntets mounted on the (outer) floater, moving relative to a set of coils attached to the inner cylinder. The bottom of the floater adopted the shape of The Berkeley Wedge[1] shape, which has been demonstrated to effectively reduce viscous effects by 70% [40]. It can be shown that this device is able to produce 300 kW peakpower in 3 m height waves with a 12 m diameter floater, with estimated overall wave-to-wire efficiency of 32% [60].

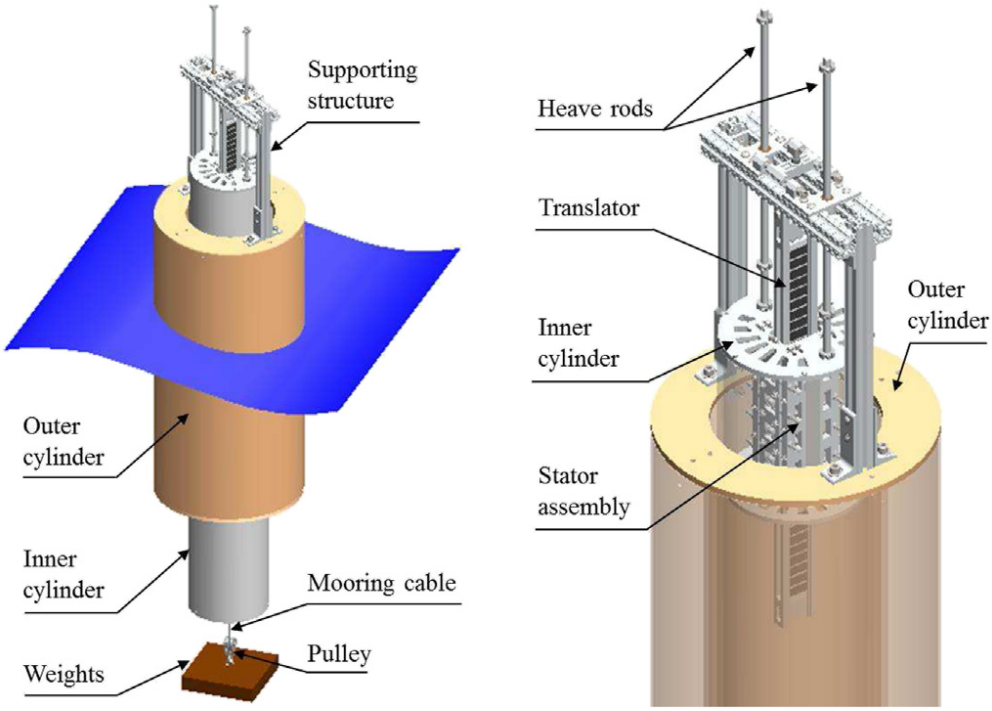

Figure 1.3: Overview of the developed co-axial cylinder system.

With the fully-developed single point absobrer, the current work will investigate the performance of an array of heaving point absorbers. Emphasis is to be put on the difference between the performance of a WEC array and that of multiple isolated devices. First of all, a general method for efficiently computing hydrodynamic coefficients and wave-exciting forces for an array of oscillating truncated cylinders will be proposed. The cylinders will be allowed to have six degrees of freedom individually. Power production for WEC arrays in optimal operating condition will then be evaluated for a large range of wave frequencies and wave-incident angles with the assumption of no physical constraint considered. To find out how practical constraints on the devices affect the power production, a constrained optimal controller was formed based on the Model-Predictive Control (MPC). With the goal of applying the controller to an array of devices, computational efficiency of the MPC

[1]Energy-capturing floating breakwater, USPTO #9,416,766
http://pdfpiw.uspto. gov/.piw?Docid=09416766.

needs to be considerably improved, with real-time implementation possibilities. Effectiveness of the controller will be first tested on a single heaving point absorber and validated by comparisons with the existing simulation results for the developed co-axial cylinder absorber. Then, the controller will be applied to a wave farm. Results will provide insights on how the individual devices behave in a farm mode to generate an optimal result for the group. Furthermore, implementation of the control strategy using the developed PMLG will be discussed. With the wave-interaction effect taken into account, constrained optimal control applied, and control inputs implemented by hardware PTO systems, realistic simulations will be performed in the end for a WEC array operating in sea states of seven sites in the westcoast of the U.S.

1.3 Outline of the Dissertation

The work is outlined in the following chapters.

Chapter 2 develops a semi-analytical method to investigate surface-wave interactions among an array of truncated cylinders. The matched eigen-function expansions method is applied to solve the wave radiation problem. A new, generalized form of the Haskind relation for an array of arbitrary configuration is derived and used to evaluate wave-exciting forces and moments on an individual cylinder or a group of cylinders, situated among an array, which only requires the solution to the radiation problem. Such efficient computation then enables the study on a wide range of factors that impacts the optimal power production from a heaving point-absorber array, including wave frequencies, wave-incident angles, the number of devices, the spacing among the devices, and the layout geometry on power extraction.

Chapter 3 describes a constrained optimal control method based on the model-predictive control (MPC). The problem of maximizing the energy production from WECs with restrictions is modeled as a constrained optimization problem, which is then cast into a Quadratic Programming (QP). A new penalty term was introduced in the cost function, which is used to guarantee the convexity of the QP. Effectiveness and efficiency of the formed MPC are verified by performing simulations with the model of co-axial cylinder and compraring results with previously developed nonlinear MPC. Also discussed is the effect of reactive power.

Chapter 4 presents a coordinated control strategy for an array of WECs based on the MPC developed in Chapter 3. The QP formulation with the convexity guaranteed makes the problem of finding optimal control inputs for a WEC array practically solvable. Wave-interaction effects among the element devices were taken into account in the dynamic model. Discussions of the results focus on the wave-interaction effects on the optimal performance of an array with constraints taken into account. Also, how individual devices would react at the optimal operating condition in waves of different angle and frequency.

Chapter 5 discusses the implementation of the coordinated control using the in-house designed PMLG. The MPC will take into account a new constraint to eliminate the requirement of the reactive power and have the optimization problem remained as a convex QP, at a cost of reduced absorbed power. The reactive power is defined as the power flowing from

the PTO unit to the absorber. Additionally, such a control force input will be approximately achieved in a form of a varying PTO damping, multiplied by the current heaving velocity of the absorber, and realized by the PMLG. Comparisons will be made among the results using the nonlinear MPC which directly takes the PTO damping as the optimal variable, the newly formed MPC with no requirement on the reactive power, and such a MPC with the control force achieved by the varying PTO damping. Lastly, the performance of a three-device array with the PMLG controlled by the MPC will be evaluated in sea states of seven sites in the west coast of the U.S.

Chapter 6 concludes the dissertation with a summary and contributions and proposes future work.

Chapter 2

Hydrodynamics of a Wave-Energy Converter Array

2.1 Overview

Economic decision drives the operation of ocean-wave energy converters (WEC) to be in a "farm mode". For a wave farm, wave interactions among the units can have significant effects on the power production of the array, compared to the one produced by multiple isolated devices, when the devices are closely spaced. Avoiding those effects requires the WECs placed farther apart, which can increase the cost of production and operation. Thus, for optimizing the layout design of a WEC array, wave-interaction effects need to be considered to accurately estimate the generated power from an array. In 1980s, expressions for evaluating optimal power generated by an array of oscillating bodies were obtained by Evans [20] and Falnes [23] respectively, where an interaction factor q was defined as the ratio of the power per device in the array to the power produced by a single device. The q factor is later widely used as an indicator for the power-capture capability of a WEC array in the layout-optimization study [12, 57]. However, solving hydrodynamic properties for each device in an array, which are required to compute the optimal power, can be a complex problem because of scattering waves among the array.

Review on existing methods for solving such hydrodynamic problems of wave interactions among a cylinder array can be found in [46, 51]. Numerical methods [10, 37] can be directly applied, but the computational cost may become prohibitive with the increase of the size of the array. Semi-analytical method based on linear theory is hence preferred for faster computation, and it also provides physical insights into the problem. In this category, point-absorber approximation used in [20, 23] and plane-wave approximation applied in [47, 59] can estimate hydrodynamic properties of an array of cylinders in a substantially simplified way. Yet, errors can be significant. As a result, these methods may not be applicable to study detailed performance of the array of absorbers. Multiple scattering method [42, 53], based on an multi-level iterative scheme, is able to achieve any order of accuracy in principle, by

increasing the order of scattering waves taken into account. Indeed, Ohkusu's [53] approach is well known. However, even for low order of accuracy, the amount of computations associated with iterations will become infeasible with increase of the number of cylinders. Kagemoto & Yue proposed an interaction theory [35] to study hydrodynamics of an arbitrary array based on the diffraction properties of its individual elements. Such an interaction theory fully takes into account the effect of multiple scattering waves, including the interaction of evanescent modes, which is considered "exact" in the context of linear theory and adopted in other studies [29, 58, 75]. In this paper, we show that the interaction of evanescent modes of scattering waves is negligible for the majority of practical cases; most importantly, neglecting evanescent modes can reduce computational efforts in solving this problem, which is essential in efficiently evaluating hydrodynamic properties and estimating power production for an arbitrary WEC arrays. This approach was pursued by Yeung & Sphaier [73] in studying tank-wall interferences.

For computing the optimal power for a WEC array, both damping coefficients from solving the radiation problem and wave-exciting forces from solving the diffraction problem are required, as explained in [20, 23]. In existing studies of WEC arrays, the two problems were treated separately. A method mentioned above will be applied twice to solve the two problems and obtained the required coefficients, which can be computationally costly for the array problems. While for a single body, it is well-known that the Haskind relation [32] can be used to obtain wave-exciting forces and moments, which does not require knowledge of diffraction properties of the structure, but rather, depends on radiation potential of the body in the far field, (see Newman [50] and Wehausen [68]). Applications can be found in Yeung [71] for a truncated vertical cylinder and Chau & Yeung [11] for dual coaxial cylinders. Here, we generalize the Haskind relation and apply it to an array of cylinders, so that all of the first-order hydrodynamic coefficients can be obtained by only solving the radiation problem, which are then used to find the optimal power of the array.

In this Chapter, a cohesive semi-analytical method is developed and used to investigate wave interaction among multiple truncated circular cylinders in arbitrary configurations. Each cylinder is considered dynamically *independent* with six degrees of freedom. Following Yeung [71] and others, we let the velocity potential of the flow field be obtained by matching eigen-function expansions for separated fluid domains. To achieve fast computation, we will indeed assume that evanescent modes of scattering waves from one cylinder will not significantly affect the pressure field around the other cylinders. These effects of neglecting the evanescent modes in the interaction will be assessed. Then the newly generalized Haskind relation will be derived for an individual, or a group of cylinders, situated among an array of cylinders. Results from this formula will be compared with those from directly solving the diffraction problem, a much more lengthy procedure. Added mass, damping coefficients and wave-exciting loads for arrays of different configurations will be presented as results to demonstrate the importance of interference effects. Most importantly, the wave-interaction effects on the optimal power captured by an array, represented by the "q" factor, was computed for arrays of up to 24 heaving point absorbers in various configurations with different wave conditions. Discussion is made regarding achieving configurations of constructive wave-

interaction effects.

2.2 Modeling Analysis of a System of Bodies

Within the context of linearized potential flow theory, consider N floating vertical cylinders of finite draft d, oscillating harmonically in water of depth h. We define N local cylindrical coordinates (r_j, θ_j, z) $(j = 1, 2, \ldots, N)$ fixed in the undisturbed free surface with the origin O_j on the axis symmetry of the body and z-axis pointing upwards, as shown in Fig. 2.1. The motion of j-th cylinder in q-th mode can be described by:

$$\zeta_q^j(t) = \mathrm{Re}\left[\bar{\zeta}_q^j e^{-i\sigma t}\right], \quad q = 1, 2, \ldots 6 \tag{2.1}$$

where $\bar{\zeta}$, being time-independent, is the complex amplitude of motion of cylinder, with $q = 1, 2, \ldots, 6$ corresponding to surge, sway, heave, roll, pitch, and yaw, σ the angular frequency of the motion, and $i = \sqrt{-1}$. The velocity potential of the fluid can be expressed

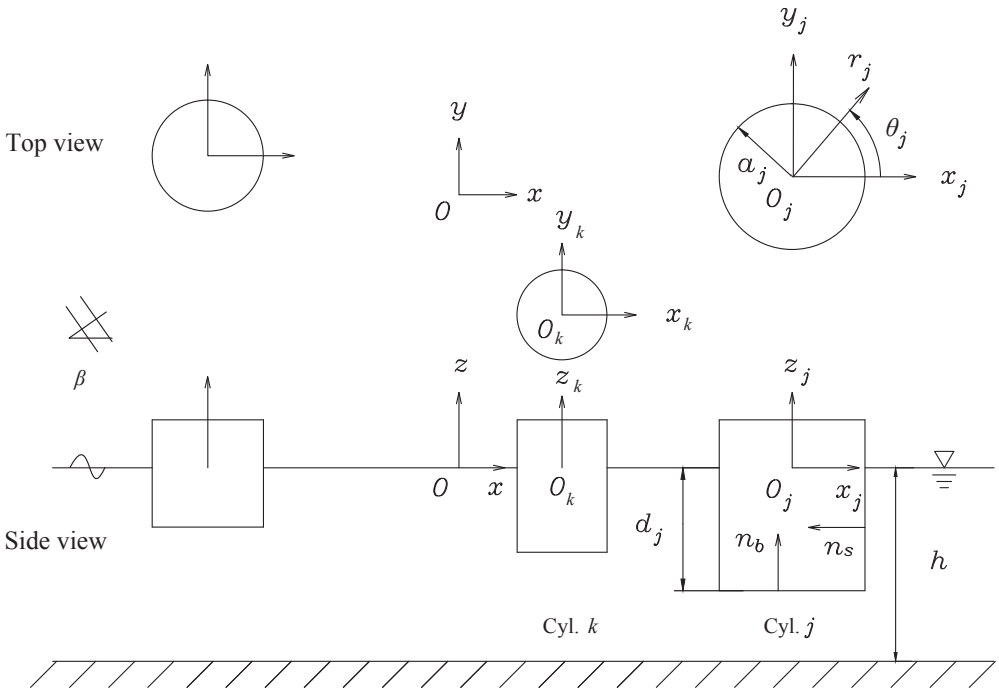

Figure 2.1: Illustration of a group of truncated vertical cylinders

by

$$\Phi(r, \theta, z, t) = \mathrm{Re}\left[\phi(r, \theta, z) e^{-i\sigma t}\right] \tag{2.2}$$

where $\phi(r, \theta, z)$ is the complex spatial potential and it needs to satisfy the following governing equations

$$\nabla^2 \phi = 0 \tag{2.3a}$$

$$\frac{\partial \phi}{\partial z} - \nu \phi = 0 \qquad \text{at } z = 0 \tag{2.3b}$$

$$\frac{\partial \phi}{\partial z} = 0 \qquad \text{at } z = -h \tag{2.3c}$$

$$\frac{\partial \phi}{\partial n^j} = U_n^j \qquad \text{on } S_j,\ j = 1, 2, \ldots, N \tag{2.3d}$$

with $\nu = \sigma^2/g$ where g is the gravitational acceleration. Here $U_n^j = \sum_{q=1}^{6} U_q^j n_q^j$ is the normal velocity of the surface of cylinder j, with the unit normal vector pointing into the body; and U_q^j as the complex amplitude of the velocity can be obtained from (2.1) as:

$$U_q^j = -i\sigma \overline{\zeta}_q^j, \quad q = 1, 2, \ldots, 6 \tag{2.4}$$

An additional radiation condition at large radial distance r from the structural array needs to be satisfied:

$$\lim_{r \to \infty} \sqrt{r} \left(\frac{\partial \phi}{\partial r} - i k_0 \phi \right) = 0 \tag{2.5}$$

where k_0 is wave number related with σ by dispersion relation to be discussed later.

Following Yeung [71], we divide the fluid domain into two kinds of regions, interior regions underneath the cylinders and an exterior region surrounding all the cylinders, as shown in Fig. 2.2, then use matched eigen-function expansions method to find the velocity potential in each domain.

Expressions in Interior Regions

The interior solution for the region under cylinder j, denoted by $\phi^{(I_j)}$, can be written as the sum of a homogeneous solution $\phi_H^{(I_j)}$ and a particular solution $\phi_P^{(I_j)}$:

$$\phi^{(I_j)} = \phi_H^{(I_j)} + \phi_P^{(I_j)} \tag{2.6}$$

with $\phi_H^{(I_j)}$ and $\phi_P^{(I_j)}$ satisfying following boundary conditions:

$$\left.\frac{\partial \phi_H^{(I_j)}}{\partial z}\right|_{z=-d_j} = 0, \qquad \left.\frac{\partial \phi_H^{(I_j)}}{\partial z}\right|_{z=-h} = 0 \tag{2.7a}$$

$$\left.\frac{\partial \phi_P^{(I_j)}}{\partial z}\right|_{z=-d_j} = U_{n_b}^j, \qquad \left.\frac{\partial \phi_P^{(I_j)}}{\partial z}\right|_{z=-h} = 0 \tag{2.7b}$$

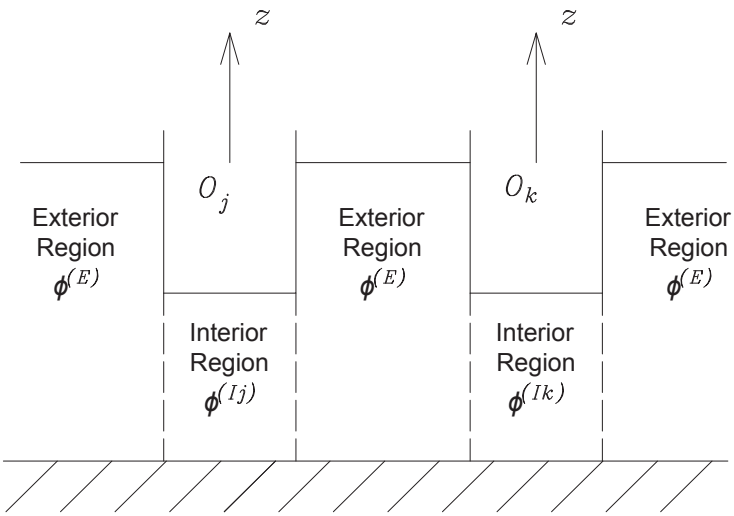

Figure 2.2: Decomposition of the fluid domain

where n_b denotes the normal vector at the bottom of the cylinder.

Separation of variables in cylindrical coordinates yields the following homogeneous solution:

$$\phi_H^{(I_j)}(r_j,\theta_j,z) = \sum_{m=-\infty}^{\infty} e^{im\theta_j}\left[\frac{\alpha_{m0}^j}{2}\left(\frac{r_j}{a_j}\right)^{|m|} + \sum_{s=1}^{\infty}\alpha_{ms}^j \frac{I_m(\lambda_s r_j)}{I_m(\lambda_s a_j)} g_s(z)\right] \tag{2.8a}$$

$$g_s(z) = \cos(\lambda_s(z+h)), \qquad \lambda_s = \frac{s\pi}{h-d_j} \tag{2.8b}$$

with the coefficients α_{ms}^j $(s = 0, 1, \dots)$ to be determined, and I_m being the m-th order modified Bessel function of the first kind.

To find the particular solution, we first compute the normal velocity at the bottom of cylinder as $U_{n_b}^j = \sum_{q=1}^{6} U_q^j n_{b,q}^j = U_{n_b}^j = U_3^j + U_4^j r\sin\theta - U_5^j r\cos\theta$, where U_q^j $(q = 3, 4, 5)$ is obtained in (2.4), and $n_{b,q}^j$ is the q-th component of unit normal vector at the bottom. We write $\phi_P^{(I_j)}$ as

$$\phi_P^{(I_j)}(r_j,\theta_j,z) = \sum_{m=-\infty}^{\infty} e^{im\theta}\varphi_{P,m}^{(I_j)}(r_j,z) \tag{2.9}$$

as shown in [58]. Then substitution of (2.9) and $U_{n_b}^j$ in (2.7b) yields

$$\left.\frac{\partial\phi_P^{(I_j)}}{\partial z}\right|_{z=-d_j} = \sum_{m=-\infty}^{\infty} e^{im\theta}\frac{\partial\varphi_{P,m}^{(I_j)}}{\partial z} \tag{2.10}$$

where

$$\left.\frac{\partial \varphi_{P,m}^{(I_j)}}{\partial z}\right|_{z=-d_j} = \begin{cases} U_3 & m=0 \\ -\frac{1}{2}U_5 r - \frac{1}{2}imU_4 r & m=\pm 1 \\ 0 & \text{otherwise} \end{cases}$$

Based on potentials for a single cylinder [71], the particular solution satisfying (2.10) can be expressed as

$$\phi_P^{(I_j)} = \sum_{m=-\infty}^{\infty} e^{im\theta} \varphi_{P,m}^{(I_j)} \tag{2.11}$$

where

$$\varphi_{P,m}^{(I_j)} = \begin{cases} U_3 \cdot \frac{1}{2(h-d_j)}[(z+h)^2 - r^2] & m=0 \\ (-\frac{1}{2}U_5 - \frac{1}{2}imU_4) \cdot \frac{1}{2(h-d_j)}[(z+h)^2 r - \frac{r^3}{4}] & m=\pm 1 \\ 0 & \text{otherwise} \end{cases}$$

Substituting homogeneous solution (2.8a) and particular solution (2.11) in (2.6), we can obtain $\phi^{(I_j)}$ as

$$\phi^{(I_j)} = \sum_{m=-\infty}^{\infty} e^{im\theta} \left[\varphi_{Pm}^{(I_j)} + \frac{\alpha_{m0}^j}{2} \left(\frac{r_j}{a_j}\right)^{|m|} + \sum_{s=1}^{\infty} \alpha_{ms}^j \frac{I_m(\lambda_s r_j)}{I_m(\lambda_s a_j)} g_s(z) \right] \tag{2.12}$$

with $g_s(z)$ given earlier by (2.8b) and $\varphi_{P,m}^{(I_j)}$ by (2.11).

Expression in Exterior Region

The exterior region, as shown in Fig. 2.2, has boundaries at the bottom of sea, the free surface, the side of all of cylinders, interfaces with all of interior regions, and a surface at infinity. The total potential is the summation of potentials for scattering waves from all the cylinders, i.e.

$$\phi^{(E)} = \sum_{j=1}^{N} \phi^{(e_j)} \tag{2.13}$$

where $\phi^{(e_j)}$ is potential for scattering waves from cylinder j and can be expressed in j-th local coordinates as:

$$\begin{aligned} \phi^{(e_j)} = f_0(z) \sum_{m=-\infty}^{\infty} e^{im\theta_j} \beta_{m0}^j \frac{H_m^{(1)}(k_0 r_j)}{H_m(k_0 a_j)} \\ + \sum_{p=1}^{\infty} f_p(z) \sum_{m=-\infty}^{\infty} e^{im\theta_j} \beta_{mp}^j \frac{K_m(k_p r_j)}{K_m(k_p a_j)} \end{aligned} \tag{2.14}$$

where $H_m^{(1)}$ and K_m are the m-th order Hankel function of the first kind and modified Bessel function of the second kind respectively, β_{mp} unknown wave coefficients, $f_0(z)$ and $f_p(z)$ the

depth function. The first term in (2.14) represents propagating wave modes which has a slow decaying rate with distance from the center of cylinder j, while the second term is for evanescent modes, and decays fast with the increase of the distance. Functions $f_0(z)$ and $f_p(z)$ form a normalized orthogonal set and can be written as

$$f_0(z) = \frac{\cosh k_0(z+h)}{(N_0 h)^{1/2}}, \quad N_0 = \frac{1}{2}\left[1 + \frac{\sinh(2k_0 h)}{2k_0 h}\right] \tag{2.15a}$$

$$f_p(z) = \frac{\cos k_p(z+h)}{(N_p h)^{1/2}}, \quad N_p = \frac{1}{2}\left[1 + \frac{\sin(2k_p h)}{2k_p h}\right] \tag{2.15b}$$

where wave numbers k_0 and k_p, $p = 1, 2, \ldots$, are positive and real roots obtained from the dispersion relations:

$$k_0 \tanh k_0 h = \nu \tag{2.16a}$$

$$k_p \tan k_p h = -\nu, \quad p = 1, 2, \ldots \tag{2.16b}$$

Direct substitution of (2.14) in (2.13) will yield the total potential

$$\begin{aligned} \phi^{(E)} = &\sum_{k=1}^{N} f_0(z) \sum_{m=-\infty}^{\infty} e^{im\theta_k} \beta_{m0}^k \frac{H_m^{(1)}(k_0 r_k)}{H_m(k_0 a_k)} \\ &+ \sum_{k=1}^{N} \sum_{p=1}^{\infty} f_p(z) \sum_{m=-\infty}^{\infty} e^{im\theta_k} \beta_{mp}^k \frac{K_m(k_p r_k)}{K_m(k_p a_k)} \end{aligned} \tag{2.17}$$

To apply boundary conditions (2.3d) on cylinder j, we will use Graf's addition theorem [67] to express (r_k, θ_k) in terms of (r_j, θ_j). Before we proceed with this transformation, we take advantage of the fact that the evanescent modes decay fast with the increase of distance, and neglect the ones induced by one cylinder in the near field of its neighboring cylinders; then (2.17) yields

$$\begin{aligned} \phi^{(E)} = &\sum_{k=1}^{N} f_0(z) \sum_{m=-\infty}^{\infty} e^{im\theta_k} \beta_{m0}^k \frac{H_m(k_0 r_k)}{H_m(k_0 a_k)} \\ &+ \sum_{p=1}^{\infty} f_p(z) \sum_{m=-\infty}^{\infty} e^{im\theta_j} \beta_{mp}^j \frac{K_m(k_p r_j)}{K_m(k_p a_j)} \end{aligned} \tag{2.18}$$

Since the leading evanescent mode is governed by the value of $k_1 r$ where k_1 satisfies $k_1 h > \pi/2$, the neglected terms would be of the order $\exp(-\pi L/2h)$, i.e. exponentially decays with the increase of the spacing between two cylinders, L. Direct calculation based on the ratio of L and water depth h can show that the requirement on spacing between cylinders can be satisfied by the majority of practical cases. Most importantly, neglecting evanescent modes in wave interaction enables us to reduce the number of unknowns required to be solved simultaneously, which saves considerable computational time and memory, especially for a large group of cylinders.

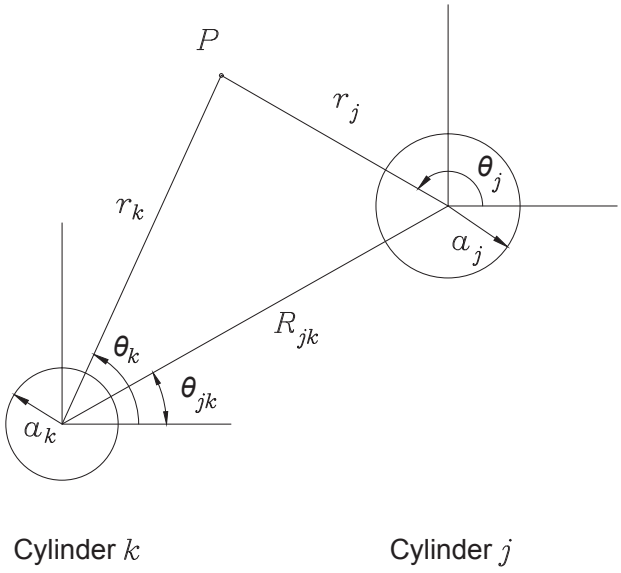

Figure 2.3: Illustration for Graf's Addition Theorem

Graf's Addition Theorem (Watson [67]) is applied to transform coordinates for (2.18), which has the form of

$$H_m(k_0 r_k)e^{im\theta_k} = \sum_{l=-\infty}^{\infty} H_{m-l}(k_0 R_{jk})e^{i\theta_{jk}(m-l)} J_l(k_0 r_j)e^{il\theta_j} \tag{2.19}$$

where R_{jk} is the distance between the origins O_j and O_k, θ_{jk} the azimuthal angle of O_k relative to O_j, as shown in Fig. 2.3, and J_l is the Bessel function of the first kind of order l. Then (2.18) can be written as

$$\begin{aligned}\phi^{(E)}(r_j,\theta_j,z) =& f_0(z)\sum_{m=-\infty}^{\infty} e^{im\theta_j}\beta_{m0}^j \frac{H_m(k_0 r_j)}{H_m(k_0 a_j)} \\ &+\sum_{p=1}^{\infty} f_p(z)\sum_{m=-\infty}^{\infty} e^{im\theta_j}\beta_{mp}^j \frac{K_m(k_p r_j)}{K_m(k_p a_j)} \\ &+\sum_{\substack{k=1\\k\neq j}}^{N} f_0(z)\sum_{m=-\infty}^{\infty}\beta_{m0}^k \sum_{l=-\infty}^{\infty}\frac{H_{m-l}(k_0 R_{jk})}{H_m(k_0 a_k)} e^{i(m-l)\theta_{jk}} J_l(k_0 r_j)e^{il\theta_j}\end{aligned} \tag{2.20}$$

The obtained exterior potential (2.20) needs to satisfy boundary conditions (2.3d) on the side surface of body j ($j = 1, 2, \ldots, N$). Similarly to the analysis for interior potential, we computed the normal velocity on that surface, denoted by $U_{n_s}^j$, by $U_{n_s}^j = -U_1^j \cos\theta_j -$

$U_2^j \sin\theta_j + U_4^j z \sin\theta_j - U_5^j z \cos\theta_j$ and write the boundary condition (2.3d) for ϕ^E in (2.20) as

$$\left.\frac{\partial \phi^{(E)}}{\partial n^j}\right|_{s_j} = \sum_{m=-\infty}^{\infty} e^{im\theta_j} \left.\frac{\partial \varphi_m^{(E)}}{\partial n^j}\right|_{s_j}, \qquad j = 1, 2, \ldots, N \tag{2.21}$$

where

$$\left.\frac{\partial \varphi_m^{(E)}}{\partial n^j}\right|_{s_j} = \begin{cases} \frac{1}{2}U_1^j - \frac{1}{2}miU_2^j + \frac{1}{2}U_5^j z + \frac{1}{2}miU_4^j z & m = \pm 1 \\ 0 & \text{otherwise} \end{cases}$$

Matching Interface Conditions

$\phi^{(I_j)}$ (2.12) and $\phi^{(E)}$ (2.20) and their normal derivatives need to satisfy continuity conditions on interfaces of exterior region and interior regions for pressure and local fluxes:

$$\phi^{(E)}\big|_{S_{\text{itf}}^j} = \phi^{(I_j)}\big|_{S_{\text{itf}}^j}, \qquad j = 1, 2, \ldots, N \tag{2.22a}$$

$$\left.\frac{\partial \phi^{(E)}}{\partial n^j}\right|_{S_{\text{itf}}^j} = \left.\frac{\partial \phi^{(I_j)}}{\partial n^j}\right|_{S_{\text{itf}}^j}, \qquad j = 1, 2, \ldots, N \tag{2.22b}$$

where S_{itf} denotes the interfaces. If we write (2.22) in the form of

$$\int_{-h}^{-d} \phi^{(E)}\big|_{r_j=a_j} g_s(z)\mathrm{d}z = \int_{-h}^{-d} \phi^{(I_j)}\big|_{r_j=a_j} g_s(z)\mathrm{d}z \tag{2.23a}$$

$$\begin{aligned} \int_{-h}^{0} \left.\frac{\partial \phi^{(E)}}{\partial n^j}\right|_{r_j=a_j} f_p(z)\mathrm{d}z &= \int_{-h}^{-d_j} \left.\frac{\partial \phi^{(I_j)}}{\partial n^j}\right|_{r_j=a_j} f_p(z)\mathrm{d}z \\ &\quad + \int_{-d_j}^{0} \left.\frac{\partial \phi^{(E)}}{\partial n^j}\right|_{s_j} f_p(z)\mathrm{d}z \end{aligned} \tag{2.23b}$$

and use the orthogonality of the depth function $f_p(z)$ (2.15) and $g_s(z)$ (2.8b):

$$\int_{-h}^{0} f_u(z) f_v(z)\mathrm{d}z = \begin{cases} h & u = v \\ 0 & u \neq v \end{cases} \tag{2.24a}$$

$$\int_{-h}^{-d} g_r(z) g_s(z)\mathrm{d}z = \begin{cases} h - d & r = s = 0 \\ \frac{1}{2}(h-d) & r = s \neq 0 \\ 0 & r \neq s \end{cases} \tag{2.24b}$$

we can obtain a linear system of equations for α_{ms}^j, β_{m0}^j, and β_{mp}^j with $j = 1, 2, \ldots, N$, $m = 0, \pm 1, \pm 2, \ldots$, $p = 1, 2, \ldots$, and $s = 0, 1, \ldots$. Particularly, the β_{m0}^j for all the cylinders ($j = 1, 2, \ldots, N$) are coupled, and need to be solved simultaneously. Truncating m to be $\pm N_m$, s to be N_s, and p to be N_p, we then solve (2.23) for the unknowns and obtain the potential functions for the whole fluid domain.

Hydrodynamic Coefficients

The fluid pressure p can be expressed with respect to the velocity potential by using the linearized Bernoulli equation:

$$p = -\rho\frac{\partial \Phi}{\partial t} = \mathrm{Re}\left\{i\sigma\rho\phi(r,\theta,z)e^{-i\sigma t}\right\}$$

where the second equation is upon (2.2). The first-order hydrodynamic forces (moments) on cylinder j, denoted by $\mathbf{F}^j$ ($\mathbf{M}^j$) can be obtained by direct integration of the pressure over the body surface S_j, which yields that

$$\begin{aligned}\left\{\begin{array}{c}\mathbf{F}^j\\ \mathbf{M}^j\end{array}\right\} &= \iint\limits_{S_j} p\left\{\begin{array}{c}\mathbf{n}^j\\ \mathbf{r}\times\mathbf{n}^j\end{array}\right\}\mathrm{d}S\\ &= \mathrm{Re}\left\{\iint\limits_{S_j} i\sigma\rho e^{-i\sigma t}\phi(r,\theta,z)\left\{\begin{array}{c}\mathbf{n}^j\\ \mathbf{r}\times\mathbf{n}^j\end{array}\right\}\mathrm{d}S\right\} \qquad (2.25)\end{aligned}$$

where ϕ is the radiation potential obtained from § 2.2.

In particular, in terms of added mass and damping coefficients, the p-th component of the hydrodynamic force ($p = 1, 2, \ldots, 6$) induced by the motion of k-th cylinder in q-th direction can be expressed as

$$F_{pq}^{jk} = \mathrm{Re}\left\{-(-i\sigma)^2\bar{\zeta}_q^k(\bar{\mu}_{pq}^{jk} + i\frac{\bar{\lambda}_{pq}^{jk}}{\sigma})e^{-i\sigma t}\right\} \qquad (2.26)$$

where $\bar{\mu}_{pq}^{jk}$ and $\bar{\lambda}_{pq}^{jk}$ are (dimensional) added mass and damping coefficients for the j-th cylinder. Substitution of (2.26) in (2.25) yields that

$$\bar{\mu}_{pq}^{jk} + i\frac{\bar{\lambda}_{pq}^{jk}}{\sigma} = \frac{i\rho}{\bar{\zeta}_q^k\sigma}\iint_{S_j}\phi_q^k n_p^j \mathrm{d}S \qquad (2.27)$$

where ϕ_q^k denotes the unit potential induced by the q-mode motion of cylinder k.

2.3 Wave-Exciting Forces and Moments

With potential theory, wave-exciting forces and moments on a number of cylinders can be obtained by

$$\left(\begin{array}{c}\mathbf{F}_{\mathrm{ex}}\\ \mathbf{M}_{\mathrm{ex}}\end{array}\right) = \mathrm{Re}\left\{i\sigma\rho e^{-i\sigma t}A\iint\limits_S(\phi_0+\phi_7)\left(\begin{array}{c}\mathbf{n}\\ \mathbf{r}\times\mathbf{n}\end{array}\right)\mathrm{d}S\right\} \qquad (2.28)$$

where A is the amplitude of incident waves, ϕ_0 and ϕ_7 are unit-amplitude potentials for incident waves and diffracted waves respectively, and S denotes the surface of the cylinders. The

governing equations (2.3a)(2.3b)(2.3c) and the radiation condition (2.5) should be satified for ϕ_7; and on the surface of body j, denoted by S_j,

$$\left.\frac{\partial(\phi_0+\phi_7)}{\partial n^j}\right|_{S_j}=0 \qquad j=1,2,\ldots,N \tag{2.29}$$

Given ϕ_0, solving for ϕ_7 to obtain wave-exciting forces can take the same amount of computational efforts as solving for the radiation potential. Haskind developed a relation [32] for an arbitrary body such that wave-exciting loads on the structure can be obtained based only on the radiation potential, as explained in [50] and [68]. Where, we generalize the Haskind relation to be applicable to a finite number of 3D bodies in arbitrary shape, and apply it to evaluate wave-exciting forces (moments) on either an individual cylinder, or a group of cylinders, situated among an array of cylinders using only the radiation potentials. Application of this relation can considerably simplify the computation for hydrodynamic properties of a cylinder array.

The l-th component of excitation loads in (2.28) can be written as

$$F_{\mathrm{ex}_l}=\mathrm{Re}\{AX_l e^{-i\sigma t}\}, \quad l=1,2,\ldots,6 \tag{2.30}$$

with

$$X_l=i\sigma\rho\iint_S(\phi_0+\phi_7)n_l\mathrm{d}S \tag{2.31}$$

where X_l is the complex amplitude of the unit wave-exciting force in direction l with n_l being the corresponding normal vector. With the application of Green's theorem, it can be shown that

$$X_l=i\sigma\rho\iint_{S_B}\left(\phi_0\frac{\partial\phi_l}{\partial n}-\phi_l\frac{\partial\phi_0}{\partial n}\right)\mathrm{d}S \tag{2.32}$$

where $S_B=\sum_{j=1}^{N}S_j$, denoting the surface of all the cylinders in the array, and ϕ_l is the unit radiation potential for cylinders of interest regarding computing the wave-exciting force, which can be either an individual cylinder, or a group of cylinders as a unit, oscillating in l-th mode among the array. As expressed in (2.32), X_l only depends on the incident wave potential, which is considered known, and the radiation potential obtained in §2.2. The evaluation of X_l can be taken to the far field and further simplified by

$$X_l=-i\sigma\rho\int_{-h}^{0}\int_{0}^{2\pi}\left[\phi_0\frac{\partial\phi_l}{\partial r}-\phi_l\frac{\partial\phi_0}{\partial r}\right]_{@r=R}R\mathrm{d}\theta\mathrm{d}z \tag{2.33}$$

where S_R was taken as a vertical circular cylinder about the z-axis of large radius R in the global coordinate system yields that in polar coordinates (r,θ,z). ϕ_l in (2.33) needs to be expressed in the global coordinates, for which the Graf's addition theorem was applied and

it takes a form different from (2.19) in the far field. The details of how X_l can be evaluated are provided in the Appendix A.

We consider Equation (2.33) is the generalized Haskind relation for a cylinder array. It is a remarkably simple expression for computing wave-exciting forces and moments for an individual *or* a group of cylinders, requiring the far field behavior of the corresponding radiation potential in the global coordinates.

2.4 Results of Hydrodynamic Study

To validate the present method and investigate wave interference effects on multi-cylinder structures, a computational solver was developed based on the theory in §2 and §3, and applied to a number of configurations shown in Fig. 2.4, where waves progress in a direction that makes an angle β with the x-axis. We compare results with boundary integral method by Matsui & Tamaki [41] and interaction theory by Kagamoto & Yue [35]. These methods are considered to have obtained the exact solution to the hydrodynamic interaction problem within the context of linear potential theory. The comparisons show good agreements and improved computational efficiency.

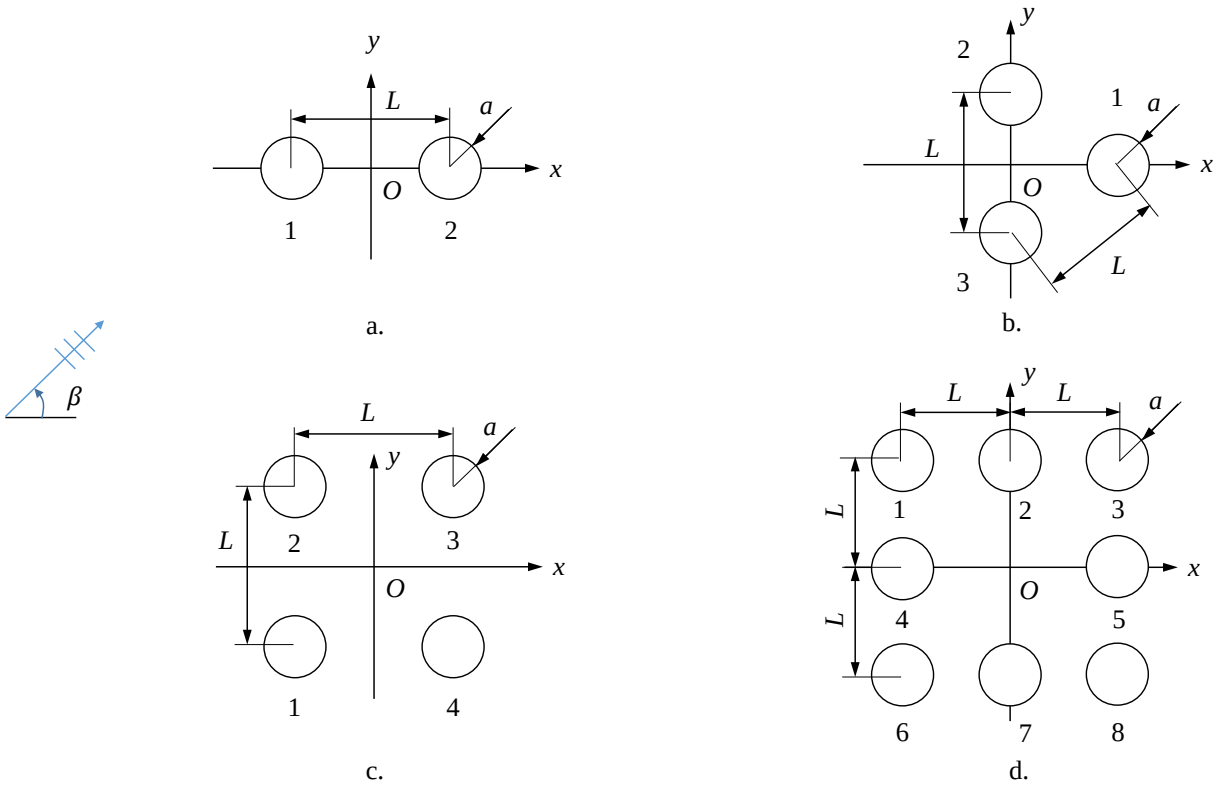

Figure 2.4: Configurations of arrays of cylinders

Analysis of Efficiency

To solve the problem, the infinite series in (2.12) and (2.20) were truncated to N_m circumferential modes, N_s radial modes for the interior solution, and N_p evanescent modes for the exterior solution, leading to linear systems of equations regarding unknown coefficients α_{ms}, β_{m0}, and β_{mp} ($m = 0, \pm 1, \ldots, \pm N_m$, $s = 0, 1, \ldots, N_s$, $p = 1, 2, \ldots, N_p$). In the process of solving the linear equations, the primary computational effort is to solve for the *interaction* coefficients β_{m0}, of which the $(2N_m + 1)$ unknowns per cylinder need to be solved simultaneously for the whole array, which results in a system with the total number of unknowns being $N_T = N(2N_m + 1)$. For the "exact" interaction theory by Kagemoto & Yue [35], such number will increase to be $N_{T,K\&Y} = N_p \times N(2N_m + 1)$ since both the propagating mode and the evanescent mode were considered in the wave interaction. Further, if an iterative scheme as in [53] were applied to study the multiple-scattering phenomenon, the number of corresponding unknowns will be multiple larger than $N_{T,K\&Y}$, depending on the number of iterations. Assuming the Gaussian elimination was used to solve the linear system, we were able to reduce computational flops by N_p^3 times, compared to the "exact" interaction theory, and $(N_p N_{it})^3$ times, compared to the iterative-scheme method with N_{it} being the number of iterations. This fact is particularly favorable for solving the problem of a relatively large group of cylinders. As an example, with the number of cylinders being $N = 30$ and typical numbers of truncated terms being $N_m = 6$, $N_p = 60$, $N_s = 60$, it can be obtained that $N_T = 390$ for the current method, while $N_{T,K\&Y} = 23,400$ for the interaction theory.

Analysis of Accuracy

We first implemented the method to compute hydrodynamic properties for two configurations: two individual cylinders computed by Matsui & Tamaki [41] and a four-cylinder array as a unit computed by Kagemoto & Yue [35]. Good agreements of results validates the assumption of neglecting evanescent mode in our method and the newly-derived generalized Haskind relation. In the following, hydrodynamic coefficients and wave-exciting forces are non-dimensionalized by

$$\mu_{pq}^{jk} = \bar{\mu}_{pq}^{jk} / \rho\pi a_j^2 d_j \quad p, q = 1, 2, 3 \tag{2.34a}$$

$$\lambda_{pq}^{jk} = \bar{\lambda}_{pq}^{jk} / \sigma\rho\pi a_j^2 d_j \quad p, q = 1, 2, 3 \tag{2.34b}$$

$$\tag{2.34c}$$

where we recall that a_j is the radius of cylinder j, and d_j the draft.

We consider two identical cylinders in tandem, as shown in Fig. 2.4(a), with radius a, draft $d/a = 0.5$, and water depth $h/a = 10$. Two cases of spacing ratio, $L/a = 3$ and $L/a = 5$, were simulated, where L is center-to-center spacing between the two cylinders. An example of convergence tests regarding N_m, N_p, and N_s is shown in Table 2.1, where added mass and damping coefficients and wave-exciting force of cylinder 1 in surge direction with the presence of cylinder 2 and were computed. Presented cases are for $k_0 a = 1.0$ and

Table 2.1: Convergence behavior: relative error (%) of hydrodynamic coefficients of two truncated columns with $L/a = 5$, $d/a = 0.5$, $h/a = 10$, $k_0 a = 1.0$

No. of terms			μ_{11}^{11}	λ_{11}^{11}	$\lvert X_1^1 \rvert$
$N_m = 2$	$N_p = 240$	$N_s = 240$	2.04×10^{-2}	8.42×10^{-2}	27.62
$N_m = 3$			8.20×10^{-4}	6.15×10^{-4}	17.96
$N_m = 6$			6.55×10^{-9}	2.53×10^{-9}	0.45
$N_m = 25$	$N_p = 30$	$N_s = 240$	2.85	2.60	1.44
	$N_p = 60$		0.82	0.80	0.44
	$N_p = 120$		0.27	0.27	0.15
$N_m = 25$	$N_p = 240$	$N_s = 30$	1.20	1.51	0.86
		$N_s = 60$	0.52	0.61	0.34
		$N_s = 120$	0.20	0.22	0.12

$L/a = 5$. We chose $N_m = 2, 3, 6, 25$, $N_p = 30, 60, 120, 240$, and $N_s = 30, 60, 120, 240$. We assumed the set of $N_m = 25$, $N_p = 240$, $N_s = 240$ gave the "exact" solution and computed relative errors in percentage for each set of parameters. As a result, $N_m = 6$, $N_p = 60$, and $N_s = 60$ was chosen for this sample case, achieving 1% accuracy. We performed the same convergence analysis for all the cases we present in this paper and found that in general: large N_p and N_s is needed for large depth-to-radius ratio; and large N_m is needed to compute wave-exciting forces and moments when wave-interaction effects get stronger.

Fig. 2.5 and Fig. 2.6 show comparisons of the hydrodynamic coefficients with those obtained by Matsui & Tamaki [41] where boundary-integral method was applied; new results were presented for high frequencies. In particular, μ_{11}^{12} and λ_{11}^{12} represented *interacting* hydrodynamic coefficients, i.e. the added mass and damping coefficients of cylinder 1 induced by the motion of cylinder 2. Good agreements were obtained over a large range of frequencies. Deviances are more noticeable when two cylinders are closer to each other ($L/a = 3$), where neglecting evanescent modes may be less valid. The result also indicates consistency with the fact that evanescent modes affect added mass more than damping coefficient, as larger discrepancies occur in μ rather than λ.

The generalized Haskind relation (2.33) is applied to obtain wave-exciting surge force on each individual cylinder. Fig. 2.7 shows that Cyl. 1 experienced larger surging force than an isolated cylinder due to the interaction effects of cylinder 2, while smaller surge force is acting on Cyl. 2 because of the sheltering effects of Cyl. 1. Good agreements were obtained in the comparison. More results on hydrodynamic coefficients in heave direction were presented in [76].

The increase in the number of devices will increase the complexity of the wave-interaction effects. To further verify the presented method, we computed hydrodynamic coefficients of a four-cylinder array, as shown in Fig. 2.4(c), moving in surge direction as a whole by simply

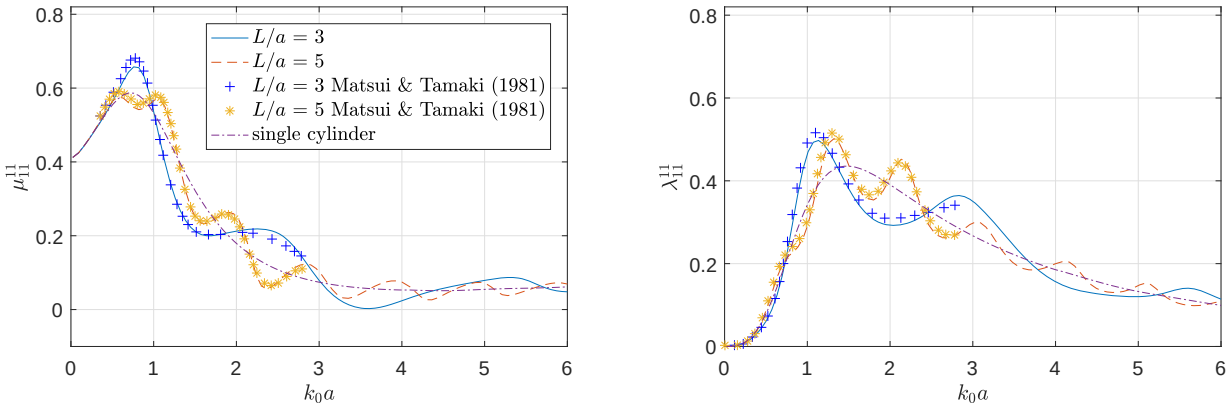

Figure 2.5: Hydrodynamic forces on cylinder 1 induced by surge motion of cylinder 1

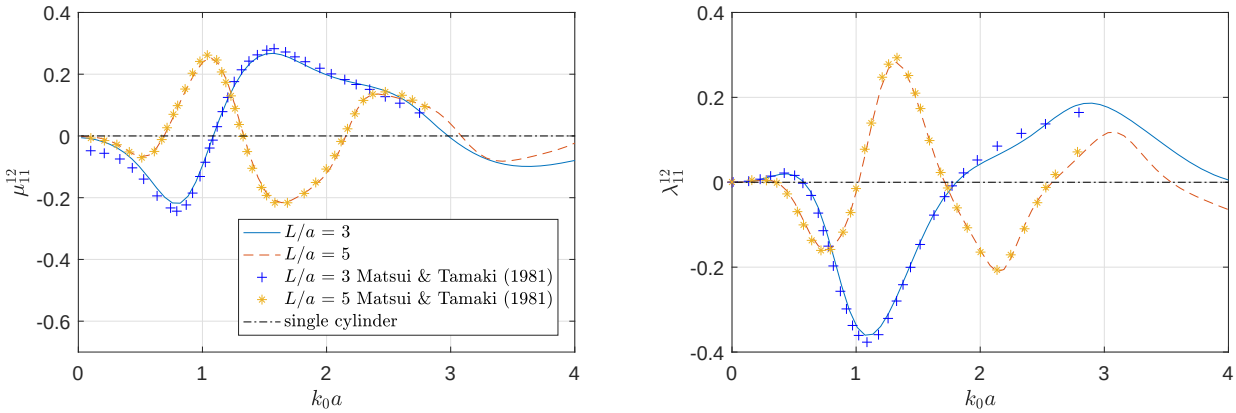

Figure 2.6: Hydrodynamic interaction forces (surge force on cylinder 1 induced by surge motion of cylinder 2)

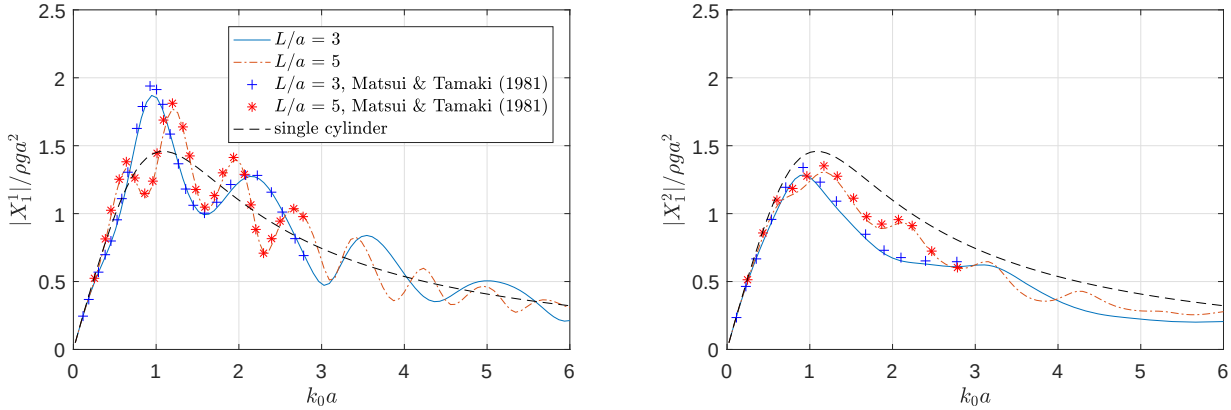

Figure 2.7: Wave-exciting surge force on cylinder 1 and 2

setting the motion of the four to be in phase and of the same amplitude. The water depth is $h/a = 4$, the draft of the cylinders $d/a = 2$, and the center-to-center spacing $L/a = 4$. Results of the hydrodynamic coefficients, as well as the surge wave-exciting force obtained by the newly generalized Haskind relation, averaged over the number of cylinders, were compared with those obtained by Kagemoto & Yue [35] and shown in Fig. 2.8 and Fig. 2.9. It can seen that results match excellently even the spacing between cylinders are relatively small ($L/a = 4$).

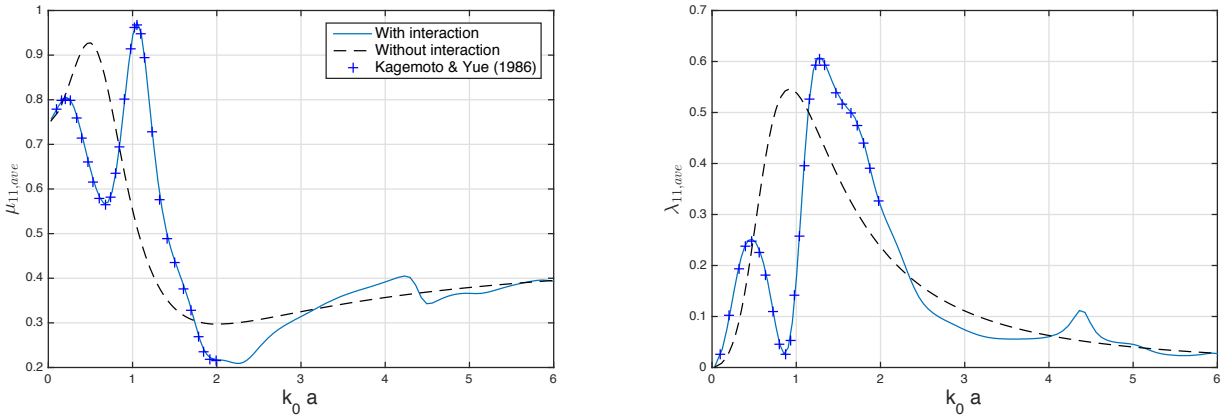

Figure 2.8: Surge hydrodynamic coefficients of a four-cylinder array

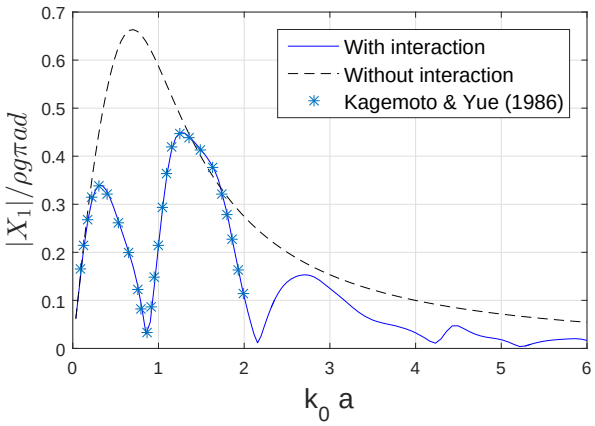

Figure 2.9: Surge wave-exciting forces on a four-cylinder array

Applications of the Generalized Haskind Relation

As can be seen from Fig. 2.9, the wave-exciting force drops to nearly 0 at certain frequencies. This is particularly interesting regarding using wave-interference effects to reduce wave loads on structures. Applying the generalized Haskind relation, we computed wave-exciting forces

for a four-cylinder array and an eight-cylinder array with configurations as shown in Fig. 2.4 (c) and (d), in heave and roll directions. The water depth is $h/a = 10$, the draft of the cylinders $d/a = 2$, and the side length of the square $l/a = 8$. Fig. 2.10 shows the damping coefficients of the two array and Fig. 2.11 presents the wave-exciting force and moment. Since the wave-exciting moment in roll of such symmetric arrays would be 0 in waves of heading angle 0, results for roll direction was shown for the wave angle being 45^o.

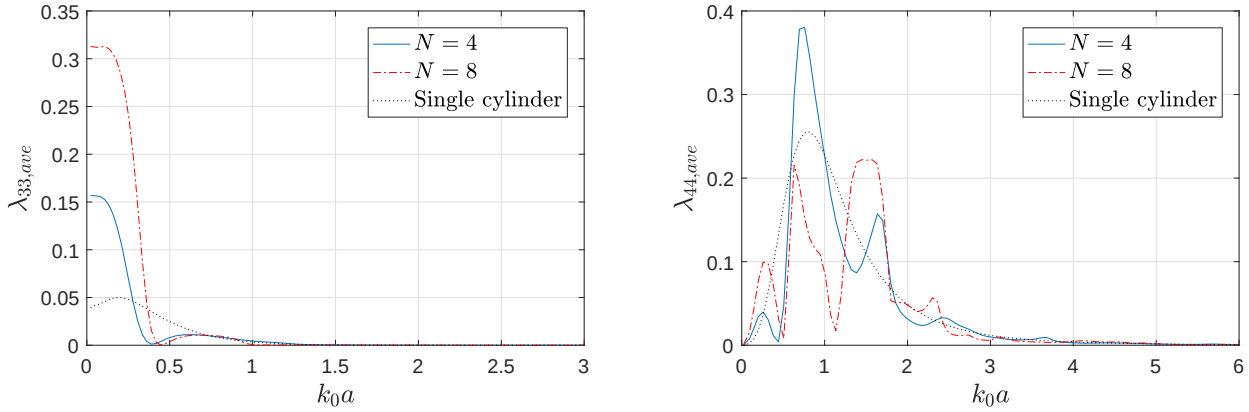

Figure 2.10: Damping coefficients of the square arrays in heave and roll motion.

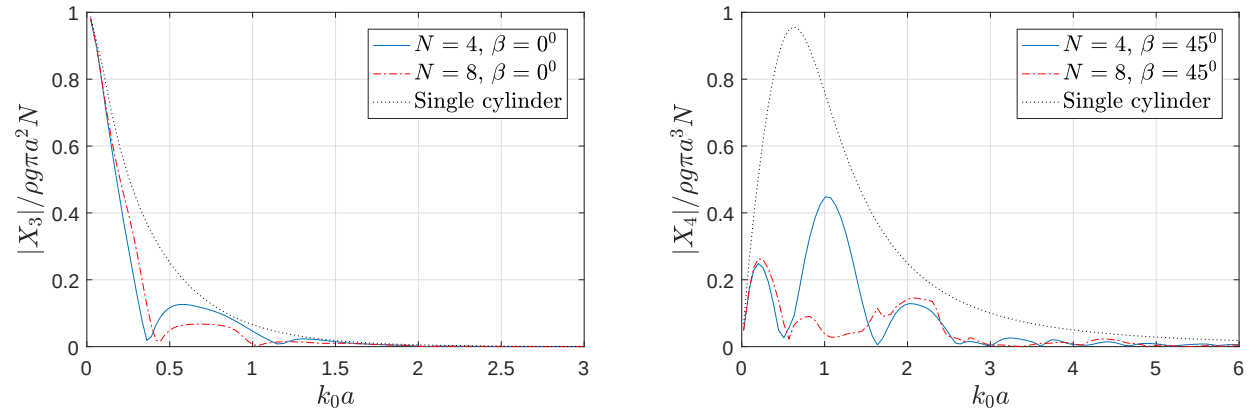

Figure 2.11: Wave-exciting moments in heave and roll direction on the square arrays with the incident-wave angle $\beta = 0^o$ for heave and $\beta = 45^o$ for roll.

It can be seen that the heave force on the array drop down to zero at the frequencies where the damping coeffients are close to zero. In addition, the eight-cylinder array, with cylinders added on sides of the square, has in general smaller wave-exciting force for each cylinder. This is especially the case for the roll moments with waves come in the 45^o direction.

2.5 Power Extraction from a WEC Array

The proposed method takes advantage of the cylindrical shape of a body and efficiently computes hydrodynamic properties for a system of independently oscillating bodies with high-order accuracy. It well fits the need of a quick estimation of wave-interaction effects for a preliminary design of a WEC array. It has been derived in [20] and [23] that the optimal power extracted by an array of oscillating bodies from regular waves can be computed as

$$P_{\text{opt}} = \frac{1}{8} F_{\text{exc}}^{*} B^{-1} F_{\text{exc}} \tag{2.35}$$

which is achieved when the velocity of cylinders satisfies

$$U_{\text{opt}} = \frac{1}{2} B^{-1} F_{\text{exc}} \tag{2.36}$$

where F_{exc} is a vector of wave-exciting forces (moments) on individual cylinders in the array with superscript asterisk denoting complex conjugate operation, and B is the NM-by-NM damping matrix, presumably non-singular, with N being the number of cylinders and M the degrees of freedom for each cylinder. For instance, given an array of heaving devices, the i-th element of F_{exc} will be AX_3^i where A is the amplitude of incoming waves, and X_3^j obtained by (2.33); the element B_{ij} in the i-th row and the j-th column of B will be $\bar{\lambda}_{33}^{ij}$, i.e. the dimensional heave damping coefficient of cylinder i induced by the heave motion of cylinder j, obtained by (2.27).

An important measure of the power-extraction ability of an array compared to a single device is the interaction factor q, which is defined as the ratio of the power captured by the array to the one captured by isolated bodies of the same number. By definition, q can be computed by

$$q = \frac{l_{\max,N}}{l_{\max,0}} = \left(\frac{1}{N} \frac{P_{\text{opt}}}{P_w} \right) / l_{\max,0} \tag{2.37}$$

where $l_{\max,N}$ and $l_{\max,0}$ are the (average) capture widths for an array of cylinders and a single cylinder respectively, and $P_w = 1/2\rho g A^2 c_g$ is the wave power with c_g being group velocity of incident waves. For a heaving cylinder, $l_{\max,0} = \lambda/2\pi$. The q factor has been widely used to evaluate the wave interaction effects on power production of a WEC array as in [12, 43, 57]. As shown in [69], the property holds for an array of heaving axisymmetric devices that the integration of the q factor over the wave-incident angle from 0 to 2π is a constant, given a wave frequency. This indicates that constructive effects from interacting waves at a certain wave condition comes along with the same amount of destructive effects at other wave conditions. Hence, evaluating the performance of an array at a specific wave condition may not be sufficient when it comes to comparing different designs of the array.

It should be pointed out that no constraint is considered in expressions (2.35) and (2.36) for evaluating the optimal power. In more practical scenarios, constraints on movements of the WECs and the machinery limits of devices can significantly affect the power performance of the array and need to be considered in the PTO control strategy. Not many

Table 2.2: Properties of the array with the maximal interaction factor

No. of cylinders	$q_{\max}$	β	k_0L	*RAO*	$\frac{\arg(\zeta_3^j)-\arg(F_{\text{exc}}^j)}{\pi}$
Two	1.66	$\frac{\pi}{2}$, $\frac{3\pi}{2}$	3.39	6.95, 6.95	0, 0
Two ($L = 8$)	1.67	$\frac{\pi}{2}$, $\frac{3\pi}{2}$	3.68	8.80, 8.80	0, 0
Two ($L = 10$)	1.67	$\frac{\pi}{2}$, $\frac{3\pi}{2}$	3.69	10.79, 10.79	0, 0
Three	1.51	0, $\frac{2\pi}{3}$, $\frac{4\pi}{3}$	3.68	3.32, 9.95, 9.95	-1.3, -0.03, -0.03
Three (5%L off)	1.60	1.35π	3.59	10.19, 10.20, 3.84	-0.11, -0.09, -4.13
Three (10%L off)	1.67	1.35π	3.51	10.33, 10.28, 4.28	-0.10, -0.14, -4.21
Four	1.59	0, $\frac{\pi}{2}$, π, $\frac{3\pi}{2}$	3.68	9.31, 9.31, 5.72, 5.72	-0.38, -0.38, 1.07, 1.07

methods exist for controlling a WEC array coordinatedly to consider the wave-interaction effect. A Model-Predictive Control strategy will be developed in Chapter 3 to optimize the power production and satisfy hard constraints on a system of heaving point absorbers, where the current method was applied to take into account the wave-interaction effect in the dynamic model. Results suggested that wave-interaction effects on a WEC array became less significant with motion constraints considered, but had similar changing trend over the wave frequency compared to the unconstrained case. In the current study, with the control strategy applied to an array of devices being the same as that applied to a single device, though unconstrained, the focus is to provide insights into wave-interaction effects brought by the array configurations with the frequency-domain analysis. This fast-evaluation method can be used at the preliminary design stage for a wave farm before running more costly simulations and enable discussions on, for example, whether more destructive or more constructive effects are to be seen for a given array at various sea states.

In the following sections, we will discuss wave-interaction effects induced by the number of devices, spacing between devices, and geometric symmetry of the layout, and perform estimations of the interaction effects on power production for an array of 24 heaving point absorbers. Simulations were first performed for arrays consisting of two, three, and four heaving absorbers in configurations as shown in Fig. 2.4(a), (b), and (c), in various wave conditions. Then changes were made to the original layouts by (1) increasing the spacing between devices and (2) moving the position of one device to break the symmetry of the layout. The maximal value of q and the corresponding wave-incident angle β, as illustrated in Fig. 2.4, and wave frequency for each configuration are listed in Tab. 2.2; also presented are the *RAO* and the phase difference between the heaving velocity and the wave-exciting force for each cylinder in the array in such a wave condition. For all configurations, the property that the q factor averaged over the wave angle is 1 holds.

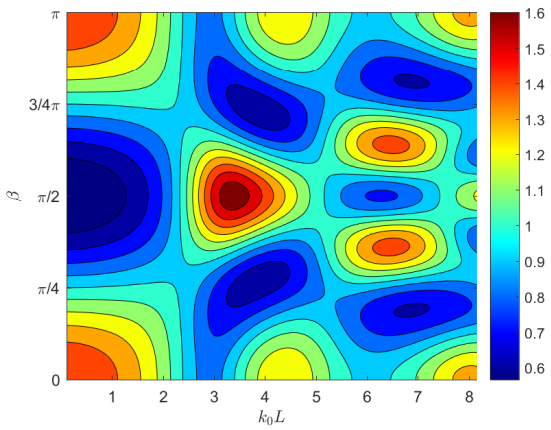

(a) Two cylinders

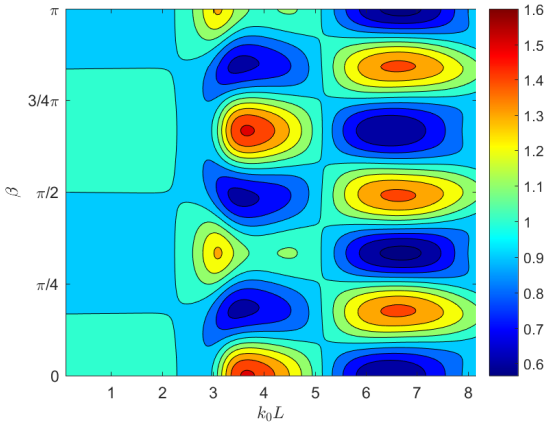

(b) Three cylinders

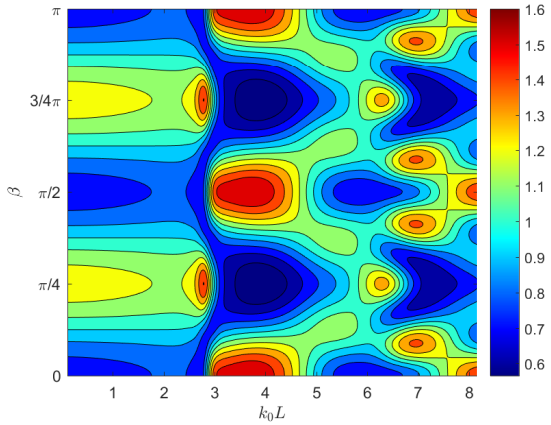

(c) Four cylinders

Figure 2.12: Contour plots of q for arrays of two, three, and four cylinders

Effects of Number of Devices

Fig. 2.12 presents the interaction factor for the array consisting of two, three, and four cylinders, changing with wave-incident angle β and non-dimensional wave frequency k_0L. The spacing was set to $L = 5a$. Taking advantage of the symmetry of the configuration, we only showed results for β being from 0 to π. The upper limit of the wave frequency was chosen such that the damping coefficient of the individual cylinder approximately reached 0. For all of the three layouts with the same spacing between closest cylinders, the maximum q was attained when waves come perpendicularly towards one side of the polygon defining the layout at the frequency k_0L around 3.5. As shown in Tab. 2.2, the cylinder(s) hit first by waves oscillated with a larger amplitude than the ones in the back along the propagation direction. In addition, because of the interacting waves, the velocity of an oscillator in an array can have a phase difference with the wave-exciting force on it at its optimal condition.

It should be pointed out that since no motion constraint is considered, the *RAO* required to achieve $q_{\max}$ may exceed the physical limits of the absorbers.

Effects of the spacing among devices

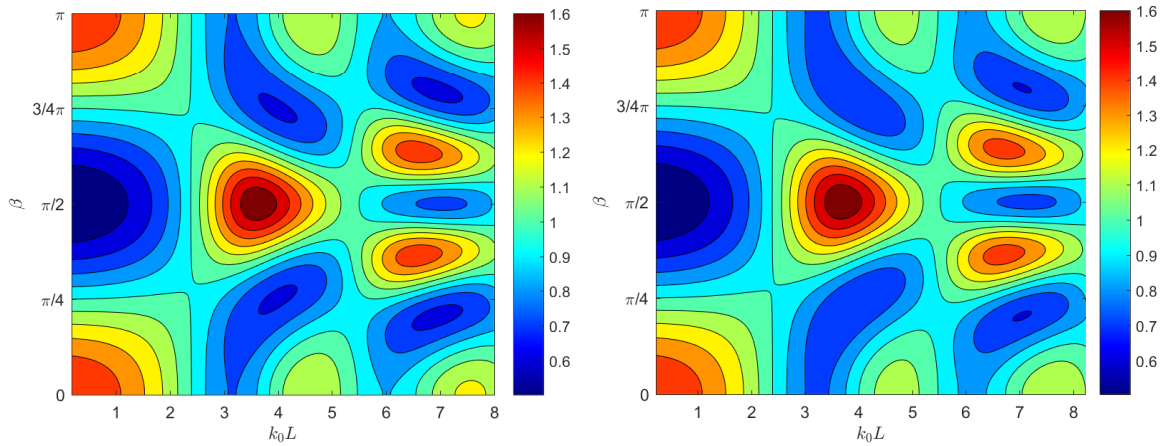

(a) $L = 8a$ (b) $L = 10a$

Figure 2.13: Contour plots of q for two cylinders with the spacing being $L = 8a$ and $L = 10a$.

Contour plots for the q factor of the two-cylinder array with the spacing changed to $L = 8a$ and $L = 10a$ are presented in Fig. 2.13. From comparisons with Fig. 2.12(a) (with $L = 5a$), it is interesting to find that the interaction factor of arrays with different separating distances have very similar changing patterns with respect to the nondimensional wave frequency k_0L. Simulations also showed that this similarity holds for arrays of three and four cylinders. This suggests that certain interaction effects, for example, the most constructive or the most destructive effect, will occur at a lower wave frequency if the devices have larger spacing L. In addition, with the increase of the distance, the two cylinders oscillate with a larger amplitude when achieving the maximum interaction q factor as shown in Tab. 2.2, which can be attributable to weaker interaction effects when cylinders are farther apart.

Effects of asymmetric layouts

Considering uncertainties in positioning the absorbers in real sea, we studied the power performance for a three-cylinder array of an equilateral triangle shape but with the cylinder 1, as shown in Fig. 2.4(b), moved along the positive y-axis by $5\%L$ and $10\%L$ respectively. Results are presented in Fig. 2.14. As the symmetry no longer exists, computations were performed for β from 0 to 2π. The wave frequency was non-dimensionalized by $L = 5a$. With the cylinder placed off-centerline, the maximum q factor occurred at the incident angle

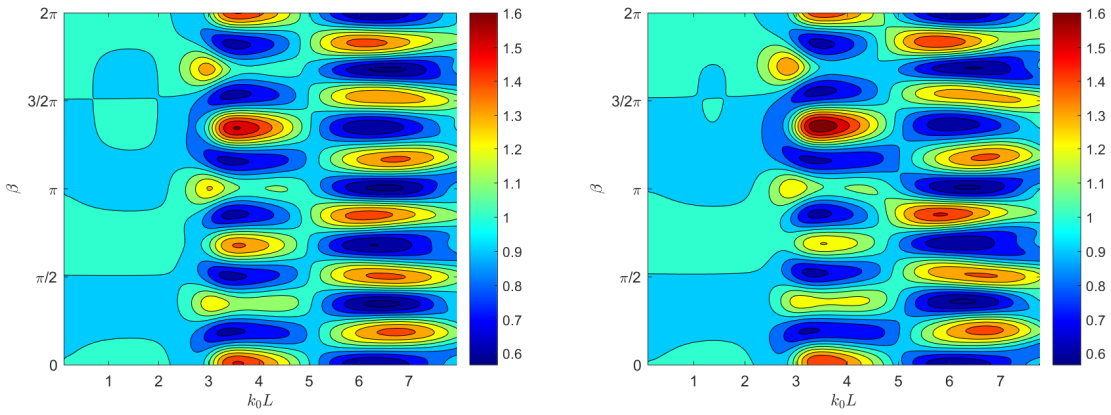

(a) 5%L off (b) 10%L off

Figure 2.14: Contour plots of q for three cylinders with the cylinder 1 positioned off the centerline.

of 243^o, which is approximately perpendicular to the shortest side of the triangle. Compared to the interaction factor for the array of symmetry, as shown in Fig. 2.12(b), the q factor for the asymmetric layout has similar regions of destructive or constructive wave effects with different extent of interaction effects. With the increase of the "misalignment" of the cylinder 1, the maximal interaction factor $q_{\max}$ was increased. Results suggested that a small amount of changes (less than 10%L) in the relative positions of cylinders should not significantly affect the prediction of power performance of the array; in addition, the asymmetry can strengthen wave-interaction effects regionally and affect the wave condition of the occurrence of $q_{\max}$. This fact can be used to adjust a symmetric configuration to accommodate the dominant wave direction at a real site.

Wave interaction among an array of 24 point absorbers

To realize commercialization of wave energy, a large WEC array is of high interests. The world's first grid-conneted wave-energy array, developed by Carnegie Clean Energy, consists of three submerged absorbers in a triangular configuration and has a peak rated capacity of $5MW$ [19]. It is possible to form a large WEC farm using multiple units of such an array, as illustrated in Fig.2.15, analogous to a wind farm consisting of $5MW$ wind turbines. Example array configurations are shown in Fig. 2.15, where the previously computed equilateral triangular array was used as the unit array. If the spacing between units are relatively large, the current method can be combined with the point-absorber approximation [20] to further gain computational efficiency in estimating the interaction effects. The basic assumption of the point-absorber approximation is that the device is small enough, relative to the wavelength of the incident waves, for it to be a weak scatter, so that scattering waves can be neglected. Regarding the combination of the current method and the point-absorber approx-

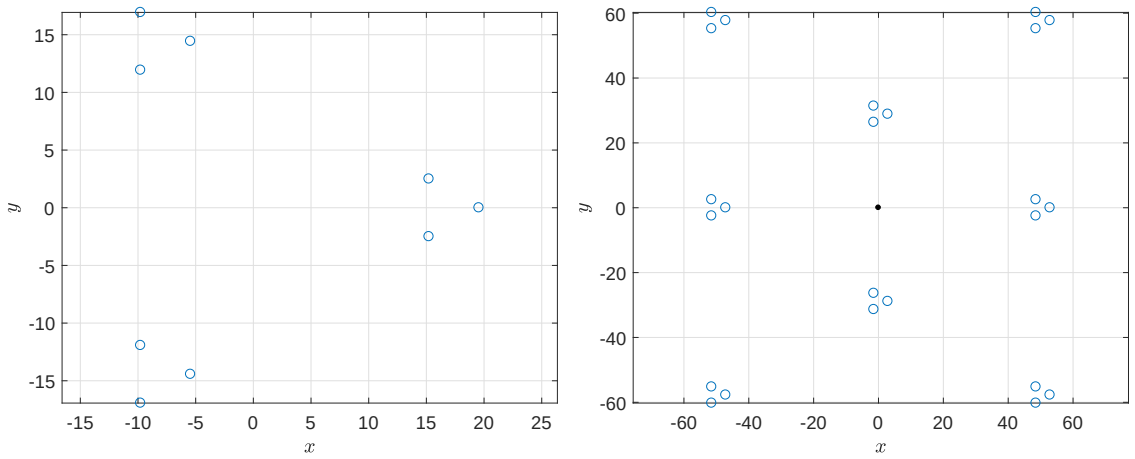

(a) (b)

Figure 2.15: Illustration of multiple units of a three-cylinder array.

imation, full interaction effects will be considered for cylinders in each unit array, while the point-absorber approximation will be used to account for interaction effects among units.

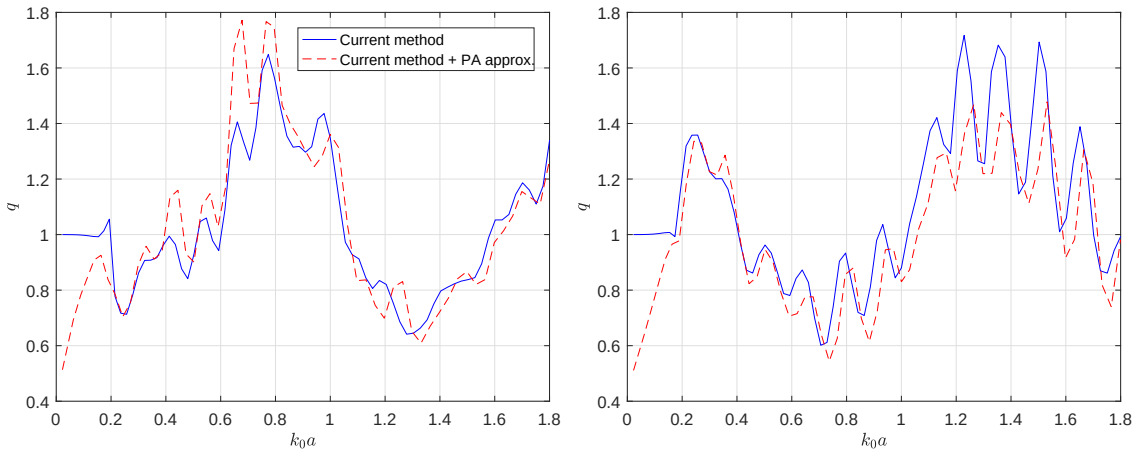

(a) $\beta = 0^o$ (b) $\beta = 90^o$

Figure 2.16: The interaction factor for three units of a triangular array with the distance between the units $L = 10r$.

To verify the accuracy of the combined method, Fig. 2.16 and Fig. 2.17 compared the interaction factor obtained by the current method considering full wave interaction and by the combined method for arrays shown in Fig. 2.15a, with the spacing between centers of the triangular units set to $L = 10r$ and $L = 20r$ respectively, where r is the radius of the excircle of the triangle for a single unit, and the wave-incident angle β is defined as in Fig. 2.4. It can be seen that good agreements were achieved, and that the accuracy of the combined

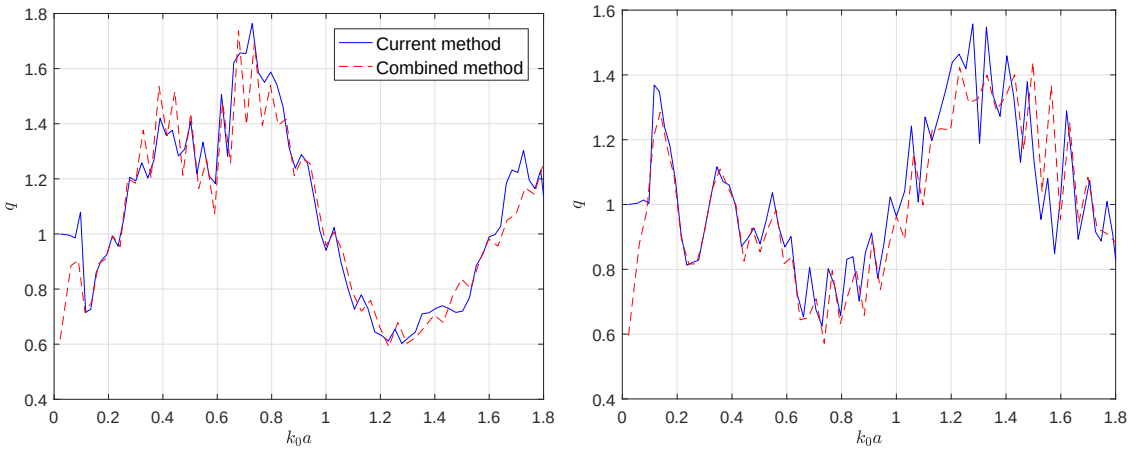

(a) $\beta = 0^o$ (b) $\beta = 90^o$

Figure 2.17: The interaction factor for three units of a triangular array with the distance between the units $L = 20r$.

method increased with the increase of the spacing between units. The combined method was then used to estimate the q factor for a large array in all wave conditions, which consists of 8 units and hence 24 cylinders, as shown in 2.15b. The center-to-center spacing between units is set to $L = 20r$. To evaluate the accuracy of the estimation, the q factor averaged over the wave angle β was presented in Fig. 2.18a, of which the value should be 1 if full interaction effects were considered. The relative difference of the presented parameter to 1 stays under 10% for most of the cases, except for the low-frequency range where the ratio of the wavelength and the spacing between units is too large that the assumption of the point absorber approximation is no longer valid. Fig. 2.18b shows the contour plot of the q factor for the 24-cylinder array in all wave conditions computed by the combined method. The maximum q reached 2.4 at $k_0 = 0.62$ and $\beta = \pi/3,\ \pi,$ and $5/3\pi$, which is 140% more than the one achieved by isolated absorbers.

It should be noticed that the optimum q is achieved by applying impedance-matching control to the WEC array, where the impedance matrix has non-zero off-diagonal elements which can be hard for implementation. More advanced control strategies will be preferred to optimize the power from a global point of view and satisfy hard constraints.

2.6 Summary Remarks

In this Chapter, the computational problem of waves interacting with an array of WECs, each modeled as a truncated cylinder, in arbitrary configurations is solved by the matched eigenfunction expansion method. Graf's addition theorem was applied to transform coordinates and express the presence of a multitude of scattering waves. To improve computational efficiency, we argued that evanescent modes generated by one cylinder are negligible in the

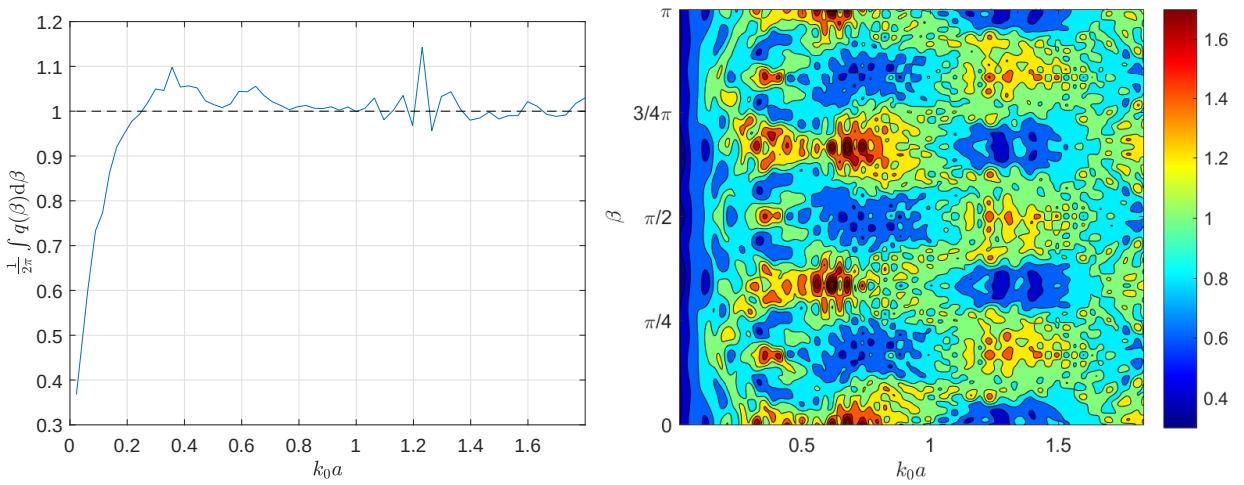

(a) q averaged over β (b) Contour plot of q

Figure 2.18: Wave-interaction effects on eight units of a triangular array with the distance between the units $L = 20r$.

near field of its neighboring cylinders, whereas the far-field radiating waves are allowed to interact. Theoretical analysis showed that the neglected terms exponentially decayed with the increase of the spacing among cylinders. Newly generalized Haskind's relation was developed to obtain wave-exciting forces and moment on an individual cylinder, or even a group of cylinders, situated among the array, without having to solve diffraction properties of the structure.

Extensive demonstrative results for added-mass and damping coefficients, and wave-exciting loads were presented for various configurations. Comparisons with numerical method and the method of "exact" interaction theory showed good agreements in a wide range of frequencies, even for arrays with relatively small spacing (the spacing-to-radius ratio $L/a \gtrsim 4$). The computed hydrodcynamic properties including damping coefficients and wave-exciting forces were then used to study the optimal power and the interaction factor q for an array of heaving point absorbers in various configurations and wave conditions. Effects of the spacing between devices, the layout symmetry, and the wave-incident angle on power extraction of the array were investigated. Also studied is a layout consisting of multiple smaller groups of point-absorber devices. A type of hierarchical method is applied to a medium size array of 24 devices, where the current method to consider intereference effects among devices in the group and the point-absorber approximation to account for the interaction among the groups, The optimal power absorption of the array under all wave conditions is presented. Key details of this research are reported in [79].

Chapter 3

MPC Control of a Single WEC

3.1 Overview

Control of a wave-energy converter (WEC) is becoming one of the key issues for wave-energy extraction to achieve higher efficiency and lower cost. Various control strategies have been developed and implemented on WECs, including resistive control, approximate complex-conjugate control, phase control by latching or clutching, etc. A comparison of selected control strategies can be found in overview articles of [5, 30].

In practice, most WECs will be subject to limitations placed on physical motion of the absorber and the capabilities of the device. These raise the need for constrained optimal control [18, 21]. In such a category of approach, model-predictive control (MPC) is attracting more and more attention because of its capability in handling hard constraints on states and inputs, which serves the objectives of maximizing wave-energy extraction and satisfying machinery requirements for safety and operations. Differing from other optimal controllers, MPC solves a constrained optimization problem on-line based on the current state of the plant, rather than determining off-line a feedback policy that provides the optimal control for all states [44]. In a real-sea environment, an on-line control strategy can better account for state changes and reject disturbances. However, this leads to the requirements that the open-loop optimal control problem has to be solvable in a reasonable amount of time (compared with plant dynamics) and that a wave-prediction unit be simultaneously incorporated to predict the dynamics of the system. In this study, we assume that there exists a wave predictor, e.g. [7, 28, 48], which can estimate the wave profile for a certain future period.

Various methods were proposed to implement an MPC on WEC systems which are known to be nonlinear and non-causal. One popular approach is to form the optimization problem in a Quadratic Programming (QP) form, so that efficient optimization algorithms can be directly applied. Nevertheless, the question of whether the constructed QP is convex or not is commonly left open. Hals et al. [31] used the heaving velocity of the WEC as the optimizer and cast the optimization problem into a QP. An arguable point for this method is that the objective function was modified such that there existed one sampling instant

delayed from the input to the output in the computation of the energy output, and the resulting QP was assumed convex. However, as shown in [38], the convexity of such a QP is not guaranteed. More importantly, the modified cost function can result in suboptimal solutions and hence less energy extraction. In addition, optimizing over the state velocity is not the same as directly optimizing over the control input in the sense that there may not be a feasible control force to achieve the "optimal velocity."

Taking the machinery force, generated by the PTO system, as the optimizer, Li and Belmont formed a novel MPC with a QP of guaranteed convexity [38]. The novelty lay in their cost function where two additional penalty terms were introduced to (a) convexify the problem, (b) penalize the consumed energy, and (c) penalize a state to ensure the feasibility of the solution. However, in their dynamic model, the wave-exciting force was assumed to be just proportional to elevation of the incoming wave, while the effects of diffracted waves were neglected, which is justifiable only for "infinitely-long waves." For long but not infinitely long waves, it can be shown that a term of order kA_0, with kA_0 being the wave slope, will contribute to the wave-exciting force. This represents the effect from the vertical acceleration of the fluid, which is derived in the Appendix A. With the less accurately predicted wave load, the generated control law would be different from the one that achieves the optimal power extraction in the certain wave condition, which also results in a sub-optimal oscillating behavior of the absorber. It should also be noticed that penalizing the heaving displacement, which can lead to an additional energy loss, may not be necessary for all cases. In the work of [14], the slew rate of the machinery force was used as the optimizer, which, in our view, can generate a less aggressive control input and hence less requirements on machines. However, convexity of the formulated problem in [14] was not guaranteed. All of the aforementioned strategies are based on a linear model. A nonlinear MPC (NMPC) for a WEC was developed first by Tom and Yeung [64], where the power-take-off (PTO) damping was used as the optimizer for the purpose of practical implementations. As a follow-on work, an improved NMPC, which took into account the mechanical-electrical energy conversion efficiency, was proposed and applied [61] to generate optimal damping profiles (time histories) off-line for a co-axial point absorber in various wave conditions.

In terms of validation by physical model tests, some pioneering work has been carried out to assess and validate the numerical simulations. PTO damping profiles generated offline by the NMPC [64] were applied to a model-scale point absorber with their in-house designed permanent magnetic linear generator (PMLG) as a PTO unit [65]. The improved NMPC was also tested in [60]. Results showed noticeable improvements on enhancing energy-extraction performance and reducing response amplitude ratio (RAO) of the absorber, compared to a simpler resistive control. Sandia National Laboratories compared various control strategies, including resistive control, latching control, linear MPC, etc., on a heaving point absorber [5]. Simulation results showed that linear MPC has strong potential for enhancing wave-energy extraction as it could produce more than twice the amount of the power on an annual basis, compared to the case with the resistive control. Recently, they conducted a wave-tank test to identify a WEC model as the first step of implementing control strategies on the WEC [4]. In the test, the machinery force was generated by a linear actuator acting as the PTO

system.

In this Chapter, a *convex* QP based on the dynamic model of a heaving point absorber will be presented, which then forms a MPC with the machinery force used as the control input and the optimizer. Such a QP can be readily applied to other types of WECs with single degree of freedom, and straightforwardly extended to systems of multi-degree of freedom. The cost function of the QP is set to maximize the extracted power and penalize changes in the control input to relieve slew-rate requirements on the PTO. It will be shown that the convexity of the problem can be guaranteed by adjusting the weight of the penalty term. Constraints on the machinery force and the oscillatory amplitude of the absorber will be added. At each time step, a standard QP solver can be adopted to *efficiently* obtain the (global) optimal solution of such a constrained optimization problem. Performances of the current MPC will be compared with those obtained from using impedance matching and existing MPC strategies in both regular and irregular wave conditions, lending credibility to our formulation. Reactive power required by the current MPC will be discussed. Part of the work has been presented in [77].

3.2 State-space Model of a Point Absorber

For demonstration, we here form the problem for a heaving point-absorber type WEC. In time domain, the equation of motion for a heaving point absorber can be written as

$$m\ddot{\zeta}_3 = f_e(t) + f_r(t) + f_h(t) + f_m(t) \tag{3.1}$$

where m and $\zeta_3(t)$ are mass and heave position of the absorber. Additionally, $f_e(t)$, $f_r(t)$, $f_h(t)$, and $f_m(t)$ are wave-exciting, wave radiation, hydrostatic restoring, and machinery forces, where $f_h(t)$ and $f_r(t)$ have forms of

$$f_h(t) = -K\zeta_3(t) \tag{3.2a}$$

$$f_r(t) = -\mu_{33}(\infty)\ddot{\zeta}_3(t) - \lambda_{33}(\infty)\dot{\zeta}_3(t) - \int_{-\infty}^{t} K_r(t-\tau)\dot{\zeta}_3(\tau)\mathrm{d}\tau \tag{3.2b}$$

where K is the hydrostatic stiffness coefficient, μ_{33} and λ_{33} are added-mass and damping coefficients, and $K_r(t)$ is known as the retardation function. $K_r(t)$ can be obtained by taking the inverse Fourier transform of the damping coefficients as

$$K_r(t) = \frac{2}{\pi}\int_0^{\infty} [\lambda_{33}(\sigma) - \lambda_{33}(\infty)]\cos(\sigma t)\mathrm{d}\sigma \tag{3.3}$$

Substitution of Eqn. (3.2) into Eqn. (3.4) yields

$$\begin{aligned}(m + \mu_{33}(\infty))\ddot{\zeta}_3(t) + (\lambda_{33}(\infty) + \lambda_{vis})\dot{\zeta}_3 + K\zeta_3(t) \\ + \int_{-\infty}^{t} K_r(t-\tau)\dot{\zeta}_3(\tau)\mathrm{d}\tau = f_e(t) + f_m(t)\end{aligned} \tag{3.4}$$

where a corrective linear viscous damping coefficient λ_{vis} obtained from experiments [64] was included to account for fluid viscosity. λ_{33} approaches 0 as $t \to \infty$ in general. The convolution of $K_r(t)$ and $\dot{\zeta}_3(t)$, denoted by y_r, can be approximated by a state-space model:

$$\dot{z}_r(t) = A_r z_r(t) + B_r \dot{\zeta}_3(t) \tag{3.5a}$$
$$y_r = C_r z_r(t) + D_r(t)\dot{\zeta}_3(t) \tag{3.5b}$$

where $z_r \in \mathbb{R}^{n_r}$ with n_r being the number of states in this model.

Thus, the state-space model of the dynamic system Eqn. (3.4) can be expressed as

$$\dot{x} = A_c x + B_c(u + w) \tag{3.6a}$$
$$y = C_c x \tag{3.6b}$$
$$z = C_{zc} x \tag{3.6c}$$

where the state vector $x := [\zeta_3, \dot{\zeta}_3, z_r]^T$, $y := \dot{\zeta}_3$, $z := \zeta_3$, $u := f_m$, and $w := f_e$,

$$\begin{aligned} A_c &= \begin{bmatrix} 0 & 1 & 0 \\ -K/M & -(\lambda_{vis} + D_r)/M & -C_r/M \\ 0 & B_r & A_r \end{bmatrix} \\ B_c &= [0, 1/M, 0_{1\times n_r}]^T \quad C_c = [0, 1, 0_{1\times n_r}] \quad C_{zc} = [1, 0, 0_{1\times n_r}] \end{aligned} \tag{3.7}$$

with $M := m + \mu_{33}(\infty)$.

The state-space model Eqn. (3.7) is discretized using zero-order hold [31], where inputs are assumed to be piecewise constant over the sampling time T_s. As a result, we obtained the discrete-time model:

$$x_{k+1} = Ax_k + B(u_k + w_k) \tag{3.8a}$$
$$y_k = Cx_k \tag{3.8b}$$
$$z_k = C_z x_k \tag{3.8c}$$

where the subscript k indicates the time instant k.

3.3 Model-Predictive Control Formulation

The optimization problem

We assume that at each sampling instant wave profile for a certain future period of time can be estimated by wave prediction algorithms. The goal is to maximize the energy E extracted by the PTO system over a predicted time horizon T_h, where

$$E = \int_0^{T_h} P(t)\mathrm{d}t = \int_0^{T_h} -f_m(t)\dot{\zeta}_3(t)\mathrm{d}t \tag{3.9}$$

Using the discrete-time model Eqn. (3.8), E can be written as $E = T_s \sum_{k=0}^{N-1}(-u_k y_k)$, where N is the number of sampling time instants during the time horizon T_h, i.e. $T_h = NT_s$. Hence, the objective is to find a series of inputs u_k $(k = 0, 1, \ldots, N-1)$ such that

$$\max_{[u_0,u_1,\ldots,u_{N-1}]} E = \min_{[u_0,u_1,\ldots,u_{N-1}]} (-E) = \min_{[u_0,u_1,\ldots,u_{N-1}]} T_s \sum_{k=0}^{N-1} u_k y_k \tag{3.10}$$

which is equivalent to set the cost function to be

$$J_0 = \sum_{k=0}^{N-1} u_k y_k \tag{3.11}$$

and minimize J_0 over the control inputs. For safety and long-term operation, constraints on the heaving motion of the absorber z and the machinery force u need to be included:

$$|z_k| \leq \zeta_{3,\max} \tag{3.12a}$$
$$|u_k| \leq f_{m,\max} \tag{3.12b}$$

where $k = 0, 1, \ldots, N-1$. However, it can be shown that the constrained optimization problem formed by Eqn. (3.11) and Eqn. (3.12) will result in a non-convex QP [38], for which the global optimal solution is not guaranteed. One alternative approach is to use a modified objective function as shown in [14, 31]: $J_{\text{approx}} = \sum_{k=0}^{N-1} u_k y_{k+1}$. Nevertheless, the convexity of the resulted QP cannot be guaranteed, and the one-step time delay in u can cause significant loss of extracted energy in certain cases, as demonstrated in [38].

In this paper, we construct the cost function to be:

$$J = \sum_{k=0}^{N-1} (u_k y_k + r|\Delta u_k|^2) \tag{3.13}$$

where $\Delta u_k = u_k - u_{k-1}$ for $k = 0, 1, 2, \ldots, N-1$. $\Delta u_0 := u_0 - u_{-1}$ where u_{-1} is defined as the control input obtained in the previous time horizon, and $u_{-1} = 0$ initially. In [38], the cost function included a penalty term on the control input, of which the penalty weight was used to convexify the problem. In a similar way, the convexity of the current cost function J in Eqn. (3.13) can be guaranteed: when r is tuned to be larger than a certain value, the Hermitian matrix in the QP will be positive definite. Such a value of r can be determined by checking the minimal eigenvalue of the Hermitian matrix. In addition, the current controller can achieve a smaller slew rate and hence less energy consumption, by having a larger penalty weight r, instead of adding constraints on the slew rate; the latter can induce additional computational costs. Nevertheless, it should be pointed out that a larger weight r on penalizing the slew rate can result in a larger loss in the energy extraction. For cases simulated here, a small r ($r << 1$) is sufficient to guarantee the convexity of the cost function. With the smallest r, the impact of the term on energy extraction is negligible.

Quadratic programming formulation

We will cast the problem into a QP. The following notations will be used:

$$U_0 := [u_0, u_1, \ldots, u_{N-1}]^T \quad W_0 := [w_0, w_1, \ldots, w_{N-1}]^T \tag{3.14}$$

which represent the series of inputs u and w at time instants $k = 0, 1, \ldots, N-1$, where we recall that u and w denote the machinery force and the wave-exciting force respectively. The optimization problem can then be written as

$$\min_{U_0} \quad J = \min_{U_0} \quad \sum_{k=0}^{N-1} (u_k y_k + r|\Delta u_k|^2) \tag{3.15a}$$

$$\text{subj. to} \quad |z_k| \leq \zeta_{3,\max} \quad k = 0, 1, \ldots, N-1 \tag{3.15b}$$

$$|u_k| \leq f_{m,\max} \quad k = 0, 1, \ldots, N-1 \tag{3.15c}$$

where x_k, y_k, z_k, and u_k ($k = 0, 1, \ldots, N-1$) should satisfy the dynamic equation Eqn. (3.8).

To form a QP, we can propagate the state equation Eqn. (3.8a) and use Eqn. (3.8b) to obtain

$$\hat{y}(k+i|k) = CA^i x_k + \sum_{j=0}^{i-1} CA^{i-j-1} B(\hat{u}(k+j|k) + \hat{w}(k+j|k)) \tag{3.16}$$

where $i = 0, 1, 2, \ldots, N-1$, $\hat{y}(k+i|k)$ denotes the state y_{k+i} estimated at time k, and the same meaning holds for $\hat{u}(k+j|k)$ and $\hat{w}(k+j|k)$. If we stack the output state $\hat{y}_{k+i}$ to form a vector, i.e. $Y_0^{N-1} = [\hat{y}(k|k), \hat{y}(k+1|k), \ldots, \hat{y}(k+N-1|k)]^T$, we can express Y_0^{N-1} in a matrix form as:

$$Y_0^{N-1} = S_x x_k + S_u(U_0 + W_0) \tag{3.17}$$

where

$$S_x = \begin{bmatrix} C \\ CA \\ CA^2 \\ \vdots \\ CA^{N-1} \end{bmatrix}, \; S_u = \begin{bmatrix} 0 & & & & \\ CB & 0 & & & \\ CAB & CB & \ddots & & \\ \vdots & \vdots & \ddots & 0 & \\ CA^{N-2}B & CA^{N-3}B & \ldots & CB & 0 \end{bmatrix} \tag{3.18}$$

In a similar form, we can express the vector of states $\hat{z}(k+i|k)$, $i = 0, 1, \ldots, N-1$, denoted by Z_0^{N-1} as

$$Z_0^{N-1} = S_{x,z} x_k + S_{u,z}(U_0 + W_0) \tag{3.19}$$

where we substitute C_z for C in Eqn. (3.18) to obtain $S_{x,z}$ and $S_{u,z}$. In matrix form, the slew input vector $\Delta U := [\Delta u_0, \Delta u_1, \Delta u_2, \ldots, \Delta u_{N-1}]^T$ can be written as

$$\Delta U = T_\Delta U_0 - g_u \tag{3.20}$$

where

$$T_\Delta = \begin{bmatrix} 1 & & & & \\ -1 & 1 & & & \\ & -1 & \ddots & & \\ & & \ddots & 1 & \\ & & & -1 & 1 \end{bmatrix}_{N\times N}, \; g_u = \begin{bmatrix} u_{-1} \\ 0 \\ \vdots \\ \\ 0 \end{bmatrix}_{N\times 1} \tag{3.21}$$

with u_{-1} being the control input applied to the system currently and $u_{-1} = 0$ initially. In the MPC, $u_{-1}$is the input obtained from the previous receding-horizon computation.

The cost function J in Eqn. (3.15a) can then be written in a compact form:

$$J = U_0^T Y_0^{N-1} + (T_\Delta U_0 - g_u)^T R (T_\Delta U_0 - g_u) \tag{3.22}$$

with $R = r \times \mathcal{I}_{N-1}$. Substituting Eqn. (3.17) and Eqn. (3.20) in Eqn. (3.22) and neglecting the constant term, we can write J in a quadratic form

$$J = \frac{1}{2} U_0^T H U_0 + f^T U_0 \tag{3.23}$$

where

$$H := S_u + S_u^T + 2S_R \tag{3.24a}$$
$$f := S_x x_k + S_u W_0 - 2S_g \tag{3.24b}$$

with $S_R := (T_\Delta)^T R T_\Delta$ and $S_g = (T_\Delta)^T R g_u$.

It can be seen that without penalizing the slew rate, the cost function will have a corresponding Hessian matrix $H_0 = S_u + S_u^T$ where S_u in Eqn. (3.18) has zero diagonal elements, which leads to an indefinite H_0 and hence a non-convex problem. The addition of S_R, aside from controlling the slew rate, adds positive values on the diagonal of the matrix H Eqn. (3.24a). By tuning r such that the minimal eigenvalue of H is larger than 0, we can have a positive definite H and hence a convex J.

The constraints Eqn. (3.15b) and Eqn. (3.15c) can be written in a component-wise inequality

$$A_u U_0 \leq b_u \tag{3.25}$$

where, using Eqn. (3.19)

$$A_u = \begin{bmatrix} I \\ -I \\ S_{u,z} \\ -S_{u,z} \end{bmatrix}, \quad b_u = \begin{bmatrix} U_{\max} \\ U_{\max} \\ Z_{\max} - S_{x,z} x_k - S_{u,z} W_0 \\ Z_{\max} + S_{x,z} x_k + S_{u,z} W_0 \end{bmatrix} \tag{3.26}$$

with $U_{\max} = f_{m,\max} \times \underbrace{[1, \ldots, 1]^T}_{\text{N}}$ and $Z_{\max} = \zeta_{3,\max} \times \underbrace{[1, \ldots, 1]^T}_{\text{N}}$.

In summary, the QP with the cost function Eqn. (3.23) subject to the constraints Eqn. (3.25) can be written as

$$\min_{U_0} \quad J = \frac{1}{2} U_0^T H U_0 + f^T U_0 \tag{3.27a}$$

$$\text{subject to} \quad A_u U_0 \leq b_u \tag{3.27b}$$

MPC scheme

The MPC scheme is as follows: at time instant k, with the knowledge of estimated states and the predicted wave profile, the QP in Eqn. (3.27) is solved, and a sequence of optimal control inputs $U_0^* = \text{argmin}(J)$ is generated; the first control input in the sequence is applied; the system dynamics is then moved forward to the next time step, and the optimization procedure is repeated. In this paper, we will assume the knowledge of a certain future period of the incoming waves.

3.4 Simulation Results in Regular Waves

We applied the MPC formulated in Section 3.3 to point-absorber models. Results are shown for both unconstrained and constrained cases. Comparisons will be made to a nonlinear MPC which has been implemented off-line for wave-tank tests. The quadprog solver in MATLAB was used to solve the QP. All simulations were performed on a Thinkpad W550s, 2.60 GHz.

Under linear theory, the wave-exciting force induced by a regular wave of frequency σ can be obtained by

$$f_e(t) = A_0 \Re\{|X_3(\sigma)|e^{i\delta}\} \sin(\sigma t) \tag{3.28}$$

where A_0 is the amplitude of an incoming wave, and X_3 is the complex amplitude of the wave-exciting force corresponding to a unit-amplitude wave of frequency σ. $X_3 = |X_3|e^{i\delta}$ with δ being the phase of the force relative to wave elevation, which can be obtained from frequency-domain hydrodynamic analysis of an absorber [68]. In the discrete-time model, the wave-exciting force is obtained by

$$w_k = A_0 \Re\{|X_3(\sigma)|e^{i\delta}\} \sin(\sigma k T_s) \tag{3.29}$$

where $k = 0, 1, \ldots, N-1$.

Unconstrained and constrained MPC

We first apply the MPC with no constraints on a cylindrical point absorber of radius 5 m and draft 8 m floating in deep water, The same model was used in [14]. The hydrodynamic coefficients of the cylinder and wave-exciting forces are obtained by an in-house code using

the method in [71]. No viscosity is considered, i.e. $\lambda_{vis} = 0$. A fifth order state-space model for the radiation subsystem is used, of which the impulse response denoted by $K_{r,SS}(t)$, was shown in Fig. 3.1 and compared to the $K_r(t)$ obtained by the inverse Fourier transform in Eqn. (3.3). Also presented in Fig. 3.1 is the damping coefficient λ_{33} obtained in the frequency domain. For simulations in this section, the sampling time T_s is set to 0.05 s, and the weight $r = 10^{-5}$ to guarantee the convexity and also reduce the impact of the penalty term on the energy absorption to a minimum.

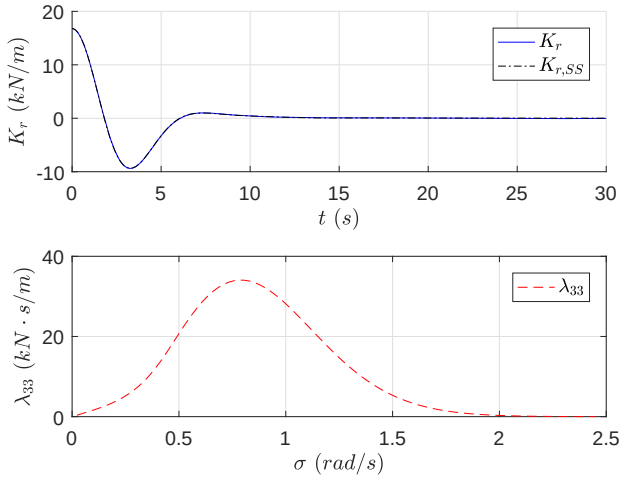

Figure 3.1: Impulse response of the radiation subsystem and damping coefficients with respect to wave frequency.

Fig. 3.2 shows a comparison of the averaged absorbed power $\overline{P}_a$ obtained by the current MPC, the MPC constructed by Cretel et. al [14], and the impedance matching method [24]. Results are obtained for prediction horizon T_h being T_w and $2T_w$ where $T_w = 2\pi/\sigma$ is the wave period. $\overline{P}_a$ is computed by

$$\begin{aligned}\overline{P}_a &= \frac{1}{T}\int_{T_0}^{T_0+T} [P_e(t) - P_r(t) - P_l(t)]\,\mathrm{d}t \\ &= \frac{1}{T}\int_{T_0}^{T_0+T} [f_e(t) - f_r(t)]\,\dot{\zeta}_3(t)\mathrm{d}t \end{aligned} \tag{3.30a}$$

where P_e and P_r are excitation power and radiation power respectively, and P_l is the lost power due to friction, etc., and assumed to be 0. T is chosen to be $5T_w$, and the starting time T_0 can be any point after the system reaches the steady state. As $P_{a,\mathrm{opt}} = \frac{1}{2}\lambda_{33}|\dot{\zeta}_{3,\mathrm{opt}}|^2$ based on the impedance matching theory [24], $\overline{P}_a$ indicates the optimal amplitude of the heaving velocity of the absorber.

Good agreements are obtained for relatively high frequencies. In low frequencies, the less power absorbed by the current MPC can be explained by the additional penalty term on the slew rate of the control input. It can be shown that an extremely large oscillation amplitude

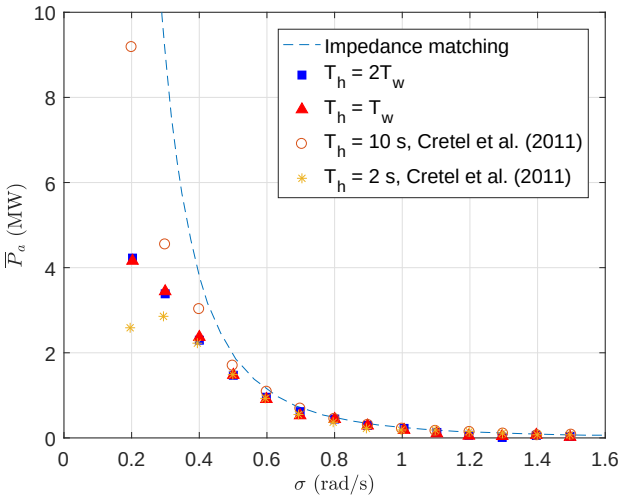

Figure 3.2: Averaged absorbed power by an unconstrained point absorber plotted over the angular frequency.

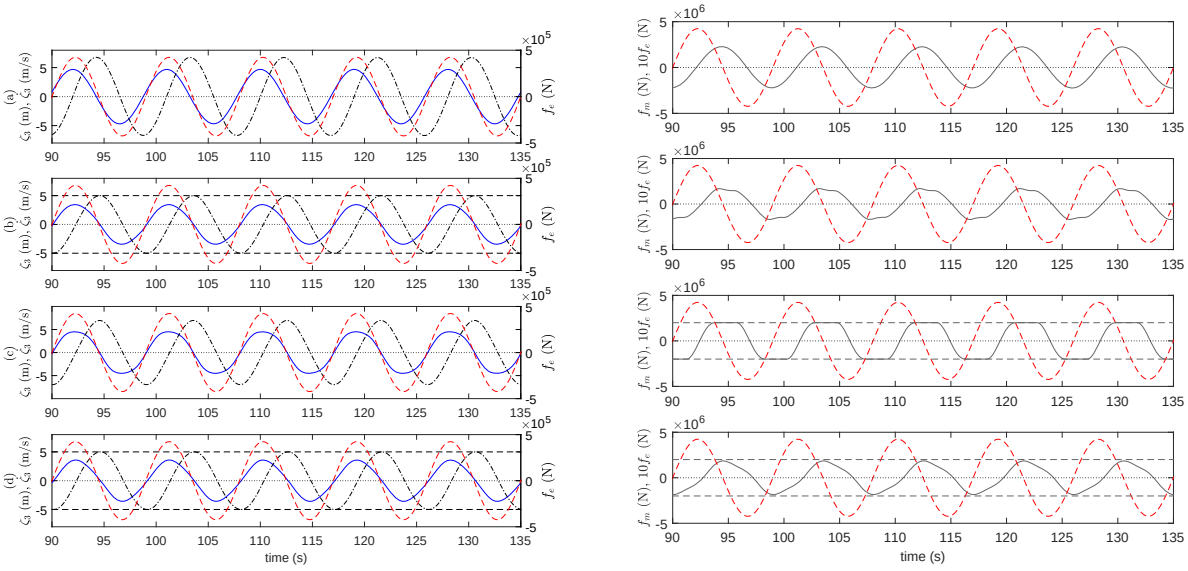

Figure 3.3: Time histories of $\dot{\zeta}_3$ (blue), ζ_3 (black, dash-dotted), and f_e (red, dashed) on the left, and f_m (grey, dash-dotted) and f_e on the right, for the absorber in regular waves with amplitude of 1 m and period of 9 s. Constraints, if any, are shown by dashed lines, values of which are set to $\zeta_{3,\max} = 5$m, and $f_{m,\max} = 2$ MN. Simulated cases are (a) no constraints, (b) constraints on the heaving motion, (c) constraints on the machinery force, and (d) constraints on both of the heaving motion and the machinery force.

of the absorber is required to achieve the optimal absorbed power in the low-frequency range. For example, at $\sigma = 0.4$ rad/s, the RAO of the absorber needs to be approximately 65. As a result, large control inputs and hence large slew rates are required given a fixed T_s, which is, however, penalized in the cost function. In terms of implementations, the cases of large RAO are impractical because of machinery restrictions. Hence, the optimal absorbed power in the unconstrained condition can be hardly achieved in real applications. It is interesting to notice that results from Cretel et al. [14] indicates a longer prediction horizon can yield a better performance for capturing energy, though the authors also pointed out such an observation needs to be treated with caution. It is shown by current results that this observation is not always the case. The averaged absorbed power is approximately the same for T_h being one wave period and two wave periods. This may be explained by the fact that the incoming waves for these cases are regular and the interval T for computing $\overline{P}_a$ is a multiple of T_w. For demonstrative simulations presented in this section, $T_h = T_w$ was used to save computational time.

If a larger penalty weight r were used in the MPC, there would be less absorbed power, especially at low wave frequencies; nevertheless, the trend of $\overline{P}_a$ with respect to σ as shown in Fig. 3.2 would be followed. This can be explained by the fact that at low frequencies, with no constraints added, a large RAO is required for the absorber to achieve the optimal condition for power extraction, which would require large control inputs and hence large slew rates of the inputs given a fixed time interval. Increasing the penalty weight means placing more restrictions on the control input, and hence the optimal condition can no longer be satisfied at certain frequencies. This leads to reduced extracted energy. More discussion on effects of the penalty weight r will be presented in Section 3.4.

Fig. 3.3(a) shows the heaving motion ζ_3 and velocity $\dot{\zeta}_3$ of the absorber in the wave of amplitude 1 m and period 9 s, as well as the wave-exciting force f_e and the control input, machinery force f_m, acting on the absorber. It can be seen that the optimal phase condition was achieved: the velocity of the absorber is in phase with the wave-exciting force. However, the heaving amplitude under the optimal condition is too large for operations. We hence applied constraints on the heaving motion or the machinery force, or both, to investigate effects of constraints on the dynamics and power extraction of the WEC system. Results are shown in Fig. 3.3(b)-(d). It can be seen that all the constraints were satisfied.

It is observed that for all of the constrained cases, the phase of the velocity is driven to match the phase of the wave-exciting force by the control input. Because of the penalty on the change in f_m, the slew rate of f_m is relatively small, which is favorable for implementations. Restricting only the machinery force yields a bang-bang type of control with a milder changing slope. For the four cases, the absorbed power is respectively (a) $\overline{P_a} = 6.17 \times 10^5$W, (b) $\overline{P_a} = 5.36 \times 10^5$W, (c) $\overline{P_a} = 6.12 \times 10^5$W, and (d) $\overline{P_a} = 5.38 \times 10^5$W. It is expected that adding constraints decreases the absorbed energy; nevertheless, more than 75% of maximal absorbed energy, obtained by the impedance matching theory for the unconstrained case, is achieved for the most restrictive case (d). In terms of computational time, obtaining solutions for one wave period takes twice as long on average for the case with both constraints added.

Comparisons with a nonlinear MPC

A nonlinear MPC (NMPC) with a non-negative damping coefficient as the control input was developed in [64] and implemented off-line in a wave-tank test [65]. This MPC was then applied to a co-axial cylinder WEC [62] with the bottom shape modified such that the viscous effect was significantly reduced. By using the non-negative dapming coefficient as the optimizer in the MPC, no reactive power will be generated in the process. However, solving the resulted nonlinear and nonconvex problem can be computationally demanding. As a comparison, the convex formulation for the optimization problem of the current MPC can enhance the computational efficiency; however, it is required that the PTO system of the WEC act as a motor since it is the machinery force that was used as the control input, which generates reactive power. We here compare the current MPC to the NMPC regarding the energy-capture capability, the required reactive power, and the computational time.

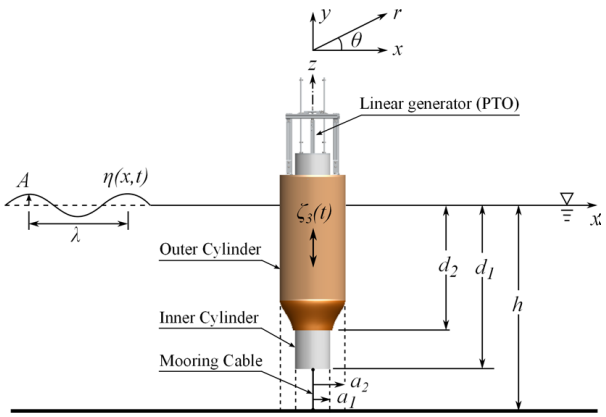

Figure 3.4: Schematic of the dual coaxial-cylinder system in [62].

The WEC model was shown in Fig. 3.4 from [62], of which the (outer) cylinder has radius of 0.254m and draft of 0.635m with water depth being 1.5m. The total mass, including the added mass, of the WEC device is 103.63 kg, and the hydrostatic stiffness coefficient is 1285.6 N/m. Additionally, the linear-viscous damping factor $\lambda_{vis} = 1.7\lambda_{33} = 9.68\text{N} \cdot \text{s/m}$ obtained from experiments [62] is adopted. A 4-th order state-space model was used to approximate the radiation subsystem, for which the radiation damping coefficients were obtained by an in-house code [11]. The case "Active, $\eta_{el} = 1$" in [62] is simulated here, for which the power-conversion efficiency is not taken into account. In order to make the comparison, the oscillating amplitude of the absorber for current cases is constrained to be no larger than the maximal RAO obtained by the NMPC [62]: $\zeta_{3,\max} = 5.1A_0$. In addition, the maximal machinery force is computed by $f_{m,\max} = B_{g,\max}\zeta_{3,\max}\sigma$, where σ is the angular frequency of incident waves and the maximal damping $B_{g,\max} = 150$ N·s/m according to [62]. The waves have amplitude of $A_0 = 0.0254$m. The simulations were carried out for $20T_w$ with 80 time steps per wave period. The sampling time was chosen such that the restrictive effect of the cost function on the slew rate is small at the minimal value of r.

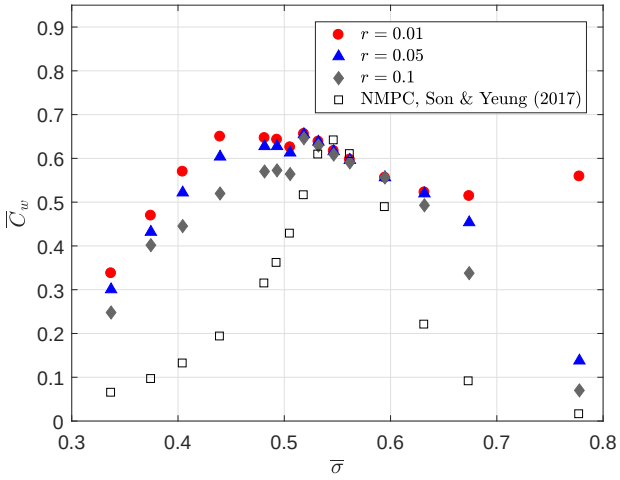

Figure 3.5: Comparisons of capture width by current method with those using NMPC.

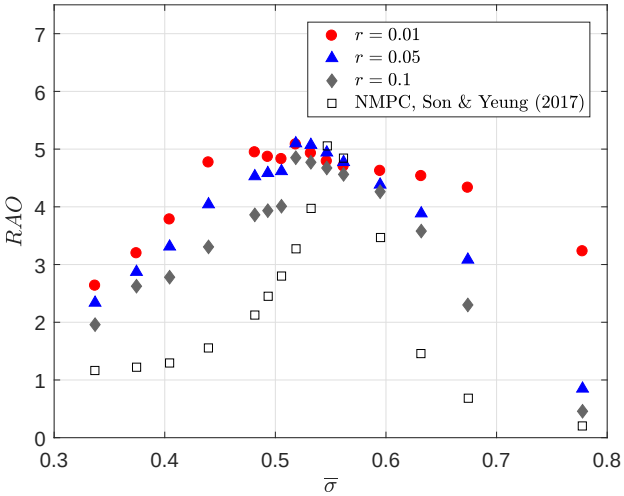

Figure 3.6: Comparisons of RAO by current method with those using NMPC.

Simulations were conducted for the penalty weight r being 0.01, 0.05, and 0.1 respectively with 0.01 being the minimum to guarantee convexity, so that the effect of r on performances of WEC and PTO system can be investigated. Results are shown in Fig. 3.5 and Fig. 3.6 and compared with those obtained by NMPC, where the non-dimensional capture width $\overline{C}_w$, the RAO of the absorber, and the non-dimensional frequency $\overline{\sigma}$ are defined by

$$\overline{C}_w = \frac{C_w}{2a} = \frac{1}{2a}\frac{\overline{P_u(t)}}{P_{\text{wave}}}, \quad RAO = \frac{|\zeta_3|}{A_0}, \quad \overline{\sigma} = \sigma\sqrt{\frac{a}{g}} \tag{3.31}$$

with a being the radius of the cylinder, g the gravitational acceleration, P_{wave} the wave power, and $\overline{P_u(t)} = \frac{1}{T}\int_{T_0}^{T_0+T} f_m(t)\dot{\zeta}_3(t)\mathrm{d}t$ the time averaged useful power, indicating the energy extracted by the PTO unit. For a regular wave of amplitude A_0 and group velocity v_g, the wave power can be obtained by $P_{\text{wave}} = 1/2\rho g A_0^2 v_g$, where $v_g = \frac{1}{2}\frac{g}{\sigma}$ in deep water. It should be noticed that since the input $f_m(t)$ is not sinusoidal in general, the energy stored in the WEC system is not 0, and hence the useful power $\overline{P_u(t)}$ is not the same as the absorbed power $\overline{P_a(t)}$.

It is observed that the current MPC broadened capture-width bandwidth for all three values of r. Near the resonance frequency $\overline{\sigma}_{\text{res}} = 0.5668$, the RAO of the absorber reaches its maximal value, and $\overline{C}_w$ stays around 0.63, close to the maximum obtained by the NMPC. The larger r, indicating more penalty on the changing rate of the control input, leads to a smaller RAO of the absorber, but also a loss of the useful power. At frequencies farther away from the resonance, the current MPC was able to extract more useful power than the NMPC. However, it should also be pointed out that the current MPC requires consuming power as a motor in order to achieve the optimal conditions, while the NMPC does not have such a requirement.

Fig. 3.7 presents the ratio of the power flowing from the PTO unit to the absorber (reactive power $\overline{P}_{react}$) to the power flowing from the absorber to the PTO unit (so-called "active power" $\overline{P}_{act}$) at various frequencies. The useful power is the net power of the two, i.e. $\overline{P}_u = \overline{P}_{act} - \overline{P}_{react}$. No reactive power is required for the NMPC, which was plotted for comparison. It can be seen that by using the current MPC, more than 50% of the "active power" turns to useful power for most of the cases. The closer the frequency is to the resonance frequency, the less the reactive power is. At resonance, more than 95% of the "active power" serves as the useful power, with the rest consumed to accomodate the constraints and the penalty on the slew rate of the control input. At a higher frequency, much more reactive power is required to drive the absorber to match the phase of the incoming waves, where more than 70% of the "active power" may be needed to achieve the most power extraction with $r = 0.01$. With the increase in r, the reactive power ratio is noticeably reduced, especially at frequencies far away from the resonance. As the PTO conversion efficiency is never perfect, tuning r to achieve a balance between the consumed power and extracted power can provide a more practical solution to the problem.

To evaluate the enhancement in computational efficiency by the convex formulation of the current MPC, we compare the computational time used by the current MPC and the

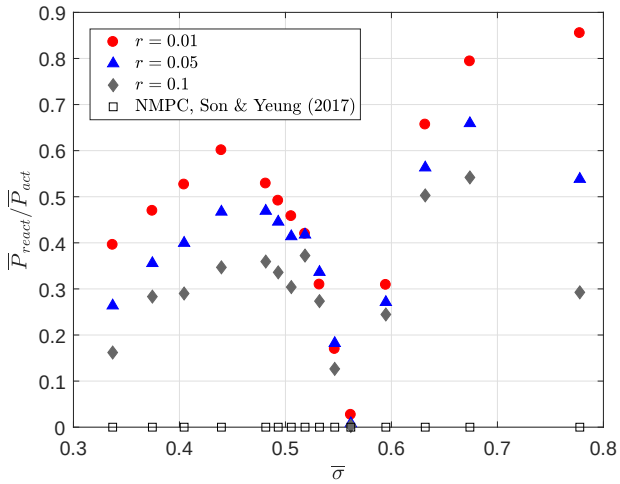

Figure 3.7: The ratio of the reactive power to the power flowing from the absorber to the PTO unit (so-called "active power").

NMPC in Fig. 3.8. The "tic" and "toc" functions in MATLAB were adopted to record the time used for computation. The nonlinear programming (NP) for the NMPC was formulated according to [62]. The same solver, the Ipopt [66] solver, was adopted to solve the NP with the same simulation settings as in [62], including the time horizon, the time interval, etc. We here used the Multi-Parametric Toolbox 3.0 [33] and the OPTI Toolbox [15] to run the Ipopt solver in MATLAB. As shown, the ratio of the computational time per wave period to the wave period obtained by the current MPC was approximately 2 orders smaller than the one obtained by the NMPC. Further, the computational time for generating control law for one wave period is approximately in the same order of the wave period. With code optimization and the scaling ratio between the prototype and the model test taken into account, the current MPC has great potential for real-time applications.

3.5 Simulation Results in Irregular Waves

The proposed MPC was then applied to study the performance of a WEC in irregular wave conditions. A modified Pierson-Moskowitz spectrum for fully developed seas was used to

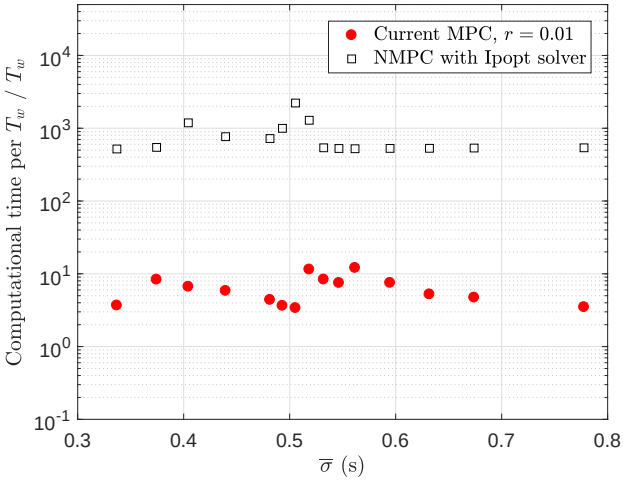

Figure 3.8: Computational time for simulated cases of regular waves.

construct the irregular wave profile:

$$S(\sigma) = H_s^2 T_1 \frac{0.11}{2\pi} \left(\frac{\sigma T_1}{2\pi}\right)^{-5} \exp\left[-0.44\left(\frac{\sigma T_1}{2\pi}\right)^{-4}\right] \tag{3.32a}$$

$$T_1 = 0.7713 T_p \tag{3.32b}$$

$$A(\sigma_j) = \sqrt{2S(\sigma_j)\Delta\sigma} \tag{3.32c}$$

$$\eta(t) = \sum_{j=1}^{N} A(\sigma_j)\sin(\sigma_j t + \varepsilon_j) \tag{3.32d}$$

$$f_e(t) = \sum_{j=1}^{N} |X_3(\sigma_j)| A(\sigma_j)\sin(\sigma_j t + \delta_j + \varepsilon_j) \tag{3.32e}$$

where H_s, T_p, A_j, and δ_j are the significant wave height, peak period, wave amplitude, and phase angle of the wave-exciting force the j^{th}-component, respectively, and ε_j is the random phase angle of the the wave components. The random phase angles are uniformly distributed between 0 and 2π and constant with time. The range of angular frequencies used in the construction of Eqn. (3.32) was between 0.1 rad/s and 8.75 rad/s spaced at 0.05 rad/s. The simulation runs for $H_s = 7.62$ cm (3.0 in) and varying T_p, carried out for 1000 peak wave periods with 40 time steps per peak period and $T_h = 2T_p$. The RAO is constrained to be half of the significant wave height, i.e. $\zeta_{3,\max} = H_s/2$, which was the maximal RAO obtained by the NMPC. The maximal machinery force is computed in the same way as in 3.4 with $\sigma = 2\pi/T_p$, and the penalty weight r was 0.01, 0.05, and 0.1 respectively. Results of the time-averaged useful power at different T_p and the ratio of the reactive power to the "active" power are shown in Fig. 3.9 and Fig. 3.10. When the minimal r was used, more than 25% increase in the useful power was achieved compared to the results

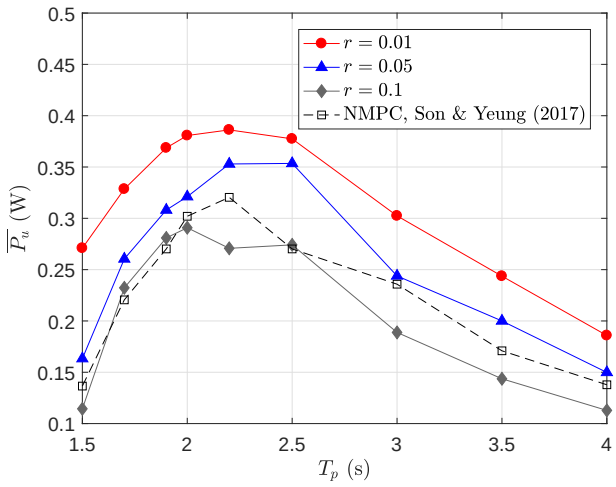

Figure 3.9: Time-averaged useful power in irregular waves.

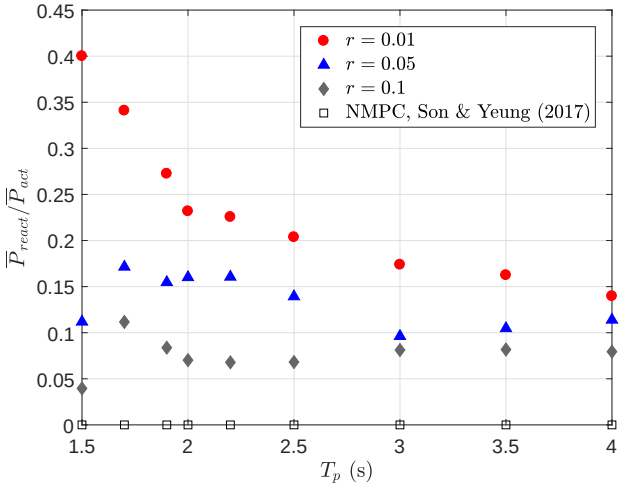

Figure 3.10: The ratio of reactive power to "active power" in irregular waves.

of NMPC. As the resonance frequency of the WEC system corresponds to $T_{\text{res}} = 1.784$s, higher useful power was obtained when T_p is closer to T_{res}. It can also be observed that in general less reactive power ratio was required in irregular waves than in regular waves. This is expected as the composition of waves of different frequencies reduces the efforts required from the PTO unit to drive the absorber in phase with waves, compared to the case where the frequency of the monochronic wave is substantially different from the resonance frequency. This fact is favorable for applications in real-sea environments. In addition, r also serves as a tuning parameter to adjust the reactive power ratio. The computational time was shown in Fig. 3.11. For all simulated cases, the ratio of the computational time per peak wave period to the peak wave period is not larger than 1, by using just a 2.60GHz Thinkpad W550s, and approximately 2 orders smaller than that of the NMPC. Fig. 3.12 shows the time histories

for the velocity and position of the absorber, the wave-exciting force, and the machinery force at $T_p = 2.2$s. It can be seen that the phase of the velocity is driven to match the phase of the exciting force and mild slew rates are attained for the control input f_m.

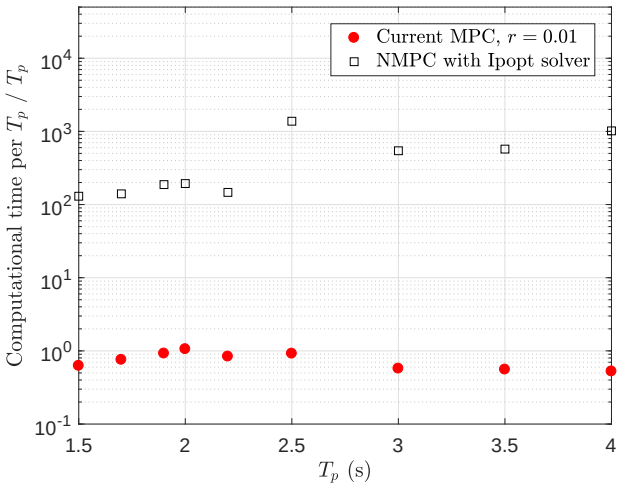

Figure 3.11: Computational time for simulated cases of irregular waves.

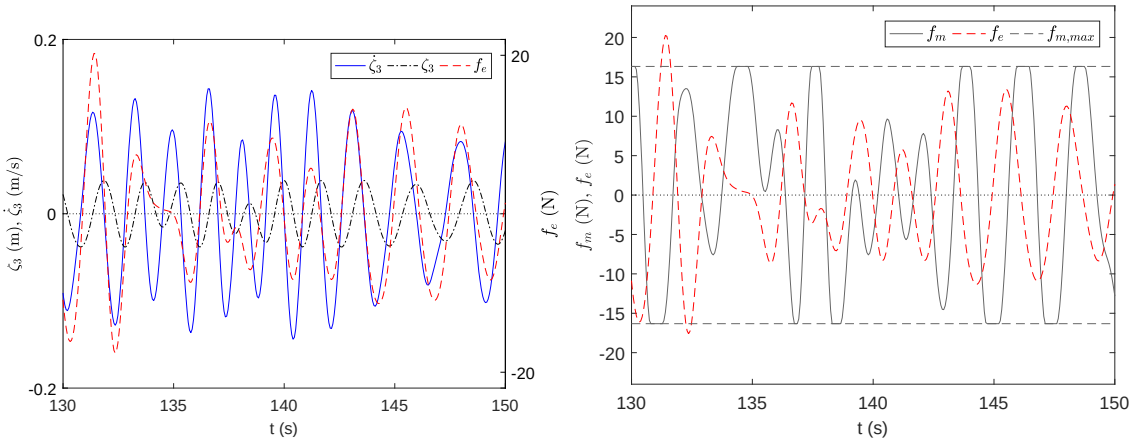

Figure 3.12: Time histories of $\dot{\zeta}_3$, ζ_3, and f_e on the left, and f_m and f_e on the right, for the absorber in irregular waves of $T_p = 2.2$ s.

3.6 Summary remarks

In this Chapter, an MPC formulation was proposed to generate the optimal control law for maximizing the energy extraction of a WEC under constraints. The constrained optimization problem was formed as a Quadratic Programming (QP). A newly added penalty term on

the slew rate of the PTO force was used to guarantee the convexity of the formed QP, which ensures the computational efficiency of the MPC.

The MPC was tested on a single heaving point absorber. Comparisions between the unconstrained MPC and the impedance matching theory showed that good agreements were obtained in the high-frequency range. Differences at lower frequencies were explained by the fact that the added penalty term prevented large changes in the PTO force, i.e. the control input, which are required for achieving the maximal absorbed power, from happening. Constraints were added to the RAO of the absorber and the machinery force (f_m). More than 75% of the optimal power obtained for the unconstrained case, was achieved by the current MPC when both constraints on RAO and the PTO force were considered. Comparisons were also made between the current MPC and a nonlinear MPC using the variable PTO damping as the control input. Results showed that the current MPC is able to broaden the bandwidth of the capture-width, at the cost of recurring reactive power. In irregular wave, becaused of the spread of sea states, the amount of required reactive power was in general reduced compared to simulation cases in regular waves, which makes it favorable for implementations in a real-sea environment.

In terms of the computation efficiency, the amount of the computational time for obtaining the control law for one wave period cost by the current MPC was in the same order of the wave period, and 2 orders smaller than the time cost by the NMPC. With code optimization and the scaling ratio between the prototype and the model test taken into account, the current MPC has great potential for real-time applications. Highlights of this research is reported in [77].

Chapter 4

MPC Control of a WEC Array

4.1 Overview

Because of the wave interference effects happening among the WEC array, the optimal power generated by the array, especially with physical constraints of the mechanical system considered, has raised lots of research interests since 1980s. The maximal power generated by a point-absorber array, with no constraint added on the devices, has been obtained by frequency-domain analysis as derived independently by Evans [20] and Falnes [23], where the control strategy used is known as the complex-conjugate control or impedance-matching control. Wave-interaction effects were taken into account in the hydrodynamic properties of the array, including damping coefficients and wave-exciting forces for devices in the array. Those coefficients are commonly obtained by boundary-element solvers, for example, WAMIT and Nemoh, which can take the full wave-interaction effect into account but can also be computationally extensive. This approach of estimating the maximal power has been widely applied for evaluating and comparing energy-absorption capabilities of different WEC arrays (e.g. [25], [45], [69], etc.). However, in addition to the inherent difficulties in handling motion and machinery constraints, the complex-conjugate control also has difficulties in dealing with the nonzero off-diagonal elements in the radiation-resistance matrix, which represents the resistance caused by radiating waves from one device on the others. In some studies of optimal configurations for a WEC array [1, 12], resistive control was applied instead, as a sub-optimal solution, where the damping coefficients of the power take-off (PTO) units on individual devices show up as tuning parameters for achieving optimal power generation of the entire array.

As described in Chapter 3, recent developments of wave-energy technology has revealed the need to controlling a WEC array with physical and machinery constraints. Model-predictive control (MPC) is attracting more and more attention because of its capability of handling hard constraints and generating optimal control inputs in real time given future predictions of wave conditions [22]. While studies showed that operating the devices in a coordinated manner can improve the array performance compared to independent control

actions on isolated devices [6, 39], MPC can be computationally demanding, if not impractical, when it comes to an array of WEC devices. Li and Belmont applied the centralized MPC with a convex formulation as developed in [38] to an array of two cylinders in irregular sea waves [39]; a distributed MPC was also presented and applied to a seven-cylinder array. This is a novel approach in the area of controlling a WEC array by MPC. However, wave-interaction effects were underestimated because the point-absorber approximation [24] adopted in this study assumes that only radiating waves from the motion of the devices need to be considered and all scattering waves caused by the presence of neighboring devices can be neglected. Nevertheless, the convex formulation was shown as a desired and necessary property for applying the MPC to a WEC arrray.

The MPC formed in Chapter 3 has the convexity of the optimization problem guaranteed by adjusting the penalty weight on the slew rate of the control input, which eliminates the necessity of penalizing the power consumption and having negatively impacts on the power absorption. Additionally, the method developed in Chap. 2 was used for fast computation of the wave-interaction effects among a WEC array. Because of the high computational efficiency, the hydrodynamic modeling in Chap. 2 is particularly attractive for evaluating relatively large arrays in real-sea waves.

In this Chapter, the MPC developed in the Chapter 3 for a single WEC is applied to an array of WECs, in both regular and irregular waves, further, in conjunction with full interaction hydrodynamics by the fast computation method developed in Chap. 2. To investigate the optimal operating condition for an array of WECs in real-sea states and with constraints considered, we will form a central controller for a WEC array subject to constraints applied on the control force and the oscillation amplitude of each device. We will also adopt the PA approximation to consider the wave-interaction effects in the plant model of the controller. The optimal control input obtained for the PA model will be fed into the "exact" dynamic model with the exact wave forces taken into account. By comparing the results, we will quantify the effect of the model inaccuracy induced by the PA approximation on the power generation estimation. Also studied is the difference in energy absorption of individual devices in the group. Since the MPC requires that a wave-prediction unit be simultaneously incorporated to predict the dynamics of the system, we will assume in this work that there exists a wave predictor, e.g. [28] and [48], which can estimate the wave elevation at a designated location for a certain future time window with a good degree of confidence.

4.2 Modeling an Array of Point Absorbers

A farm of wave-energy devices can act independently in a seaway or in a coordinated manner with possible communication among themselves. Ideally, we assume the incident wave field is known and if a global controller is intelligent enough, the system may act cohesively to achieve the best global performance subject to some hardware or physical constraints. It is not difficult to envision each device may have its own controller communicating with a

global controller. In what follows, we set up a framework so that the master controller would direct the members to act in "the best interest of the community."

The Equations of Motion

Without loss of generality, we consider the bodies in the array to be different in size. As initially described in Chapter 3, the equations of motion of a heaving point absorber, the j-th in an array of N bodies, can be written in the time domain as

$$m^j \ddot{\zeta}_3^j = f_e^j(t) + f_r^j(t) + f_h^j(t) + f_m^j(t) \tag{4.1}$$

where m^j and $\zeta_3^j(t)$ are mass and heave displacement of the absorber. Here, $f_e^j(t)$, $f_r^j(t)$, $f_h^j(t)$, and $f_m^j(t)$ are wave-exciting ("e"), wave-radiation ("r"), hydrostatic restoring ("h"), and applied machinery forces ("m") on the cylinder j, respectively. Here, $f_h^j(t)$ and $f_r^j(t)$ take the forms:

$$f_h^j(t) = -K_j \zeta_3^j(t) \tag{4.2a}$$

$$f_r^j(t) = -\mu_{33}^{jj}(\infty)\ddot{\zeta}_3^{jj}(t) - \sum_{l=1}^{N} \int_{-\infty}^{t} K_r^{jl}(t-\tau)\dot{\zeta}_3^l(\tau)\mathrm{d}\tau \tag{4.2b}$$

with K_j being the hydrostatic stiffness coefficient, and μ_{33}^{jj} the added-mass coefficients at infinite frequency. The convolution integrals represent the fluid memory effects where $K_r^{jl}(t)$ $(j, l = 1, 2, \ldots, N)$ is the impulse response function with the superscripts indicating the effect of cylinder l on cylinder j. The K_r^{jl} can be obtained by the inverse Fourier transform of the damping coefficients in frequency domain (see [68]) as

$$K_r^{jl}(t) = \frac{2}{\pi} \int_0^{\infty} [\lambda_{33}^{jl}(\sigma) - \lambda_{33}^{jl}(\infty)] \cos(\sigma t)\mathrm{d}\sigma \tag{4.3}$$

Note that wave damping at infinite frequency vanishes, i.e. $\lambda_{33}^{jl}(\infty) = 0$. For $l \neq j$, the λ_{33}^{jl} represents the effect of the motion of the cylinder k on the wave forces of cylinder j. The wave-exciting force can be expressed as:

$$f_e^j(t) = \int_{-\infty}^{\infty} K_e^j(t-\tau)\eta(0,t)\mathrm{d}\tau \ , \tag{4.4}$$

for a given $\eta(0,t)$, which denotes the incident-wave elevation at the vertical axis of the body. The impulse response function $K_e^j(t)$ of j-th cylinder can be evaluated by the inverse Fourier transform of the complex amplitude X_3^j of the wave-exciting force induced by unit-amplitude waves of frequency σ as:

$$K_e^j(t) = \frac{1}{2\pi} \Re \left\{ \int_{-\infty}^{\infty} X_3^j(\sigma) e^{i\sigma t} \mathrm{d}\sigma \right\} \tag{4.5}$$

As full knowledge of the incoming waves is presumed in this paper, we will compute the wave forces based on the frequency-domain analysis under linear wave theory, see e.g. [64].

Substituting Eqn. (4.2) into Eqn. (4.1), we obtain

$$\begin{aligned}(m_j + \mu^j_{33}(\infty))\ddot{\zeta}^j_3(t) + \lambda_{vis}\dot{\zeta}^j_3 + K_j\zeta^j_3(t) \\ + \sum_{l=1}^{N}\int_{-\infty}^{t} K^{jl}_r(t-\tau)\dot{\zeta}^l_3(\tau)\mathrm{d}\tau = f^j_e(t) + f^j_m(t)\end{aligned} \tag{4.6}$$

where a corrective linear viscous damping coefficient λ_{vis}, obtained from experiments [64], is included to account for viscosity-based dissipation. Here, K^{jl}_r and f^j_e contain the effects of interacting waves; the corresponding coefficients λ^{jk}_{33} and X^j_3 will be obtained by solving the radiation problem for the array and applying the new Haskind relation by the method described in Chapter 3.

State-Space Model

To form a state-space (SS) model for the controller based on the dynamics presented in Eqn. (4.6), we denote the convolution of K^{jl}_r and $\dot{\zeta}_3(t)$ by y^{jl}_r, and approximate it using the following linear sub-system: u

$$\dot{\boldsymbol{z}}^{jl}_r(t) = A^{jl}_r \boldsymbol{z}^{jl}_r(t) + B^{jl}_r\dot{\zeta}^l_3(t) \tag{4.7a}$$

$$y^{jl}_r = C^{jl}_r \boldsymbol{z}^{jl}_r(t) + D^{jl}_r(t)\dot{\zeta}^l_3(t) \tag{4.7b}$$

where $z^{jl}_r \in \mathbb{R}^{n^{jl}_r}$ with n^{jl}_r being the number of states in this model. Since $\lambda^{jl}_{33} = \lambda^{lj}_{33}$ which implies $K^{jl}_r = K^{lj}_r$ per Eqn. (4.3), the two can be modeled by the same sub-system, i.e. $A^{jl}_r = A^{lj}_r$, $B^{jl}_r = B^{lj}_r$, $C^{jl}_r = C^{lj}_r$, and $D^{jl}_r = D^{lj}_r$. A reduced-order model obtained by MATLAB function *balmr* was used to reduce the number of states and in the meantime capture the characteristics of the impulse responses.

Following the notation in [39] and using Eqn. (4.7), we can write the equation of motion for the j-th cylinder as:

$$\dot{\boldsymbol{x}}^j = A_j\boldsymbol{x}^j + \sum_{l=1,\, l\neq j}^{N} F_{jl}\boldsymbol{x}^l + B_j(u^j + w^j) \tag{4.8a}$$

$$y^j = C_j\boldsymbol{x}^j \tag{4.8b}$$

$$z^j = C_{z,j}\boldsymbol{x}^j \tag{4.8c}$$

where $y := \dot{\zeta}_3^j$, $z := \zeta_3^j$, $u^j := f_m^j$, $w^j := f_e^j$, and

$$A_j = \left[\begin{array}{ccc|ccccccc} 0 & 1 & 0 & 0 & \dots & 0 & 0 & \dots & 0 \\ -\frac{K_j}{M_j} & -\frac{(\lambda_{vis}+D_r^{jj})}{M_j} & -\frac{C_r^{jj}}{M_j} & -\frac{C_r^{j1}}{M_j} & \dots & -\frac{C_r^{jj-1}}{M_j} & -\frac{C_r^{jj+1}}{M_j} & \dots & -\frac{C_r^{jN}}{M_j} \\ 0 & Br_r^{jj} & Ar_r^{jj} & 0 & \dots & 0 & 0 & \dots & 0 \\ \hline 0 & 0 & 0 & A_r^{j1} & 0 & \dots & \dots & \dots & 0 \\ \vdots & \vdots & \vdots & 0 & \ddots & 0 & \dots & \dots & 0 \\ \vdots & \vdots & \vdots & 0 & \dots & A_r^{jj-1} & 0 & \dots & 0 \\ \vdots & \vdots & \vdots & 0 & \dots & 0 & A_r^{jj+1} & \dots & 0 \\ \vdots & \vdots & \vdots & 0 & \dots & \dots & \dots & \ddots & 0 \\ 0 & 0 & 0 & 0 & \dots & \dots & \dots & \dots & A_r^{jN} \end{array}\right]$$

$$F_{jl} = \left[\begin{array}{ccc|ccc} 0 & 0 & 0 & 0 & \dots & 0 \\ 0 & -\frac{D_r^{jl}}{M_j} & 0 & \vdots & \dots & \vdots \\ 0 & 0 & 0 & 0 & \dots & 0 \\ \hline 0 & 0 & 0 & 0 & \dots & 0 \\ 0 & B_r^{jl} & 0 & \vdots & \dots & \vdots \\ \vdots & 0 & \vdots & \vdots & \dots & \vdots \\ \vdots & \vdots & \vdots & \vdots & \dots & \vdots \\ 0 & 0 & 0 & 0 & \dots & 0 \end{array}\right]$$

$$B_j = [0, 1/M, \mathbf{0}_{1\times N_r^j}]^T \quad C_j = [0, 1, \mathbf{0}_{1\times N_r^j}], \quad C_{z,j} = [1, 0, \mathbf{0}_{1\times N_r^j}]$$

where $M := m_j + \mu_{33}^j(\infty)$, B_r^{jl} occupies the same rows as A_r^{jl}, and $N_r^j = \sum_{l=1}^{N} n_r^{jl}$ is the total number of states for the "interaction" radiation subsystems.

The centralized model for a system of N WECs can be written as

$$\dot{\boldsymbol{x}} = A_c\boldsymbol{x} + B_c(\boldsymbol{u} + \boldsymbol{w}) \tag{4.9a}$$

$$\boldsymbol{y} = C_c\boldsymbol{x} \tag{4.9b}$$

$$\boldsymbol{z} = C_{z,c}\boldsymbol{x} \tag{4.9c}$$

where $\boldsymbol{x} = [\boldsymbol{x}^1; \boldsymbol{x}^2; \ldots; \boldsymbol{x}^N]$, $\boldsymbol{u} = [u^1; u^2; \ldots; u^N]$, $\boldsymbol{w} = [w^1; w^2; \ldots; w^N]$, and

$$A_c = \begin{bmatrix} A_1 & F_{12} & \ldots & \ldots & F_{1N} \\ F_{21} & A_2 & F_{23} & \ldots & F_{2N} \\ F_{31} & F_{32} & A_3 & \ldots & F_{3N} \\ \vdots & \vdots & \vdots & \ddots & \vdots \\ F_{N1} & F_{N2} & F_{N3} & \ldots & A_N \end{bmatrix}$$

$$B_c = \text{blkdiag}(B_1, B_2, \ldots, B_N)$$

$$C_c = \text{blkdiag}(C_1, C_2, \ldots, C_N)$$

$$C_{z,c} = \text{blkdiag}(C_{z,1}, C_{z,2}, \ldots, C_{z,N})$$

where blkdiag is a command in MATLAB that constructs a block diagonal matrix with the input matrices.

The state-space model Eqn. (4.9) is discretized using zero-order hold ([31]), where inputs are assumed to be piecewise constant over the sampling time T_s. As a result, we obtain the following discrete-time model:

$$\boldsymbol{x}_{k+1} = A\boldsymbol{x}_k + B(\boldsymbol{u}_k + \boldsymbol{w}_k) \tag{4.10a}$$

$$\boldsymbol{y}_k = C\boldsymbol{x}_k \tag{4.10b}$$

$$\boldsymbol{z}_k = C_z\boldsymbol{x}_k \tag{4.10c}$$

where the subscript k indicates the time instant k.

Point-Absorber Approximation

The hydrodynamic coefficients used in the formulated SS model have considered the full wave-interference effects. Yet, because of the complexity of solving such a hydrodynamic problem, the point-absorber approximation was oftentimes adopted to model the WEC system. As indicated in [45], the basic assumption of the point absorber approximation is that the devices are small enough, relative to the wavelength of the incident waves, for the structure to be a weak scatterer. Based on this assumption, only the far-field radiating waves induced by the motion of one device on the other were considered; all scattered waves were neglected in the computation of interaction effects. The wave-exciting force on an individual device is hence the same as the one on an isolated body except for a potential phase change dependent on the coordinate origin of the device. The damping coefficient λ_{33}^{jj} representing the hydrodynamic force induced by the motion of the j-th cylinder itself will also not be affected by interacting waves. The "interaction" damping coefficient λ_{33}^{jl} with $j \neq l$, representing the force on the body j caused by the motion of the body k, will be considered and dependent on the relative position of two neighboring devices. As derived in [20], the damping coefficients λ_{33}^{jl} with the j-th cylinder located at a global (cylindrical) coordinates (r_j, α_j) and the l-th cylinder at (r_l, α_l) can be expressed as

$$\lambda_{33}^{jl} = \lambda_{33} J_0(k d_{jl}) \tag{4.11}$$

where λ_{33} is the radiation damping coefficient for the isolated cylinder, J_0 is the zero-th order Bessel function, k is the wave number of the incoming waves, and

$$d_{jl} = \sqrt{r_j^2 + r_l^2 - 2r_j r_l \cos(\alpha_m - \alpha_n)}$$

is the distance between the j-th and l-th body with $j, l = 1, 2, \ldots, N$. Note that $\lambda_{33}^{jl} = \lambda_{33}$ if $j = l$, and $\lambda_{33}^{jl} = \lambda_{33}^{lj}$. Substitution of Eqn. (4.11) into Eqn. (4.3) yields the retardation function $K_r^{jl}(t)$. In addition, as derived by [20], the complex amplitude X_3^j of the wave-exciting force on cylinder j with a phase shift because of the location of the cylinder j can be obtained by

$$X_3^j(\sigma) = X_3(\sigma) e^{ikr_j \cos(\beta - \alpha_j)} \tag{4.12}$$

where β is the incident angle of the waves measured from the x-axis and X_3 is the complex amplitude of the wave force for an isolated cylinder, which can be obtained from frequency-domain hydrodynamic analysis [68] of the single device.

It can be seen that the PA approximation significantly simplifies the hydrodynamic problem and provide a straightforward estimation for hydrodynamic properties of individual devices in an array. However, the model inaccuracy induced by the PA approximation may affect the array performance. To investigate such an effect, we will form a second SS model as expressed in (4.10) with the damping coefficient λ_{33}^{jl} obtained in (4.11) and the wave-exciting force X_3^j in (4.12) and proceed the MPC procedure.

4.3 Model-Predictive Control Formulation with Convexity

A convex formulation for the model-predictive control on a single WEC was proposed in Chapter 3. With the state-space model constructed in Section 4.2, we can apply the same procedure of the MPC formulation as described in Chapter 3 to build a MPC controller for multiple WECs.

The Optimization Problem

The goal is to maximize the total energy E extracted by all of the PTO systems over a predicted time horizon T_h, where

$$E = \int_0^{T_h} P(t)\mathrm{d}t = -\int_0^{T_h} \sum_{j=1}^{N} f_m^j(t)\dot{\zeta}_3^j(t)\mathrm{d}t \tag{4.13}$$

With the use of the discrete-time model Eqn. (4.10), E can be written as $E = T_s \sum_{k=0}^{N_h-1} (-\boldsymbol{u}_k^T \boldsymbol{y}_k)$, where N_h is the number of sampling time instants during the time horizon T_h, i.e. $T_h = N_h T_s$.

Hence, the objective is to find a series of inputs $\boldsymbol{u}_k$ $(k = 0, 1, \ldots, N_h - 1)$ such that

$$\begin{aligned} \max_{[\boldsymbol{u}_0, \boldsymbol{u}_1, \ldots, \boldsymbol{u}_{N_h-1}]} E &= \min_{[\boldsymbol{u}_0, \boldsymbol{u}_1, \ldots, \boldsymbol{u}_{N_h-1}]} (-E) \\ &= \min_{[\boldsymbol{u}_0, \boldsymbol{u}_1, \ldots, \boldsymbol{u}_{N_h-1}]} T_s \sum_{k=0}^{N_h-1} \boldsymbol{u}_k^T \boldsymbol{y}_k \end{aligned} \tag{4.14}$$

This is equivalent to setting the cost function to be

$$J_0 = \sum_{k=0}^{N_h-1} \boldsymbol{u}_k^T \boldsymbol{y}_k \tag{4.15}$$

and minimize J_0 over the control inputs. For safety and long-term operation, constraints on the heaving motion of the absorber z and the machinery force u need to be included:

$$|z_k^j| \leq \zeta_{3,\max} \tag{4.16a}$$

$$|u_k^j| \leq f_{m,\max} \tag{4.16b}$$

where $k = 0, 1, \ldots, N_h - 1$ and $j = 1, 2, \ldots, N$. However, it has been shown in [38] that the constrained optimization problem formed by Eqn. (4.15) and Eqn. (4.16) will result in a non-convex QP, for which a global optimal solution is not guaranteed.

In this paper, we construct the cost function to be:

$$J = \sum_{k=0}^{N_h-1} (\boldsymbol{u}_k^T \boldsymbol{y}_k + r_1 ||\Delta \boldsymbol{u}_k||_2^2 + r_2 ||\boldsymbol{u}_k||_2^2) \tag{4.17}$$

where $\Delta \boldsymbol{u}_k = \boldsymbol{u}_k - \boldsymbol{u}_{k-1}$ for $k = 0, 1, 2, \ldots, N_h - 1$, $||\cdot||_2$ represents the l^2 norm, and $r_1,\ r_2$ (≤ 0) are penalty weights. $\Delta \boldsymbol{u}_0 := \boldsymbol{u}_0 - \boldsymbol{u}_{-1}$ where $\boldsymbol{u}_{-1}$ is defined as the control input obtained in the previous time horizon, and $\boldsymbol{u}_{-1} = 0$ initially. To attain a convex QP, we set $r_2 = 0$ and tune r_1 so that the Hermitian matrix for the cost function Eqn. (4.17) is positive definite, in a way similar to [38]. In this way, the QP is convex regardless of the value of r_2 which serves as the second tuning parameter for penalizing energy consumption. For cases simulated here, a small r_1 ($r_1 << 1$) is sufficient to guarantee the convexity of the cost function. Compared to directly increasing the penalty on the power consumption to convexify the cost function as proposed in [38], the current approach of penalizing the slew rate of the control input can better avoid over-penalizing the energy consumption, which sacrifices absorbed energy.

Quadratic Programming Formulation

We will cast the problem into a QP. The following notations will be used:

$$\begin{aligned} U_0 &:= [\boldsymbol{u}_0; \boldsymbol{u}_1; \ldots; \boldsymbol{u}_{N_h-1}] \\ W_0 &:= [\boldsymbol{w}_0; \boldsymbol{w}_1; \ldots; \boldsymbol{w}_{N_h-1}] \end{aligned} \tag{4.18}$$

which represent the series of inputs $\boldsymbol{u}$ and $\boldsymbol{w}$ at time instants $k = 0, 1, \ldots, N_h - 1$, where we recall that $\boldsymbol{u}$ and $\boldsymbol{w}$ are column vectors denoting the machinery forces and the wave-exciting forces on all of the WECs, as defined in Eqn. (4.9). The optimization problem is composed of the cost function Eqn. (4.17) and constraints Eqn. (4.16) with the dynamics in Eqn. (4.10) satisfied.

To form the QP, we propagate the state equation Eqn. (4.10a) and use Eqn. (4.10b) to obtain $\hat{y}(k+i|k)$, which denotes the state y_{k+i} estimated at time k and stacks the output states to form the vector $Y_0^{N_h-1} := [\hat{y}(k|k), \hat{y}(k+1|k), \ldots, \hat{y}(k+N_h-1|k)]^T$. $Y_0^{N_h-1}$ can then be expressed in a matrix form as:

$$Y_0^{N_h-1} = S_x x_k + S_u(U_0 + W_0) \tag{4.19}$$

where

$$\begin{aligned} S_x &= \left[C; CA; CA^2; \ldots; CA^{N_h-1}\right] \\ S_u &= \begin{bmatrix} 0 & & & & \\ CB & 0 & & & \\ CAB & CB & \ddots & & \\ \vdots & \vdots & \ddots & 0 & \\ CA^{N_h-2}B & CA^{N_h-3}B & \ldots & CB & 0 \end{bmatrix} \end{aligned} \tag{4.20}$$

In a similar manner, we can express the vector of states $\hat{z}(k+i|k)$, $i = 0, 1, \ldots, N_h - 1$, denoted by $Z_0^{N_h-1}$ as

$$Z_0^{N_h-1} = S_{x,z} x_k + S_{u,z}(U_0 + W_0) \tag{4.21}$$

where we substitute C_z for C in Eqn. (4.20) to obtain $S_{x,z}$ and $S_{u,z}$. In matrix form, the slew input vector $\Delta U := [\Delta \boldsymbol{u}_0; \Delta \boldsymbol{u}_1; \Delta \boldsymbol{u}_2; \ldots; \Delta \boldsymbol{u}_{N_h-1}]$ can be written as:

$$\Delta U = T_\Delta U_0 - g_u \tag{4.22}$$

where

$$\begin{aligned} T_\Delta &= \underbrace{\begin{bmatrix} 1 & & & & & \\ & \ddots & & & & \\ 0 & & 1 & & & \\ -1 & 0 & & 1 & & \\ & \ddots & \ddots & & \ddots & \\ & & -1 & 0 & & 1 \end{bmatrix}_{NN_h \times NN_h}}_{N} \\ g_u &= \left[\boldsymbol{u}_{-1}; 0; \ldots; 0\right]_{NN_h \times 1} \end{aligned} \tag{4.23}$$

with $\boldsymbol{u}_{-1}$ being the control input applied to the system currently and $u_{-1} = 0$ initially. In the MPC, $\boldsymbol{u}_{-1}$is the input obtained from the previous receding-horizon computation.

The cost function J in Eqn. (4.17) can then be written in a compact form:

$$J = U_0^T Y_0^{N-1} + (T_\Delta U_0 - g_u)^T R_1 (T_\Delta U_0 - g_u) + U_0^T R_2 U_0 \tag{4.24}$$

where $R_i = r_i \times \mathcal{I}_{(NN_h)}$ $(i = 1, 2)$ with $\mathcal{I}$ being the identity matrix. Substituting Eqn. (4.19) and Eqn. (4.22) in Eqn. (4.24) and neglecting the constant term, we can write J in a quadratic form

$$J = \frac{1}{2} U_0^T H U_0 + f^T U_0 \tag{4.25}$$

where

$$H := S_u + S_u^T + 2S_R \tag{4.26a}$$
$$f := S_x x_k + S_u W_0 - 2S_g \tag{4.26b}$$

with $S_R := (T_\Delta)^T R_1 T_\Delta + R_2$ and $S_g = (T_\Delta)^T R_1 g_u$.

It can be seen that without penalizing the slew rate, the cost function will have a corresponding Hessian matrix $H_0 = S_u + S_u^T$ where S_u in Eqn. (4.20) has zero diagonal elements, which may lead to an indefinite H_0 and hence a non-convex problem. The addition of S_R, aside from controlling the slew rate, adds positive values on the diagonal of the matrix H per Eqn. (4.26a). By setting $r_2 = 0$ and tuning r_1 such that the minimal eigenvalue of H is larger than 0, we can have a positive definite H and hence a convex J.

The constraints Eqn. (4.16) can be written in a component-wise inequality. Thus

$$A_u U_0 \leq b_u \tag{4.27}$$

where it can be shown, with the use of Eqn. (4.21), that

$$A_u = \begin{bmatrix} I \\ -I \\ S_{u,z} \\ -S_{u,z} \end{bmatrix}, \quad b_u = \begin{bmatrix} U_{\max} \\ U_{\max} \\ Z_{\max} - S_{x,z} x_k - S_{u,z} W_0 \\ Z_{\max} + S_{x,z} x_k + S_{u,z} W_0 \end{bmatrix} \tag{4.28}$$

with $U_{\max} = f_{m,\max} \times \underbrace{[1, \ldots, 1]}_{NN_h}^T$ and $Z_{\max} = \zeta_{3,\max} \times \underbrace{[1, \ldots, 1]}_{NN_h}^T$.

In summary, the QP with the cost function Eqn. (4.25) subject to the constraints Eqn. (4.27) can be written as:

$$\min_{U_0} \quad J = \frac{1}{2} U_0^T H U_0 + f^T U_0 \tag{4.29a}$$
$$\text{subject to} \quad A_u U_0 \leq b_u \tag{4.29b}$$

MPC Scheme Implementation

The MPC scheme as presented is implemented as follows: at time instant k, with the knowledge of estimated states and the predicted wave profile, the QP in Eqn. (4.29) is solved, and a sequence of optimal control inputs $U_0^* = \text{argmin}(J)$ is generated; the first set of the control inputs in the sequence is applied; the system dynamics is then moved forward to the next time step, and the optimization procedure is repeated. In this paper, we will assume the knowledge of a certain future period of the incoming waves is available.

Regarding the study of the PA approximation, the plant model in the MPC controller is built with the hydrodynamic coefficients obtained under the approximation. The control inputs generated from the MPC will be fed into the "real" dynamic model of the WEC array where the wave-interaction effects were accurately captured as formed in §4.2.

4.4 Performance of a Constrained WEC Array

We will apply the MPC formulated in Section 4.3 to arrays of point-absorber type WECs with configurations shown in 4.1. The heaving point absorber adopted for simulations in this paper is shown in Fig. 4.2, which was developed in [64, 72] with both simulations and model tests. The cylinder or floater has a radius of $a = 0.1365$ m and a draft of $d = 0.6126$ m, and the WEC device has a total mass of $M = 42.1$ kg (including the added mass), and hydrostatic stiffness coefficient of $K = 574.2$ N/m. The water depth is 1.5 m. In addition, an equivalent linear-viscous damping factor $\lambda_{vis} = 5.0\text{N} \cdot \text{s/m}$ was used, which was obtained from experiments in [64]. In this section, performances of three devices shown in 4.1(b) will be evaluated in both regular and irregular wave conditions. Power absorbed by the array with the current MPC formulation will be compared with those obtained by passive damping control. Also discussed is the performance of the array, with wave interacting among devices, compared to that of isolated devices. For such purpose, an interaction factor q will be used, which presents the ratio of the power absorbed by an array averaged over the number of devices and the power absorbed by a single cylinder, as defined in the following

$$q = \frac{P_u}{NP_{u,s}} \tag{4.30}$$

where P_u is the useful power obtained by multiple absorbers, $P_{u,s}$ is the power absorbed by a single or isolated absorber, and N the number of devices. For the passive controller, it is assumed that each WEC will be equipped with a simple linear damper of nonnegative damping coefficient. As described in [24], the optimal linear damping of the j-th cylinder in regular waves can be obtained by

$$B_g^j(\sigma) = \sqrt{(\lambda_{33}^j(\sigma) + \lambda_{vis})^2 + (\sigma \cdot (m_j + \mu_{33}^j(\sigma)) - \frac{K_j}{\sigma})^2} \tag{4.31}$$

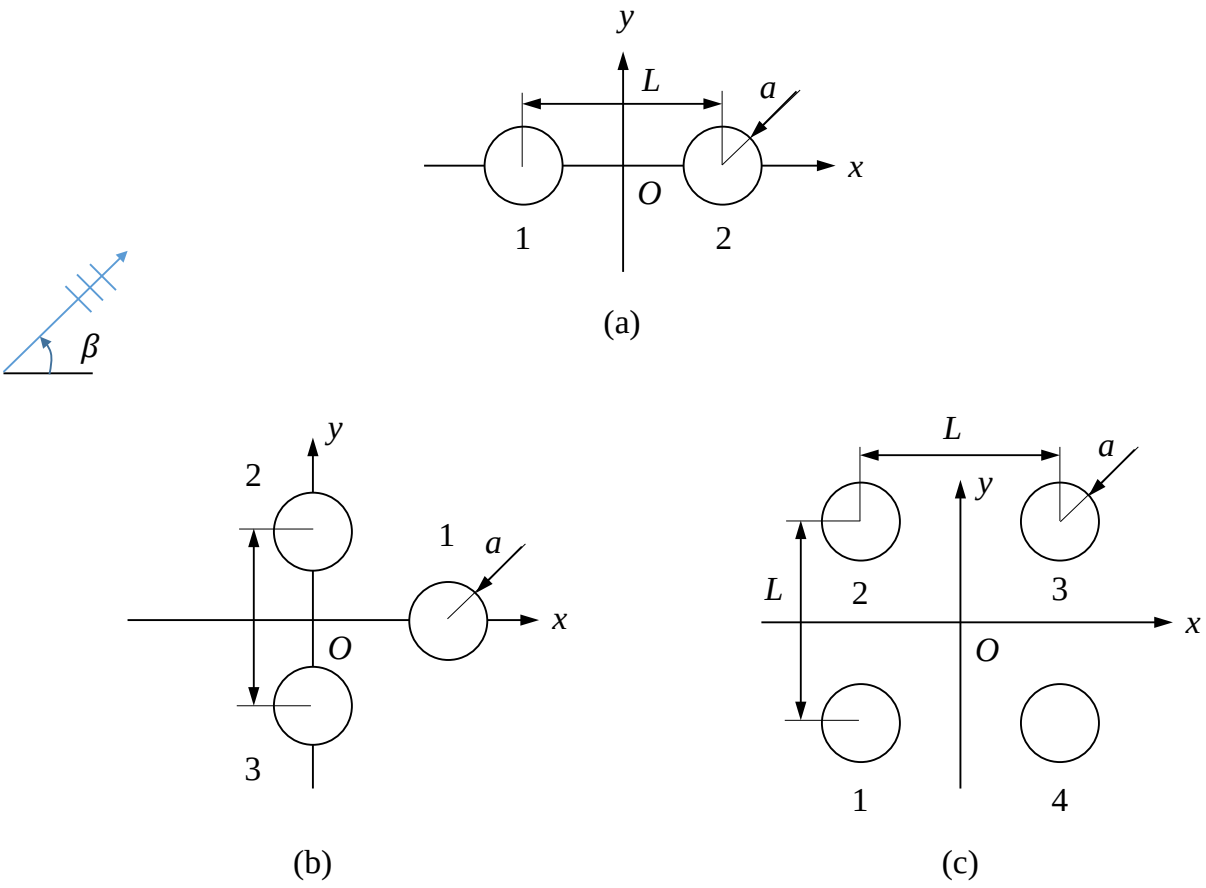

Figure 4.1: Birdseye view of the configuration of two to four identical WEC devices, separated by a distance of L as defined, with incident waves striking at an angle β.

where λ_{33} and μ_{33} are hydrodynamic coefficients for the j-th cylinder as in isolation. The PTO force can be obtained by

$$f_g^j(t) = -B_g^j \dot{\zeta}_3^j(t) \tag{4.32}$$

In irregular waves, the B_g will be tuned to correspond to the peak period of the wave spectrum.

To illustrate the modeling of effects of radiating waves, the radiation subsystem for K_r^{jl} $(j, l = 1, 2, 3)$ of a three-cylinder array is presented in Fig. 4.3 as an example, where K_r^{jj} indicates the radiation forces on device j caused by the motions of itself and K_r^{jl} $(l \neq j)$ indicates the radiation forces caused by device j on its neighbor l. The impulse response $K_r^{jl}(t)$, obtained by inverse Fourier transform (IFT) of the corresponding damping coefficients $\lambda_{33}^{jl}(\sigma)$ was plotted with the response of reduced-order state-space (SS) models. A sixth-order state-space model was used to approximate the subsystem for K_r^{11} and a seventh-order state-space model for K_r^{12} to achieve an accuracy of 0.999, evaluated by the method described in

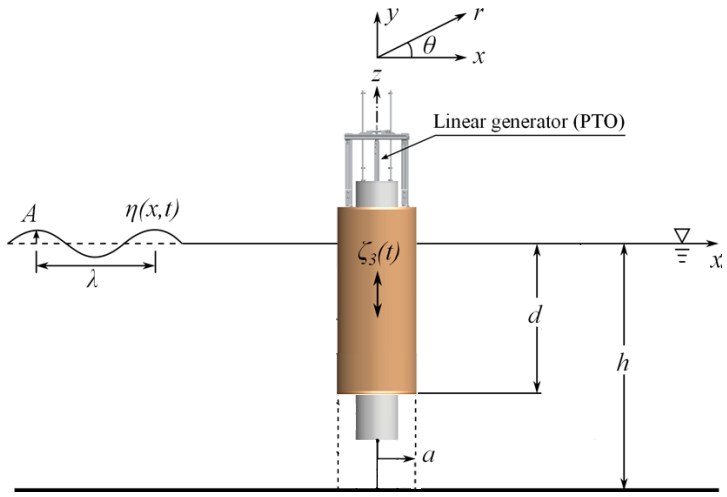

Figure 4.2: Schematic of the heaving point absorber and the PTO system developed in [64].

[62]. Because of the equilateral layout, the array has the property of $K_r^{12} = K_r^{13}$. Here, L denotes the center-to-center spacing.

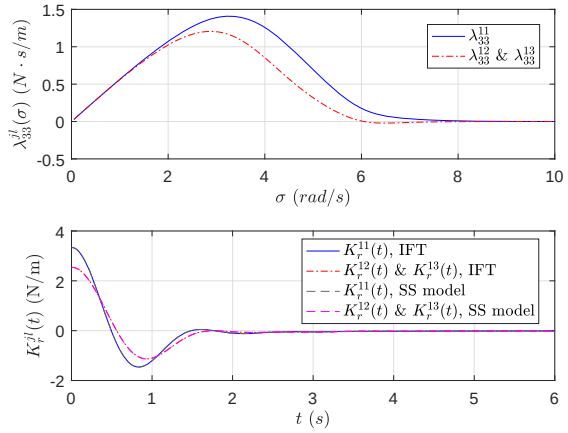

Figure 4.3: Impulse response of the radiation subsystems and the damping coefficient in heave for three cylinders with the spacing $L = 5a$. Coupling hydrodynamics is shown as superscript ^{12} and ^{13}

Constraints for the devices are considered as: (1) the maximum response amplitude operator (RAO) of absorbers is 3, i.e. $\zeta_{3,\max} = 3A_0$ with A_0 being the wave amplitude, and (2) the maximal machinery force is $f_{m,\max} = B_{g,\max}\zeta_{3,\max}\sigma$ with $B_{g,\max} = 50$ N·s/m, where σ is the angular frequency of incident waves, according to [64]. We set the penalty weight r_i

(i = 1, 2) to be $r_i = \overline{r_i}/T_w^2$, where the scaling factor T_w^2 with T_w being the wave period was used to eliminate the effect of the selected time interval. In the current study, $\overline{r_1} = 10^{-0.9}$ was chosen to be the minimal value such that the cost function Eqn. (4.17) is convex, and $\overline{r_2} = 10^{-2}$ was chosen to be the weight penalizing power consumption. The quadprog solver with the interior point algorithm in MATLAB was used to solve the QP for the MPC, which has polynomial time complexity [70] for solving convex QP.

Results in Regular Waves

Using linear theory, we can write the wave-exciting force induced by a regular wave of frequency σ on the cylinder j as:

$$f_e^j(t) = A_0 \Re\{X_3^j(\sigma) e^{-i\sigma t}\}, \quad j = 1, 2, \ldots, N \tag{4.33}$$

with A_0 being the wave amplitude. Here, we recall that X_3^j contains wave-interaction effects among the cylinders and was obtained by the method developed in Chapter 2. The wave amplitude was set to $A_0 = 0.061$ m in simulations. The wave-exciting force on cylinder j, for the discrete-time model in Eqn. (4.10), is obtained by

$$w_k^j = A_0 \Re\{X_3^j(\sigma) e^{-i\sigma k T_s}\} \tag{4.34}$$

where w_k^j denotes the f_e^j at time instant k with $k = 0, 1, \ldots, N_h - 1$. Simulations were carried out for $20T_w$ with 80 time steps per wave period.

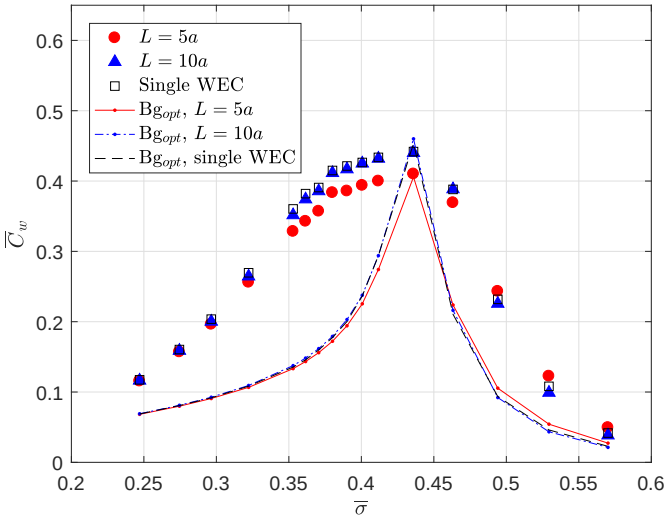

Figure 4.4: Nondimensional capture width of three WECs in regular waves with the spacing ratio $L/a = 5$ and $L/a = 10$.

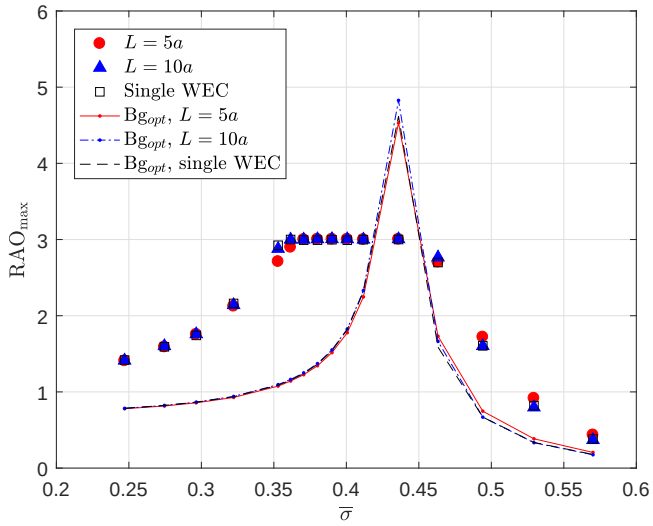

Figure 4.5: Maximal RAO of three WECs in regular waves with the spacing ratio $L/a = 5$ and $L/a = 10$.

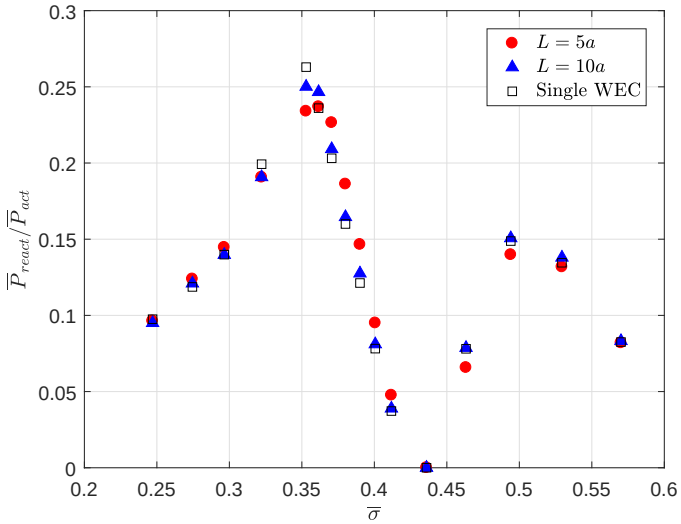

Figure 4.6: The ratio of the reactive power to the power flowing from the absorbers to the PTO units (so-called "active power") for a three-WEC array with the spacing ratio $L/a = 5$ and $L/a = 10$.

We present results for the non-dimensional capture width $\overline{C}_w$, the maximal response amplitude operator (RAO) of absorbers in the array, and the non-dimensional frequency $\overline{\sigma}$, which were defined by

$$\overline{C}_w = \frac{C_w}{2a} = \frac{1}{2a}\frac{\overline{P}_u/N}{P_{\text{wave}}} \tag{4.35a}$$

$$\text{RAO}_{\max} = \max(\frac{\zeta_3^1}{A_0}, \frac{\zeta_3^2}{A_0}, \ldots, \frac{\zeta_3^N}{A_0}) \tag{4.35b}$$

$$\overline{\sigma} = \sigma\sqrt{\frac{a}{g}} \tag{4.35c}$$

with g being the gravitational acceleration, P_{wave} the incident-wave power flux, and

$$\overline{P_u(t)} = \frac{1}{T}\int_{T_0}^{T_0+T} f_m^j(t)\dot{\zeta}_3^j(t)\mathrm{d}t$$

representing the time-average energy extracted by the WEC array, which is summed over j, then averaged over N bodies. Fig. 4.4-Fig. 4.6 show results for a three-cylinder array with the spacing to radius ratio $L/a = 5$ and $L/a = 10$ respectively in head seas ($\beta = 0$); also shown were results obtained by the (unconstrained) passive control.

It can be seen that the MPC significantly out-performed the passive controller in terms of broadening the capture-width bandwidth, even with strictly restricted RAOs and control inputs. It should be noted that the current MPC, taking the machinery force as the control input, will require power to motor the system, i.e. the so-called "reactive power" is employed, while the passive control of the damping do not need driving power. In Fig. 4.6, we present the ratio of the reactive power ($\overline{P}_{react}$) to the power flowing from the absorbers to the PTO units (so-called "active power" $\overline{P}_{act}$). Near the resonance frequency $\overline{\sigma} = 0.4356$ of the single device, the MPC was able to produce nearly the same amount of power as the one produced by the passive controller, with the RAO constrained and the consumed power being approximately 0. This result suggests that the current MPC is capable of maximizing the extracted energy and satisfying hard constraints on the absorbers. Also, by penalizing energy consumption in the cost function, the reactive power required by the MPC system is controlled to be less than 30% of the total power, i.e. more than 70% of the absorbed power can be transformed to the useful power. When the spacing among the devices increases to $10a$, i.e. 5 diameters, the difference caused by the wave-interaction effects appears to be very small. More discussion on the wave-interaction effects on power production from the array will be presented in a later section.

Time histories of heaving velocities of the three devices with spacing ratio $L/a = 5$ in head seas ($\beta = 0$) in the Fig. 4.7, as well as the instantaneous power and the machinery force, i.e. the control force. Because of the geometric symmetry, Cyl.2 and Cyl.3 behaved the same in waves of $\beta = 0$. Wave-interaction effects can be seen from the phase difference between the heaving velocity and the wave-exciting force for the array in waves of a frequency near the resonant frequency of the device, which has a period of $T_w = 1.7$s. If there were no

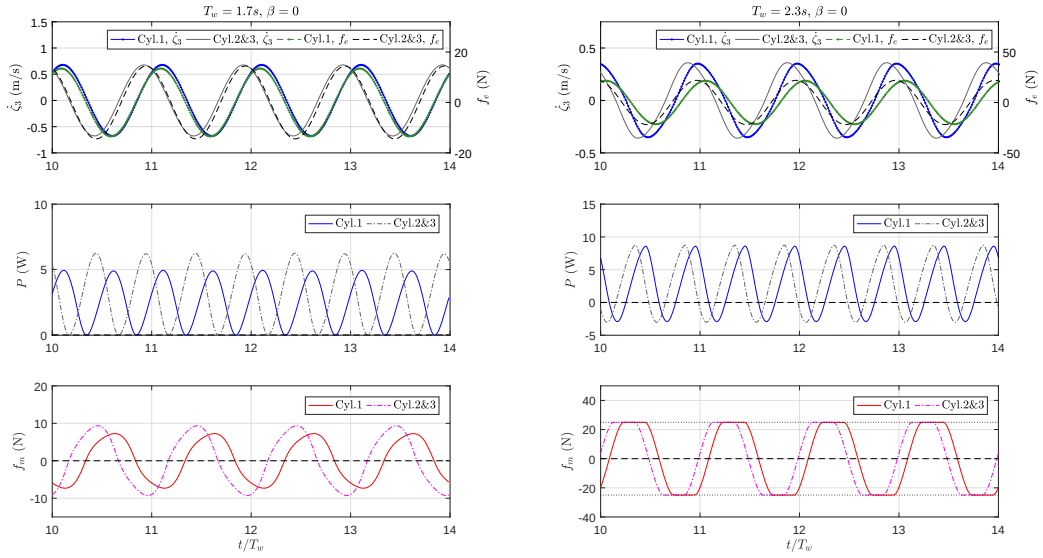

Figure 4.7: Time histories of the heaving velocity $\dot{\zeta}_3$, the wave-exciting force f_e, the instantaneous power P, and the machinery force f_m for a three-device array at two selected wave periods, showing rather different behavior ($L/a = 5$).

wave interference, the two should be in phase at the resonance. Also, in such waves, Cyl.1 extracted less power than Cyl.2&3 because of sheltering effects from the upstream cylinders. In waves of $T_w = 2.3$s, at the frequency $\overline{\sigma} = 0.322$ corresponding to longer waves, cylinders in the upsteam and downstream behaved as independent and attained similar amounts of extracted energy; also, the constraint on the control force was active, which resulted in a bang-bang type of control. This suggests that at lower frequencies, effects of constraints played a more dominant role than the wave-interaction effects. In addition, in Fig. 4.7, it can be seen that there exists phase differences among the instantaneous power extracted by individual devices. Such phase differences may be used to achieve a more stable power output from the array to the grid.

Results in Irregular Waves

The performance of the controlled WEC array was evaluated in irregular waves. A modified Pierson-Moskowitz spectrum for fully developed seas was used to construct the irregular

wave profile:

$$S(\sigma) = H_s^2 T_1 \frac{0.11}{2\pi} \left(\frac{\sigma T_1}{2\pi}\right)^{-5} \exp\left[-0.44\left(\frac{\sigma T_1}{2\pi}\right)^{-4}\right] \tag{4.36a}$$

$$T_1 = 0.7713 T_p \tag{4.36b}$$

$$A(\sigma_j) = \sqrt{2S(\sigma_j)\Delta\sigma} \tag{4.36c}$$

$$\eta(t) = \sum_{j=1}^{N} A(\sigma_j)\sin(\sigma_j t + \varepsilon_j) \tag{4.36d}$$

$$f_e(t) = \sum_{j=1}^{N} |X_3(\sigma_j)| A(\sigma_j)\sin(\sigma_j t + \delta_j + \varepsilon_j) \tag{4.36e}$$

where H_s, T_p, A_j, and δ_j are the significant wave height, peak period, wave amplitude, and phase angle of the wave-exciting force the j^{th}-component, respectively, and ε_j is a random phase angle of wave components. The random phase angles are uniformly distributed between 0 and 2π and constant with time. The range of angular frequencies used in the construction of Eqn. (4.36) was between 0.1 rad/s and 8.75 rad/s spaced at 0.05 rad/s. The simulation runs for $H_s = 7.62$ cm (3.0 in) and varying T_p, carried out for 500 peak wave periods with 50 time-steps per peak period and the time horizon $T_h = 2T_p$. In this application, the RAO is constrained to be 1.5 times the significant wave height, i.e. $\zeta_{3,\max} = 1.5H_s$ and the $B_{g,\max} = 50$ N·s/m. The maximal machinery force is computed in the same way as described in Section 4.4 with $\sigma = 2\pi/T_p$. The same penalty weights $r_1 = 10^{-0.9}/T_p^2$ and $r_2 = 10^{-2}/T_p^2$ as in regular waves were used.

Results of the averaged useful power and the ratio of the consumed power for the three-WEC array with two spacings in head seas ($\beta = 0$) are shown in Fig. 4.8F̃ig. 4.9, and compared with arrays controlled by passive controllers, as described in Eqn. (4.31), and the single device with the MPC control. Performance of the MPC in irregular waves is significantly better than the passive controller. Destructive wave-interaction effects were observed for all simulated wave conditions. Increasing the spacing between devices can reduce the destructive effects by a factor of 2. Meanwhile, with the composition of waves of different frequencies, the variance of interaction factor q with the wave periods tends to be flatter, compared to that in the regular-wave cases. In irregular waves, the ratio of the reactive power increases with the increase of the peak wave period and approaches to 0.33 for the array, less than the value of 0.4 for the single device. The less portion of reactive power for array arrangements may be attributable to the energy transfer among the group members.

Computational Time

The box plot of the computational time for simulations of the coordinated control of two, three, and four devices in model scale are plotted over the number of devices in the array,

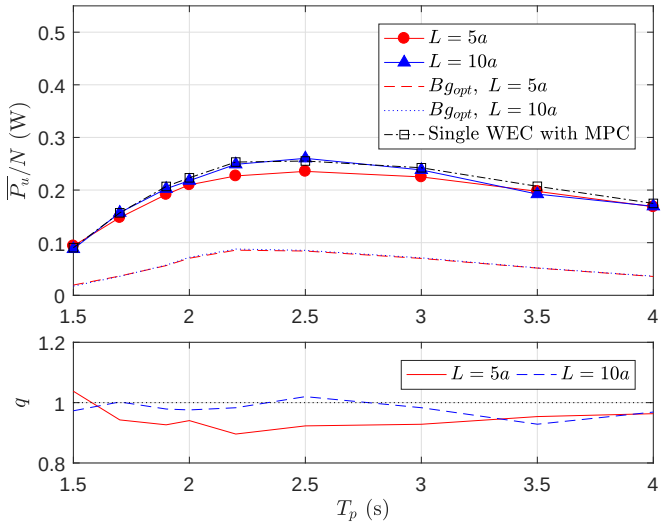

Figure 4.8: Averaged useful power for three WECs in irregular waves.

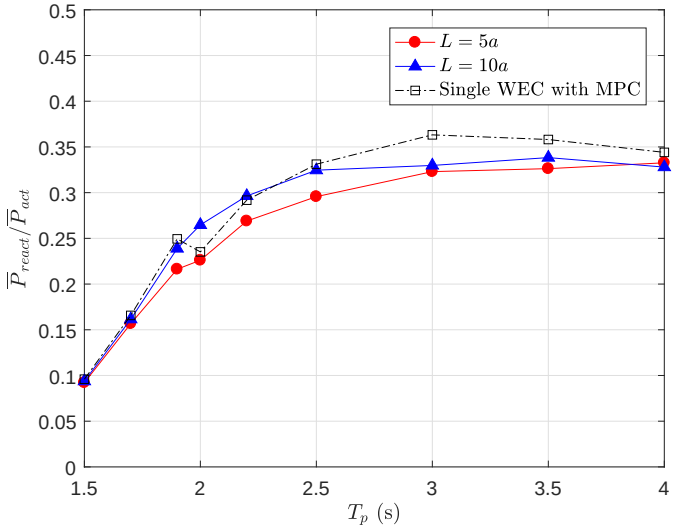

Figure 4.9: The ratio of reactive power to active power for three WECs in irregular waves.

as shown in Fig. 4.10. All simulations were performed on AMD Threadripper 16-core CPU running at 3.4 GHz. Simulations for irregular-wave cases were carried out for $500T_p$ with 50 time steps per wave period. The prediction horizon used in the MPC is 2 wave periods. Regarding the mean values of the computational time per peak wave period, increasing the number of devices can increase the computational time by an order of magnitude. Nevertheless, the results show increase in the numbder of devices did not make the computational cost prohibitively high. In addition, with code optimization and scaling ratio between prototype and model test taken into account, the method can be used for a fast evaluation of the power performance of a medium-size array.

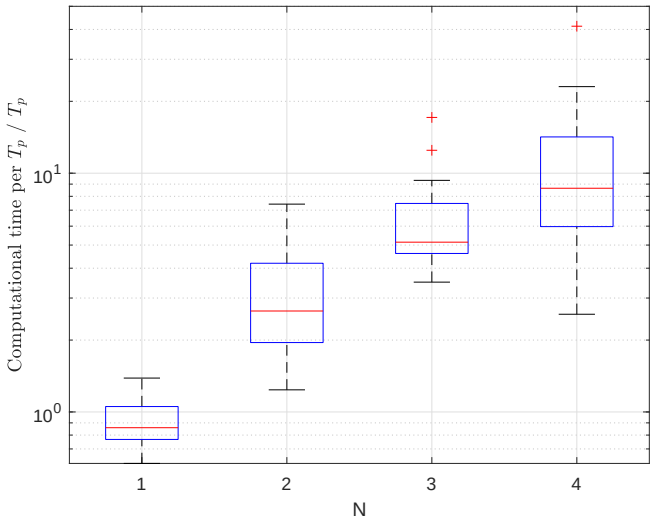

Figure 4.10: Box plot of the computational time for irregular-wave cases plotted over the number of cylinders.

4.5 Wave-Interaction Effects on Power Performance of a Constrained WEC Array

In studies of optimal wave-array configurations, constructive wave-interference effects is a primary criterion for determining the favorable configurations. However, existing studies normally do not consider physical constraints on a WEC array and oftentimes simplify hydrodynamic effects from interacting waves in the modeling. The resulted interaction factor q can differ by more than 50% in waves of different frequency and wave-incidence angles. To investigate wave-interaction effects on the power performance of a constrained array in the optimal operating condition, we here performed simulations for two, three, and four devices.

Fig. 4.11 shows the interaction factor q obtained for the three-device array with the spacing to radius ratio $L/a = 5$ and $L/a = 10$ under the MPC control (with constraints)

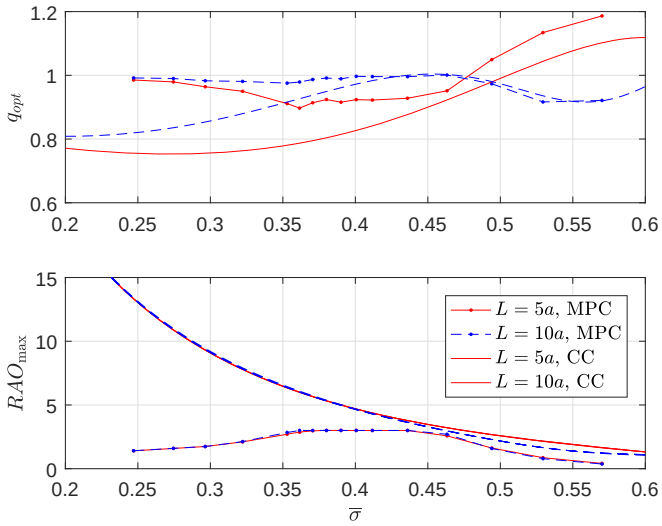

Figure 4.11: The q factor for three devices with constrained MPC control and (unconstrained) complex-conjugate (CC) control in head seas ($\beta = 0$).

and under the complex-conjugate (CC) control (without constraints) as described in [20] and [23]; also presented is the mean RAO of the three devices in the array. It can be seen that wave-interaction effects on the optimal power output were in general reduced with constraints added on devices, particularly in the low-frequency region, where an impractically large RAO was required to achieve the optimal power with unconstrained control. For a constrained array, the strongest wave-interaction effects appear near the resonance frequency of a single WEC device. While at low frequencies, the effects of constraints will become dominant over the interaction effect, which makes the individual cylinders behave as almost independent. The spacing among devices noticeable affects the wave-interaction effects. When the spacing distance between the three cylinders increases from $L = 5a$ to $L = 10a$, the maximal interaction effect was reduced approximately from 20% to 10%.

We also investigated the effect of wave-incidence angle on the power production of a constrained array. As shown in the results from Chapter 2, the power performance of a WEC array vary largely with the wave-incidence angle. Additionally, it was shown in [69] that the integration of the q factor over the wave angle from 0 to 2π should be equal to 1 for an array of heaving point absorbers under optimal unconstrained control. This means that there will be the same amount of constructive effects and destructive effects induced by waves from all directions. In the design of a wave farm, an array is normally placed such that regional waves come in the direction that makes the array generate the most power.

Such differences induced by the wave angle appeared in a different form when constraints were applied to the system. We plot the mean power generated by the array and the ones generated by individual devices for arrays consisting of two, three, and four cylinders in the waves of various incident angles, as shown in Fig. 4.12. It can be seen that the averaged

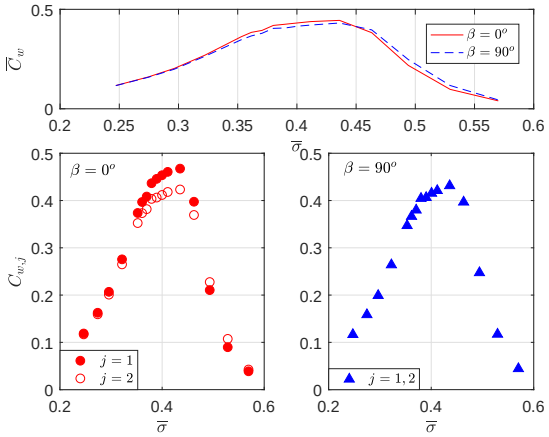

(a) Two-device array in waves of $\beta = 0$ and $\beta = \pi/2$

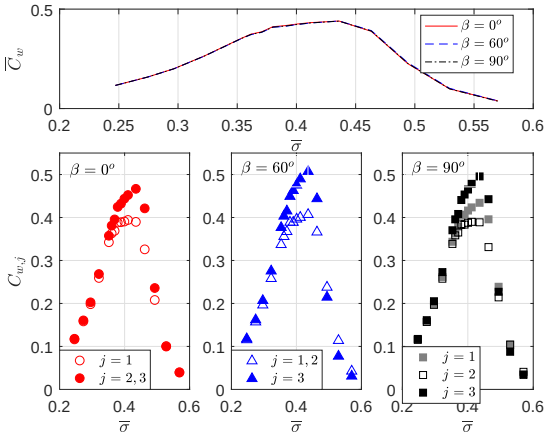

(b) Three-device array in waves of $\beta = 0$, $\beta = \pi/3$, and $\beta = \pi/2$

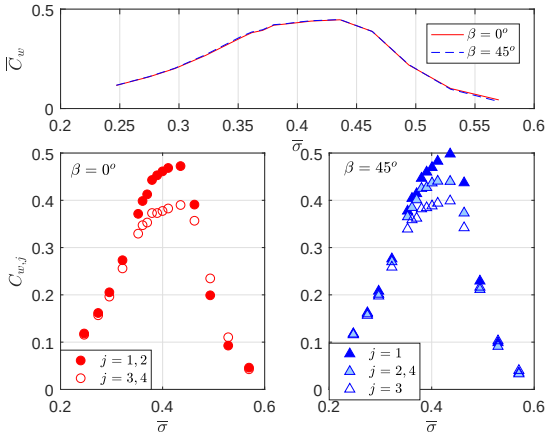

(c) Four-device array in waves of $\beta = 0$ and $\beta = \pi/4$

Figure 4.12: Power extracted by a two-device array: the upper plot shows the averaged capture width for the array and the lower ones show the capture width for individual devices.

power generated by the whole array does not appear much differences when incident waves are from different directions. However, the distribution of the absorbed energy among array elements are largly affected by the wave-incidence angle. The devices confronted with waves first, represented by the solid symbols, were able to absorb the most power in all cases, while the absorbers that are the farthest in the downstream, indicated by the hollow symbols, has the least energy absorption. The results may also be explained that when the configuration of the array has less wave-direction preferences, or in other words, appears more like a circle, the total energy that can be extracted from the array will tend to be the same amount for waves of all directions, but with the energy distributed differently among the members. Therefore, in optimizing the array configuration, it can be worthwhile to consider the energy extraction difference in individual devices, in addition to maxmizing the total energy output.

4.6 Effects of the Point-Absorber Approximation

The point-absorber (PA) approximation was commonly used in the study of control strategies for WECs because it is straightforward to apply and can provide an estimation for wave-interaction effects. In this section, we compared simulation results using a model with the "exact" wave-interaction effects and using the one with the point-absorber approximation. The evaluation was performed with the use of irregular-wave conditions for realistic scenarios.

Results for arrays of different spacing ratios are presented, since the spacing between devices will affect the accuracy of the PA approximation, i.e. the larger the spacing, the more valid the assumption of neglecting effects of scattering waves. Fig. 4.13 shows the useful energy $\overline{P}_u$ and the reactive power $\overline{P}_{react}$, obtained for the array of $L/a = 5$ with wave-interaction effects modeled by the PA approximation and the exact method respectively. It can be seen that with the "exact" wave-interaction model, the array generated $5-15\%$ more energy than the one with the PA-approximation model with a similar amount of energy consumption (reactive power). This suggest that the more information about the wave forces on the array can benefit the energy absorption of the system. With a larger spacing ratio, $L/a = 10$, the "exact" model still outperformed the PA-approximation model but the difference in the energy absorption with the two models is less than 5%, as shown in Fig. 4.14. Hence, if devices in an array have relatively large spacings, the PA approximation can be a fast and good way to consider wave-interaction effects on the power performance of the array.

4.7 Summary Remarks

In this Chapter, the MPC developed in Chapter 3 was applied to arrays of heaving point absorbers such that the absorbers will act coordinatedly to maximize the energy extraction of the whole array, with wave interactions among the devices taken into account in the dynamic model. Constraints were considered on the motion amplitudes and the PTO forces

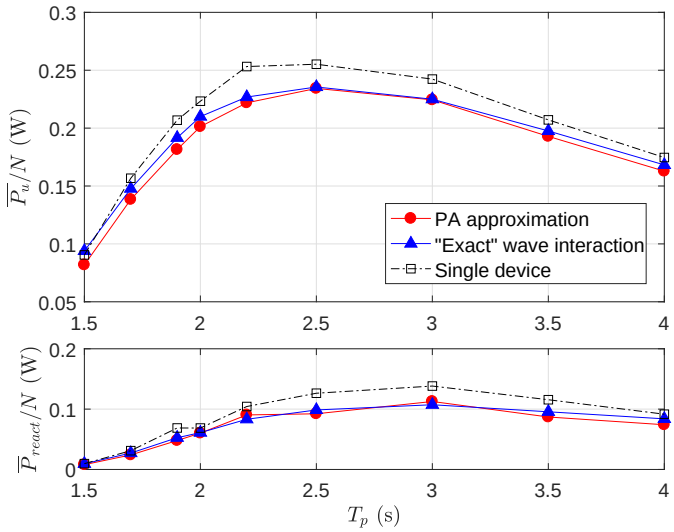

Figure 4.13: Comparisons of the performance of a three-WEC array in irregular waves with the wave-interaction effect modeled by the PA approximation and an "exact" method ($L/a = 5$).

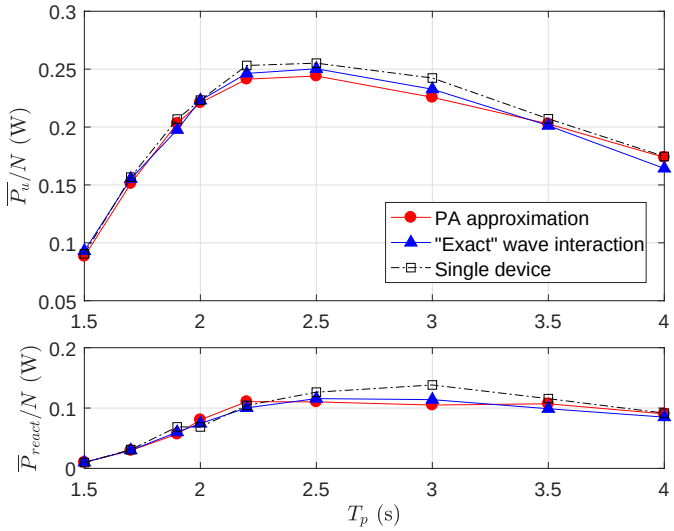

Figure 4.14: Comparisons of the performance of a three-WEC array in irregular waves with the wave-interaction effect modeled by the PA approximation and an "exact" method ($L/a = 10$).

of individual devices. The power consumption, caused by using the PTO force as the control input to ensure a linear dynamic system, was penalized with the weight acting as a free tuning parameter. Full wave-interaction effects among the array, evaluated by the fast computation method developed in Chapter 2, was taken into account in the dynamic model of the whole array.

Simulation showed that the MPC strategy successfully optimized the energy generation from a point-absorber array and satified hard contraints on the devices. Compared to the unconstrained optimal-damping control strategy, the MPC significantly broadened the capture-width bandwidth and generated nearly the same amount of maximal energy but with constraints satisfied. Additionally, the wave-interaction effect on the power production is considerably reduced because of the restricted oscillatory motion of the devices, when compared to that of unconstrained cases which is commonly used as an indicator of the power production capability of an array. Hence, the phase matching condition for indicating the condition of maximal energy extraction for an absorber, though in principle not valid for an array because of wave interferences, was approximately achieved even when the devices were less than 3 diameters apart. The interaction effects were seen as destructive, indicating the less the interaction effects, the better the power performance of the array given the design. Simulations of the array in irregular waves were also performed, enabled by the efficient computation of the convex QP formulation of the MPC; and the power consumption by the PTO systems were discussed. The ratio of computational time per peak wave period to the wave period plotted over the number of devices showed the computational efficiency of the current method and its potential in real-sea applications. Highlights of this research is reported in [78].

Chapter 5

Implementation of the control strategy on a WEC array

5.1 Overview

As it can be seen from Fig. 4.6 and Fig. 4.9, reactive power will be required during the active control process of the heaving absorber, which causes two-direction energy flow. Comparing to the resistive control by tuning the PTO damping, we observe the advantage of the current controller is that it can act an arbitraty, and desired, amount of forces on the devices, less affected by the oscillations of the devices themselves. As demonstrated in the previous Chapters, this property is able to effectively broaden the capture-width bandth of the heaving absorbers. However, the requirement of generating reactive power will add complexity on the PTO design and increase the production cost of the WECs. In addition, since the PTO system in practice is non-ideal, which means that it will send less power to the grid than that absorbed by the WEC when acting as a generator, and need more electrical power supply than the required amount when it acts as a motor. Therefore, with a non-ideal PTO, less absorbed power will be converted to useful power compared to the amount obtained with ideal PTO systems.

The useful power transimitted to the grid, with a non-ideal PTO taken into account, can be expressed by

$$P_{grid} = \eta_1 P_{act} - \frac{1}{\eta_2} P_{react} \tag{5.1}$$

where the PTO is assumed to have the efficiency of η_1 as a generator and η_2 as a motor. Recall that P_{act} denotes the active power flowing from the absorber to the grid and P_{react} denotes the reactive power. Fig. 5.1 shows the grid power captured by a single point absorber with an ideal PTO and also a non-ideal PTO with $\eta_1 = \eta_2 = 0.7$; also plotted is the power captured by the system using a nonlinear MPC which directly optimizes a non-negative PTO damping [64] and would not produce reative power. It can be seen that with an ideal PTO, allowing for the reactive power can increase the capture width especially in wave frequencies farther

away from the device's resonance frequency. However, when the PTO efficiency lowers to 70%, such an advantage of a system with reactive power allowed becomes small. The system with NMPC, without allowing the reactive power, transferred similar amounts of power to the grid as those generated by a system allowing for reactive power flow. Increasing the penalty on the power consumption, by increasing r_2 in Eqn. (4.17), can reduce the reactive power, but not fully eliminate the need of reactive power in the process.

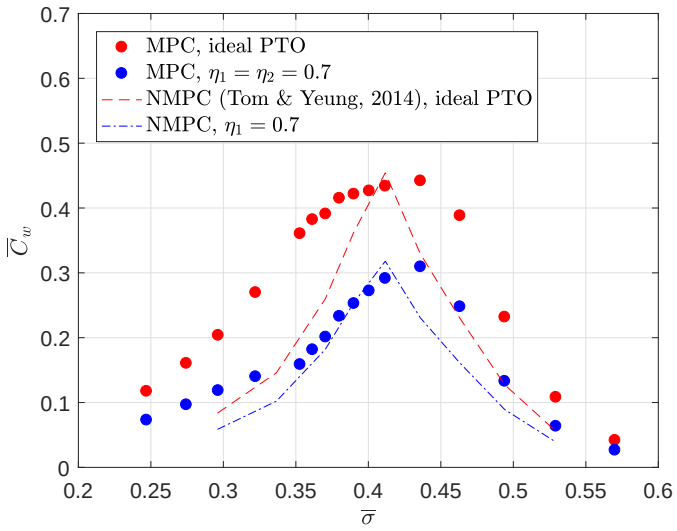

Figure 5.1: Capture width based on the grid power obtained by a single point absorber.

In this chapter, we will propose a modified optimization problem, which *seeks optimal control forces under the condition that no reactive power need be generated*. Comparisons of the useful power generated with a non-ideal PTO will be made between this new MPC and the MPC formed in Chapter 4. With no requirement on reactive power, such control forces can be implemented "approximately" by an in-house designed Permanent Magnetic Linear Generator (PMLG). The implementation and the resulted performance of the array will also be discussed. Finally, performances of a three-device array located in seven U.S. Pacific Coast regions, chosen for evaluating the Wave Energy Prize sponsored by the Department of Energy (DOE) in 2015, will be presented. Given the sea states representing the seven locations, simulations will be conducted for the array equipped with non-ideal PMLG PTO units and the coordinated control strategy. The results will significantly reduce uncertainties existing in the evaluation of technology performance level (TPL) of an array of heaving point absorbers.

5.2 Eliminating the Reactive Power

To eliminate reactive power in the system, we can directly add the following constraints to the optimization formulation in Eqn. (3.15)

$$u_k y_k \leq 0 \quad k = 0, 1, \ldots, N-1 \tag{5.2}$$

This can be expressed in a vector form as

$$\text{diag}(U_0) Y_0^{N-1} \leq 0 \tag{5.3}$$

where diag indicates the diagonal matrix with U_0 on the diagonal; $U_0 = [\boldsymbol{u}_0; \boldsymbol{u}_1; \ldots, \boldsymbol{u}_{N-1}]$ as defined in Eqn. (4.18) and $Y_0^{N-1} = S_x \boldsymbol{x}_k + S_u(U_0 + W_0)$ as defined in Eqn. (4.19). However, substituting Y_0^{N-1} in Eqn. (5.3) reveals that such a constraint is quadratic in u_k with a non-convex matrix S_u as expressed in Eqn. (4.20). The resulted optimization problem is known to be hard to solve with considerably increased computational time.

Instead, if we add the constraint only on the first control input, which is the one to be applied to the system, the convexity of the optimization problem will pertain because $y_0 = Cx_0$, not dependent on u_0, resulting in an additional *l*inear constraint. The new optimization problem then became

$$\min_{U_0} \quad J = \frac{1}{2} U_0^T H U_0 + f^T U_0 \tag{5.4a}$$

$$\text{subject to} \quad \widetilde{A}_u U_0 \leq \tilde{b}_u \tag{5.4b}$$

with H and f the same as in Eqn. (4.26) and

$$\widetilde{A}_u = \begin{bmatrix} t_1 \\ I \\ -I \\ S_{u,z} \\ -S_{u,z} \end{bmatrix}, \quad \tilde{b}_u = \begin{bmatrix} 0 \\ U_{\max} \\ U_{\max} \\ Z_{\max} - S_{x,z} x_k - S_{u,z} W_0 \\ Z_{\max} + S_{x,z} x_k + S_{u,z} W_0 \end{bmatrix} \tag{5.5}$$

where $t_1 \in R^{N \times N}$ and $t_1 = \text{diag}([\boldsymbol{y}_0; 0; \ldots; 0])$ with $\boldsymbol{y}_0 = C\boldsymbol{x}_0$. This optimization problem can then be implemented in the MPC scheme.

With no requirement of generating reactive power, the design of the PTO system can be considerably simplified. It needs to be pointed out that constraining the first control input and resulting with no reactive power leads to an optimization problem essentially different from that of finding the optimal control law for a system with no capability of generating reactive power. In fact, the current scheme assumes that the system has the capability and only that it will not the reactive power at the first time step. This formulation is a variation of the optimization problem formed in Chapter 4.

Simulation results of the capture width, computed for the grid power P_{grid} as expressed in Eqn. (5.1), of a three-device array with the two control formulations are presented in

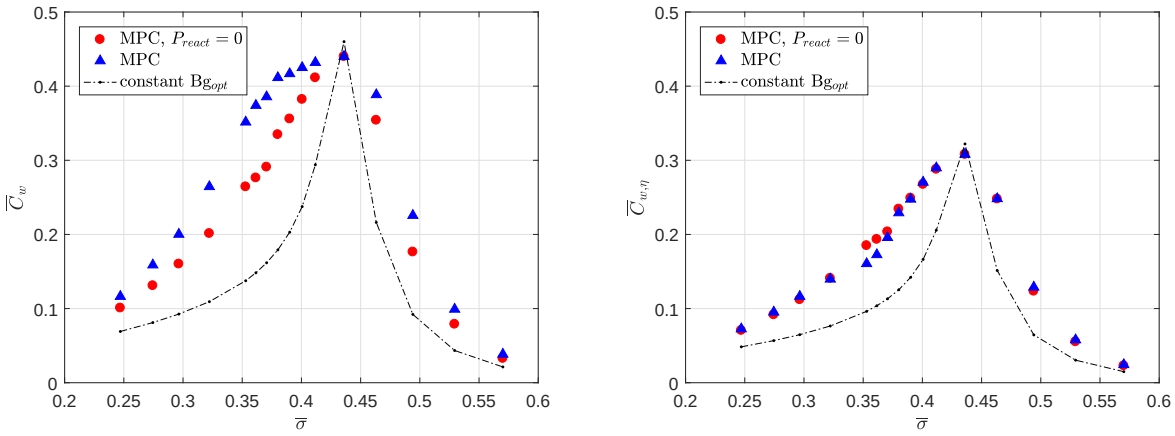

(a) Ideal PTO ($\eta_1 = \eta_2 = 1.0$) (b) Non-ideal PTO ($\eta_1 = \eta_2 = 0.70$)

Figure 5.2: Capture width based on the grid power for a three-WEC array MPC control with (blue markers) or without (red markers) reactive-power occurrence ($L/a = 10$, head-sea condition)

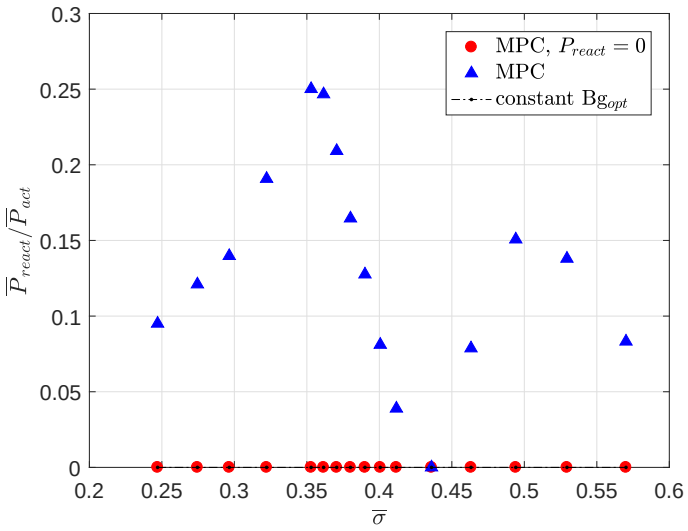

Figure 5.3: The ratio of the reactive power to the "active" power for the three-WEC array shown in Fig. 5.2.

Fig. 5.2, where Fig. 5.2a is with an ideal PTO, i.e. $\eta_1 = \eta_2 = 1$, and Fig. 5.2b is with a non-ideal PTO system and $\eta_1 = \eta_2 = 0.70$. Also presented is the ratio of the reactive power for the two control strategies. It can be seen that the strategy of adding constraints on the first control inputs eliminates the power consumption. In general, the WEC array with the ability to handle reactive power can produce more useful power. Nevertheless, with the PTO efficiency taken into account, the difference in the capture width generated by a WEC array with and without reactive power becomes noticeably smaller. When the efficiency decreases to 70% as shown in Fig. 5.2b, the array with the no-reactive-power MPC had the same or even better performance compared to the other. With consideration of both increasing the energy production and reducing the cost, the MPC with no reactive power *a*nd the convex formulation may be a favorable alternative solution.

5.3 Implementation of the MPC

A Permanent Magnetic Linear Generator (PMLG), serving as the PTO unit for a point absorber, was developed, built, and tested in a model tank at the Berkeley Marine Mechanics Lab (see [63, 64, 65]). The PMLG consists of an array of magntets mounted on the floater, moving relative to a set of coils attached to the supporting structure inside the floater. The generator damping is adjusted by varying the load resistance R and the magnet-coil gap width w_{gap} of the PMLG. With no requirement on generating reactive power, the optimal control force obtained in §5.2 can be realized by the PMLG, except for the instants at which the heaving velocity of the device is too small that the required damping value exceeds its limit.

For such a scheme, additional constraints need to be added for the PTO force on each device so that

$$|\boldsymbol{u}_0| = |f_m| \leq B_{g,max}\boldsymbol{y}_0 = B_{g,max}C\boldsymbol{x}_0 \tag{5.6}$$

where the scalar $B_{g,max}$ (> 0) is the maximal value of the PTO damping. Based on Eqn. (5.4a), the optimization problem with this additional constraint can be written as

$$\min_{U_0} \quad J = \frac{1}{2}U_0^T H U_0 + f^T U_0 \tag{5.7a}$$

$$\text{subject to} \quad \widehat{A}_u U_0 \leq \hat{b}_u \tag{5.7b}$$

where

$$\widehat{A}_u = \begin{bmatrix} t_1 \\ I \\ -I \\ S_{u,z} \\ -S_{u,z} \end{bmatrix}, \quad \hat{b}_u = \begin{bmatrix} 0 \\ \widetilde{U}_{\max} \\ \widetilde{U}_{\max} \\ Z_{\max} - S_{x,z}x_k - S_{u,z}W_0 \\ Z_{\max} + S_{x,z}x_k + S_{u,z}W_0 \end{bmatrix} \tag{5.8}$$

with

$$\widetilde{U}_{\max} = [B_{g,\max}C\boldsymbol{x}_0; f_{m,\max} \times \underbrace{[1, \ldots, 1]}_{(N-1)N_h}]$$

We first compared the performance of a single WEC controlled by the MPC with the convex formulation in Eqn. (5.7) and by a Nonlinear MPC with the PTO damping B_g as the control input as presented in [64]. Regarding the MPC setting for the comparison, both of the current MPC and the NMPC have added a term to penalize the slew rate of the control input and have the same limit on the PTO damping, while the current MPC allows for smaller heaving oscillations ($RAO \leq 3$) than the NMPC ($RAO \leq d/A_0 \approx 10$ with d being the draft of the device). The selected NMPC case for comparisons had the best power performance among all simulated cases in [64]. As shown in Fig. 5.4a, the current MPC is able to attain similar amount of power production compared to the NMPC where the PTO dampng should be optimized based on the nonlinear dynamics of the system. In addition, the current MPC, with the convex formulation of the optimization problem and hence the global optimal solution, leads to a broadened capture-width bandwidth for the WEC array. This may be explained by the fact that, at certian frequencies, the NMPC only returns to a local optimum rather than the global one. This is also seen in the facts that the highest energy absorption in the NMPC case was at a frequency lower than the resonance frequency and that the oscillating amplitude of the device did not reach its maximal capacity.

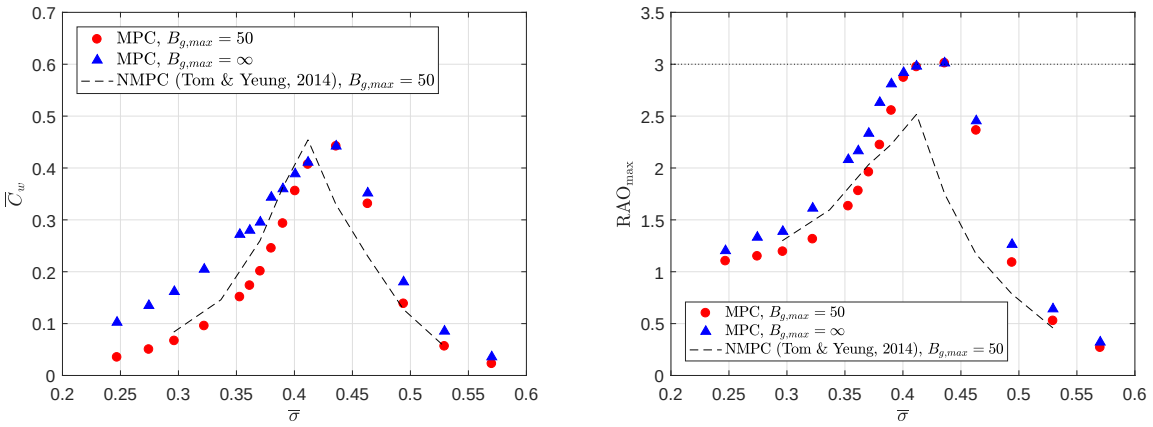

(a) Capture width (b) Maximal RAO

Figure 5.4: Comparisons of the capture width of a single WEC under MPC control with and without constraints on the PTO damping.

Fig. 5.5a and 5.5b show results of the three devices compared to those obtained with no limit on the PTO damping, i.e. the controller formulated in §5.2. It can be seen that with the generator damping restricted, the energy absorption was noticeably reduced especially at frequencies farther from the resonance frequency. The reason may be that restricting the damping coefficient $B_{g,\max}$ not only limits the actual control force $f_m = -B_g\dot{\zeta}_3$ being applied, but also affect the amplitude of heaving velocity of the absorber. As shown in the 5.5a, increasing the limit on the damping coefficient to $B_{g,\max} = 100$ can increase the power absorption.

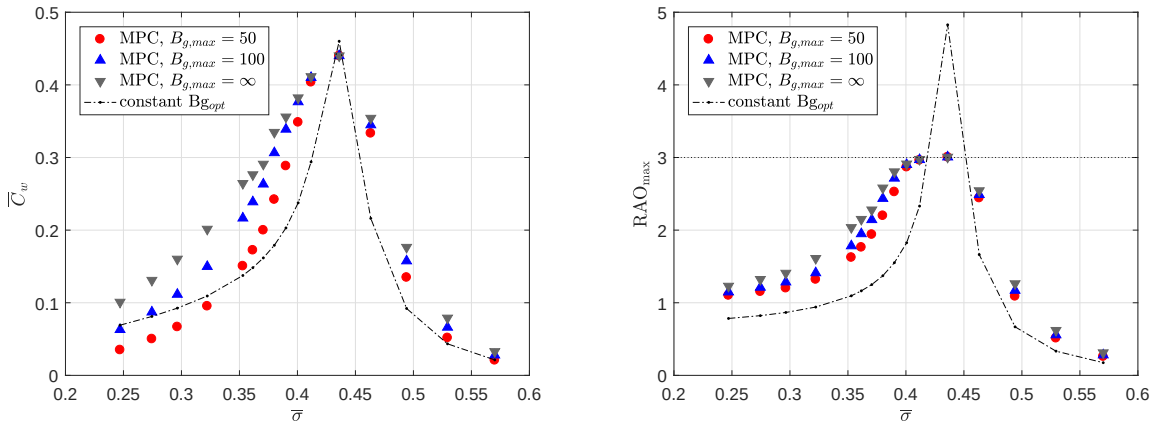

(a) Capture width (b) Maximal RAO

Figure 5.5: Comparisons of the results for a three-WEC array under MPC control with and without constraints on the PTO damping ($L/a = 10$, head-sea condition).

Simulations in irregular sea waves were also performed. Results of the capture width and RAO are shown in Fig. 5.6a and 5.6b. All the implemented control strategy does not require the PTO to handle reactive power. In irregular waves, the advantage of the MPC over the constant optimal damping control becomes even more significant. In addition, doubling the capacity of the PTO damping can have a 25% on average increase in the capture width.

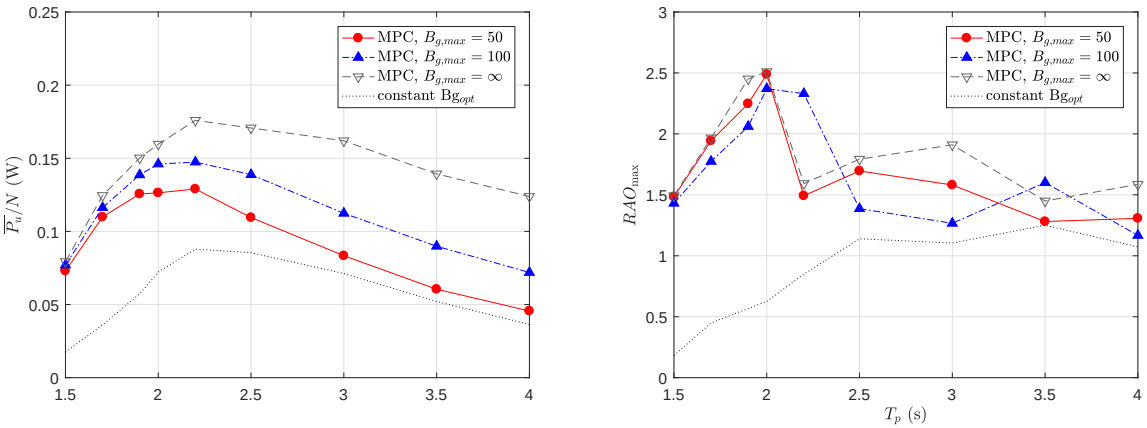

(a) Capture width (b) Maximal RAO

Figure 5.6: Comparisons of the results for a three-WEC array in irregular waves under MPC with damping control and force control ($L/a = 10$, head-sea condition).

Table 5.1: Full-Scale Properties of the Unidirectional Sea States used to calculate *ACCW*

Sea State	T_p (s)	H_s (m)	Direction (deg)
IWS 1	7.31	2.34	10.00
IWS 2	9.86	2.64	0.00
IWS 3	11.52	5.36	-70.00
IWS 4	12.71	2.06	-10.00
IWS 5	15.23	5.84	0.00
IWS 6	16.50	3.26	0.00

5.4 Performance Evaluation of a Three-Device Array in the West Coast U.S.

One of the challenges in promoting the wave-energy technology is the considerable amount of uncertainties in implementing the design at real-sea sites. With the efficient constrained optimal control strategy developed, wave-interaction effects accurately captured, and the hardware implementation method available for a WEC array, we can provide an accurate estimation of the power performance of the array in irregular waves of potential deployment sites.

The sites are the ones selected for performance evaluation of the WEC designs in the Wave Energy Prize sponsored by the U.S. Department of Energy in 2015. The Wave Energy Prize [52] (the Prize) is an 18-month public design-build-test competition, aimed to encourage the design of techno-economical WEC devices that double the energy captured from ocean waves compared to the current designs, which in turn would reduce the cost of wave energy, making it more competitive with other energy solutions. For quantifying the energy-capture capability of the proposed WEC concepts, the average climate capture width ($ACCW$) was defined and computed for each design, where the $ACCW$ represents the absorbed power of the device (kW) devided by the wave energy flux per meter crest width in kW/m, which operates in typical West Coast wave climates.

Specifically, $ACCW$ is calculated for six ($i = 1 : 6$) unidirectional long-crested irregular wave states (IWS) that are representatives of the West Coast of the U.S., including Alaska and Hawaii [55]. The full-scale sea state parameters from [55] are listed in Table 5.1, for which the select methodology is to apply the k-means algorithm on the data provided by National Data Buoy Center (NDBC), of which the details is described in [9]. These wave parameters were used with the Joint North Sea Wave Project (JONSWAP) spectrum to synthesize the wave time-series used in the simulation. The JONSWAP gamma value was assigned to 1 for each of the spectra (e.g., a Bretschneider spectrum). Hence, the wave spectrum as a function of the wave frequency σ is described by

$$S(\sigma) = \frac{1}{2\pi}\frac{5}{16}H_s^2 T_p \left(\frac{\sigma T_p}{2\pi}\right)^{-5} \exp\left[-\frac{5}{4}\left(\frac{\sigma T_p}{2\pi}\right)^{-4}\right] \tag{5.9}$$

Table 5.2: Weighting factors used to calculate the $ACCW$ and the full-scale average annual wave energy flux for the seven sites in the west coast of U.S. [9]

Sea State	Factors for each climate, Ξ_{ij}						
	Alaska $j=1$	Washington $j=2$	Northern Oregon $j=3$	Oregon $j=4$	Northern California $j=5$	Southern California $j=6$	Hawaii $j=7$
IWS 1	0.243	0.137	0.155	0.175	0.207	0.152	0.328
IWS 2	0.332	0.277	0.307	0.268	0.230	0.270	0.245
IWS 3	0.075	0.041	0.056	0.058	0.012	0.014	0.001
IWS 4	0.200	0.338	0.344	0.295	0.466	0.391	0.133
IWS 5	0.024	0.022	0.037	0.034	0.16	0.010	0.0
IWS 6	0.012	0.045	0.042	0.054	0.064	0.095	0.013
Average Annual Wave Energy Flux (kW/m)							
$C_{p,j}$	35.5	32.7	39.3	37.9	31.5	31.2	16.8

where H_s and T_p are the significant wave height and peak period of the sea state.

With the energy absorption obtained for devices in each IWS, the $ACCW$ of the devices at the jth location ($j = 1, 2, \ldots, 7$) will be computed as a linear combination of results of the six states with weighting factors of the states listed in the Table 5.2, which was obtained in the sea state selection study [9]. Then the $ACCW$ at each site, denoted by $ACCW_j$, and the averaged $ACCW$, denoted by $\overline{ACCW}$ can be computed by

$$\begin{aligned} ACCW_j &= \frac{\sum_{i=1}^{6} \Xi_{ij} AP_i}{C_{p,j}} \\ ACCW &= \frac{1}{7} \sum_{j=1}^{7} ACCW_j \end{aligned} \tag{5.10}$$

where AP_i is the average power absorbed by the WECs for the sea state i. The Prize then used the $\overline{ACCW}$ to compute the ACE, a parameter defined for evaluating the cost-effective performance of the design. Publicized is the ACE value of each awarded team, but not the ACCW value. In [3], a database was built for existing WEC designs. The capture width ratio (%), denoted by η_1 was introduced to present the power performance of the design, which is defined as the following:

$$\eta_1 = \frac{CW}{B} \tag{5.11}$$

Table 5.3: Specifications of the Controller

Controller 1	Controller 2	Controller 3	
$B_{g,\max} = 100$ $RAO_{\max} = 3$	$B_{g,\max} = \infty$ $RAO_{\max} = 3$	$F_{g,\max} = B_{g,\max} * A_0 RAO_{\max}$ with $B_{g,\max} = 100$ $RAO_{\max} = 3$	A_0: wave amplitude

Table 5.4: Capture width ratio η_1 (%) of a three-WEC array ($L/a = 5$) with different controller settings in sea states of seven sites in the West Coast of the U.S.

	Alaska $j = 1$	Washington $j = 2$	Northern Oregon $j = 3$	Oregon $j = 4$	Northern California $j = 5$	Southern California $j = 6$	Hawaii $j = 7$
Controller 1	25.8%	25.0%	24.8%	24.4%	42.9%	23.9%	23.8%
Controller 2	29.4%	29.1%	29.1%	28.7%	53.7%	28.3%	26.0%
Controller 3	40.3%	40.4%	40.5%	40.0%	77.6%	39.2%	33.8%

Here, CW is the capture width. For the seven sites in the West Coast, $CW = ACCW_j$ at location j. The B is the charateristic length of the device; for a heaving buoy, B is the diameter of the device.

We conducted simulations for a three-device array and computed the η_1 for the array in the seven sites. The mean diameter of a single heaving point absorber, according to [3], is about $10 - 12$m, and the one for devices in a point-absorber array is about 8m. Given the diameter of the model tested in the BMML being 0.2703m, a scaling factor of 30 was used to scale the results to the full size by using Froude scaling [8]. The applied controller and the corresponding specifications are listed in Tab.5.3. Controller1 was formed as in Eqn. (5.7) with a limit on the PTO damping. Controller2 was formed as in Eqn. (5.4) where the reactive power was eliminated from the system and there is no limit on the PTO damping. Controller3 was formed as in Eqn. (4.29) in §4 where the PTO was assumed to be capable of handling reactive power and constraints were added on the PTO force. Simulation results of the CWR (%) are listed in the Table. 5.4 for the array with spacing ratio $L/a = 5$. The corresponding q factors, averaged over the seven locations, are listed in the Table. 5.5 to compare the performance of the array with different controllers and different spacing ratios.

It can be seen from Table. 5.4 that the array has the best power performance in the Northern California site, which can be explained by the fact that the heaving absorber was designed for sea states in Northern California. For performances of different controllers, with

Table 5.5: Mean value of the interaction factor q over the seven sites obtained with different controllers

Mean q factor	Controller 1	Controller 2	Controller 3
Spacing ratio $L/a = 5$	0.964	0.966	0.9177
Spacing ratio $L/a = 10$	1.001	1.01	0.9655

the PTO capable of handling reactive power, the power absorption was increased by $60-80\%$ compared to the case with no reactive power allowed. The wave-interaction effects on the power production of the array appear to be mostly destructive, especially for arrays having smaller spacing ratio and experiencing larger interaction effects. When the spacing ratio increases to 5 diameters, the interaction effects are negligble when constraints on the PTO damping were applied (Controller 1). Comparing the results of Controller 3 and Controller 1, we observed that the more power the array absorbs, the more loss of energy the array experienced due to the wave-interference effects. Nevertheless, such loss of energy is relatively small: less than 5% for the damping control PTO and less than 10% for the force control PTO. In the meantime, the cost of production will be greatly reduced by the enlargement of the array size. Fig. 5.7 from [49] are the CaPex (capital cost) and OpEx (operations and maintenance cost) for arrays of different sizes, which shows a substancial decrease in the cost with an increase in the array size. With the spline interpolation, an array of size three can reduce the cost by 20%. Hence, taking into account the effects from both the destructive wave effects and the cost reduction, we can confirm that the wave farm will play a pivotal role in advancing the commercialization of wave energy technology.

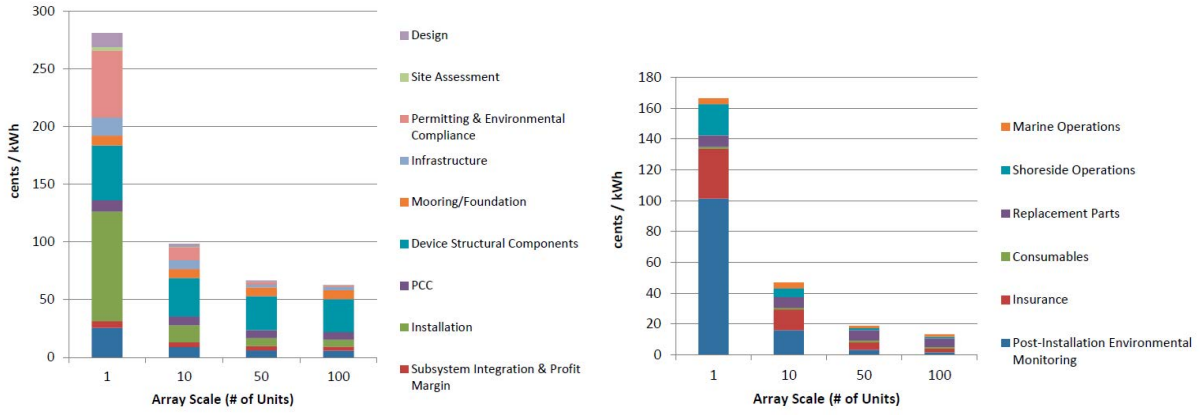

Figure 5.7: CaPex (left) and OpEx (right) contributions to LCOE (cents/kWh) per deployment scale [49].

5.5 Summary Remarks

In this Chapter, a modified MPC was proposed to compute optimal PTO forces that will not require the use of reactive power, based on the coordinated MPC for the WEC array in Chapter 4. Such control forces were realized by varying the PTO damping so that the product of the damping and the heaving velocity at the current state provides the required amount of the control force. The varied PTO damping was implemented by an in-house designed permanent magnetic linear generator (PMLG). Simulations compared the power obtained by the original MPC and by the modified MPC with no reactive power generation. The optimized PTO force from the latter was realized by changing the PTO damping, with which the power production was compared with that obtained by a nonlinear MPC (NMPC) which directly optimized the PTO damping [64]. Firstly, applying the PTO damping resulted from the MPC with convex QP achieved approximately the same amount of energy absorption as applying the NMPC, but with sigfinicantly improved computational efficiency, as demonstrated in Chapter 3. In addition, the advantage of the modified MPC was present when the PTO efficiency was taken into account. With the two-way energy flow required by the orginal MPC, the PTO system needs to consume more power when it acts as a motor and converts less power when it is a generator. As a result, the original MPC had better performance at wave frequencies away from the resonance frequency of the single device but produced similar amount of effective power compared to the damping-controlled MPC when the PTO effciency was decreased to 70%. Lastly, performances of a three-device array were evaluated in irregular sea states chosen to represent the seven sites near west coast in the U.S. The capture-width ratio and the interaction factor for the array were presented. We found that wave-interaction effects appear to be destructive in the simulated sea states. Nevertheless, the destructive efffects were less than 5% when the devices are 3 diameters apart, and less than 1% when the spacings are more than 5 diameters.

Chapter 6

Conclusions and Future Work

6.1 Conclusions

A study of the roadmap to the 100% clean and renewable all-sector energy for 139 countries by 2050 considered the contribution of the offshore wind, wave, and tidal power. It indicates that if $410,000$ wave-power plants with each power capacity of 750kW were installed, they would meet 0.58% of all-purpose load. It can be seen that (1) wave power is considered as a practical energy source and the commercialization of wave-power conversion techonlogy will likely be realized in the form of large-size wave farms and (2) the contribution of wave power to the renewable energy profile will be small in 2050 because of the low capacity factor of the wave energy devices and the current relatively immature development stage of the wave-energy extraction technology. This suggests that more human power and resources are needed to expedite the wave power extraction, since this clean ocean power has shown its enormous potential in satisfying many current energy needs.

This dissertation developed a complete set of tools for a realistic evaluation of the power performance of a point absorber array with constrained optimal control in irregular sea waves. A semi-analytical method based on potential-flow theory and linear theory were developed to compute wave-interaction effects among an arbitrary WEC array, which were incorporated in the dynamic model of the WEC controller. A model-based optimal control strategy was proposed with the energy optimization problem formulated as a convex Quadratic Programming (QP), where real-time inplementation was demonstrated successfully. The implementation of the optimized control force on the point absorber, obtained from the controller, was applied using an in-house designed permanent magnetic linear generator. Simulations were performed for a three-device array with constrained optimal control at seven sites near the west coast of the U.S.. Results showed that wave-interference effects appeared to be destructive; nevertheless, the enegy loss was less than 5% when the devices were 2.5 diameters apart and less than 1% when the spacing increased to be 5 diameters. With the cost reduction increased with the array size, we summarized that a relatively close-spacing wave farm consisting of more than 10 devices can be beneficial to the commercialization of the wave-energy

extraction technology.

Key findings are summarized below.

- Hydrodynamic modeling of a wave farm.
  - The new Haskind relation derived for an array of arbitrary geometric shape and in arbitrary layout is very useful and efficient in estimating the wave-interaction effects on the power production of the array with no constraint.
  - When there is no motion constraint, the wave-interaction effects could be either constructive or destructive, i.e. the array could extract more power than multiple isolated devices or less, depending on the wave frequency and the wave-incident angle.
  - The increase in the power absorption caused by wave-interference effects can be more than 50%. However, the integration of the interaction factor q with respect to the wave-incident angle yields a constant. This suggests that the array that experiences large constructive wave effects in waves of a certain direction can experience similar amount of destructive effects when waves come in other directions.
- constrained optimal control of a wave farm.
  - MPC is a powerful strategy in handling constraints and provides an approach to investigate the optimal power production of an array under constraints. However, the computationally-demanding property makes the MPC less attractive in real-time implementation. By using the PTO force as the control input and reformulate the optimization problem, the computational efficiency was considerably increased, with which the MPC showed potential in real-time application, especially for a single device.
  - In terms of convexifying the cost function, penalizing the slew rate of the control input has less impacts on the energy absorption than directly penalizing the power consumption, which also left the penalty weight of the latter as a free parameter for tuning the control.
  - Adding motion constraints significantly reduced the extent of wave-interaction effects on the power performance. Most importantly, the wave effects appear to be destructive for all simulation cases including different configuration, different wave frequencies, and wave-incident angles. This may lead to the preliminary conclusion that the interference effect would have negative impact on the power performance and need to be avoided. Increasing the spacing among element devices can be the simplest way, which, however, would be restricted by the acreage of the permitted area and the cost of production and operation. Optimal control may be able to take such factors into account in the future.

  - Coordinated control with a central controller was used as the primary tool in this dissertation since one of the main goals is to provide some insights on the cooperative actions of the devices at the optimal operating condition. However, it should be pointed out that taking into account the radiation forces in the system model would be increasingly hard with an increase of the WEC devices because of the complexity caused by relative positions of individual devices. Furthermore, the large number of optimization variables and constraints would make the real-time implementation less practical, even with the convex QP formulation. Simulation results show that neglecting the radiation effects, i.e. the devices acting independently with their own controllers but the surrounding waves were predicted "correctly" with scattering waves taken into account, will have less than 1% impacts on the amount of absorbed power but induce an approximate 10% increase in the reactive power. Also, the energy absorbed by each device will be less evenly distributed in particular near the resonance frequency of the device. Distributed MPC control can be a potential solution for a large wave farm consisting of hundreds of devices.

- Implementation of the optimal control force.

  - The MPC proposed with the PTO force used as the control input had an inherent "drawback" of generating reactive power. This requires that the PTO system to be both a generator and a motor, which can be hard to realize with existing PTO designs. A modified MPC was then proposed, which sacrificed a certain amount of energy capture-capability and achieved no reactive power generation with the convex formulation retained.
  - The control force obtained from the modified MPC was realized by the in-house designed permanent magnetic linear generator by varying the PTO damping.
  - Simulation results showed that the modified MPC with control force realized by changing PTO damping can achieve the same amount of energy extraction as a nonlinear MPC which directly optimizes the PTO damping. The latter leads to a nonconvex and nonlinear problem and have a two-order increase in computational time.
  - Performance evaluation of three point absorbers equipped with the advanced control and the PMLG at seven west-coast sites showed that the reduction in the absorbed power caused by the wave-interaction effects is less than 5%. The economic and environmental issues may play an essential role in the array desgin.

6.2 Future Work

The current study suggests that wave-interaction effects will reduce the power production of the array and need to be avoided. Increasing spacings among devices can be the simplest

way to reduce the interaction effects. This may not be practical since the area available for wave-farm deployment can be restricted by the usage of commercial and navy purposes, the enviromental consideration, the cost of operation and maitenance, etc. Since the levelized cost of production (LCOE) is the key parameter to determine the commercialization readiness level of a technology, an economic study for a wave farm regarding effects of the array size on the LCOE is of vital importance for determining the configuration of a wave farm.

Many other interesting problems arise in the wave-farm study:

- The hydrodynamic theory can be extended to consider devices of a more general geometry by combining the wave-interaction theory with a boundary element method [74].
- Since wave-interaction effects does not have very significant effect on the power production of the array under constraints in irregular sea states, a decentralized MPC controller may have sufficiently good performance in maximizing the power and, more importantly, further reduce the computational costs such that the MPC can be applied to wave farms of hundreds of devices.
- Wave prediciton is essential to the effectiveness of the MPC. A wave-prediction unit can be incoorporated into the current controller scheme, of which the effect on the power production needs to be investigated.
- The current study is based on theoretical analysis and computational simulation. Experimental validation for the proposed controller would be pivotal to demonstrate the applicability of the strategy.

In addition, the grid integration of the extracted wave power and the life-cycle performance of a wave farm are also critical problems that need to be looked into. In all, technology breakthroughs are greatly desired for promoting the ocean-wave technology, which will surely benefit the energy structure and the society.

Appendix A

Appendix

Development of the Haskind Relation for a Cylinder Array

In this Appendix, we develop the Haskind Relation for a cylinder array. Under linear theory, the radiation potential ϕ for a cylinder array can be written as a sum of the potentials in six modes of motion for each cylinder, i.e.

$$\phi = \sum_{k=1}^{N} \sum_{q=1}^{6} U_q^k \phi_q^k \tag{A.1}$$

where U_q^k is the complex amplitude of velocity, and ϕ_q^k the unit-velocity potential, for the q-th mode motion of the cylinder k while the other cylinders are stationary. And on the surface of body j, ϕ_q^k should satisfy that

$$\frac{\partial \phi_q^k}{\partial n^j} = \begin{cases} 0, & \text{if} \quad k \neq j \\ n_q^j, & \text{if} \quad k = j \end{cases} \tag{A.2}$$

Applying (A.2), we can write X_l $(l = 1, 2, \ldots, 6)$ in (2.31) as

$$X_l = \sum_{j=1}^{N_G} i\sigma\rho \iint\limits_{S_j} (\phi_0 + \phi_7) \frac{\partial \phi_l^j}{\partial n^j} \mathrm{d}S = \sum_{j=1}^{N_G} i\sigma\rho \iint\limits_{S_B} (\phi_0 + \phi_7) \frac{\partial \phi_l^j}{\partial n} \mathrm{d}S \tag{A.3}$$

with N_G being the number of oscillating cylinders. Further, (A.3) can be written as

$$X_l = i\sigma\rho \iint\limits_{S_B} (\phi_0 + \phi_7) \frac{\partial \phi_l}{\partial n} \mathrm{d}S \tag{A.4}$$

where $\phi_l := \sum_{j=1}^{N_G} \phi_l^j$ denotes the radiation potential when the group of cylinders oscillates as a unit with unit velocity.

Applying Green's theorem on a closed control surface S_{ctrl} consisting of bodies' surfaces S_B, free surface S_F, sea bottom S_h, and a control surface at far field S_R, we obtain that

$$\iint\limits_{S_{\text{ctrl}}} \left(\phi_7 \frac{\partial \phi_l}{\partial n} - \phi_l \frac{\partial \phi_7}{\partial n} \right) \mathrm{d}S = 0 \tag{A.5}$$

The integrand is cancelled on S_F and S_R, since both ϕ_7 and ϕ_l satisfy the linearized free-surface condition (2.3b) and radiation condition (2.5); it also vanishes on S_h because of the non-penetrating condition at sea bottom (2.3c). Hence, (A.5) yields

$$\iint\limits_{S_B} \phi_7 \frac{\partial \phi_l}{\partial n} \mathrm{d}S = \iint\limits_{S_B} \phi_l \frac{\partial \phi_7}{\partial n} \mathrm{d}S \tag{A.6}$$

Substituting (A.6) in (A.4) and applying the boundary condition (2.29) lead to the expression (2.32).

To further simplify the computation, we can take the evaluation of wave-exciting forces to the far field. Applying Green's theorem to ϕ_0 and ϕ_l on the control surface S_{ctrl} yields that

$$\iint\limits_{S_B+S_R} \left(\phi_0 \frac{\partial \phi_l}{\partial n} - \phi_l \frac{\partial \phi_0}{\partial n} \right) \mathrm{d}S = 0 \tag{A.7}$$

where the integrand vanishes on S_h and get cancelled on S_F. Hence, (2.32) can be rewritten as

$$X_l = -i\sigma\rho \iint\limits_{S_R} \left(\phi_0 \frac{\partial \phi_l}{\partial n} - \phi_l \frac{\partial \phi_0}{\partial n} \right) \mathrm{d}S \tag{A.8}$$

Taking S_R a vertical circular cylinder about the z-axis of large radius R in the global coordinate system yields the Haskind relation (2.33) in polar coordinates (r, θ, z).

In (2.33), the radiation potential ϕ_l can be obtained by evaluating the exterior potential $\phi^{(E)}$ in (2.18) in the far field ($R \to \infty$), where all of the evanescent modes can be neglected as they decay fast with the increase of distance. This yields that

$$\phi_l = \sum_{k=1}^{N} f_0(z) \sum_{m=-\infty}^{\infty} e^{im\theta_k} \beta_{m0}^k \frac{H_m(k_0 r_k)}{H_m(k_0 a_k)} \tag{A.9}$$

which should satisfy corresponding boundary conditions in (2.21). It should be noted that ϕ_l was expressed using local coordinates in (A.9). To transform coordinates to the global coordinates, the Graf's addition theorem takes a different form from (2.19) under the condition of $r_j \gg R_{jk}$ and $r_k \gg R_{jk}$ at far field, which was applied in [36] and is shown in the following

$$H_m(k_0 r_k) e^{im\theta_k} = \sum_{l=-\infty}^{\infty} J_{m-l}(k_0 R_{jk}) e^{i\theta_{jk}(m-l)} H_l(k_0 r_j) e^{il\theta_j} \tag{A.10}$$

Substituting (A.10) in (A.9) yields that

$$\phi_l = \sum_{k=1}^{N} f_0(z) \sum_{m=-\infty}^{\infty} \beta_{m0}^k \sum_{l=-\infty}^{\infty} \frac{J_{m-l}(k_0 R_{Ok})}{H_m(k_0 a_k)} e^{i(m-l)\theta_{Ok}} H_l(k_0 r) e^{il\theta} \tag{A.11}$$

where R_{Ok} and θ_{Ok} is the polar coordinates of the global origin in the local cooridinates of the cylinder k.

For regular incident waves of unit amplitude, progressing in a direction which makes an angle β with the x-axis, the velocity potential ϕ_0 expressed in coordinates of j-th cylinder can be written as

$$\phi_0 = \frac{-ig}{\sigma} \frac{\cosh k_0(z+h)}{\cosh(k_0 h)} \sum_{m=-\infty}^{\infty} I_j e^{im(\pi/2-\beta)} J_m(k_0 r_j) e^{im\theta_j} j \tag{A.12}$$

where $I_j = e^{ik_0(x_j \cos\beta + y_j \sin\beta)}$ is a phase factor associated with cylinder j locating at (x_j, y_j).

To conclude, X_l can be evaluated by substituting ϕ_0 (A.12) and ϕ_l (A.11) in (2.33).

Bibliography

[1] A.D. Andrés, R. Guanche, L. Meneses, C. Vidal, and I.J. Losada. Factors that influence array layout on wave energy farms. *Ocean Engineering*, 82:32–41, 2014.

[2] F.O. Antonio. Wave energy utilization: A review of the technologies. *Renewable and sustainable energy reviews*, 14(3):899–918, 2010.

[3] A. Babarit. A database of capture width ratio of wave energy converters. *Renewable Energy*, 80:610–628, 2015.

[4] G. Bacelli, R. Coe, D. Patterson, and D. Wilson. System identification of a heaving point absorber: Design of experiment and device modeling. *Energies*, 2017. in-press.

[5] G. Bacelli, R.G. Coe, D. Wilson, O. Abdelkhalik, U.A. Korde, R.D. Robinett, and D.L. Bull. A comparison of WEC control strategies for a linear WEC model. *Proceedings of the 4th Marine Energy Technology Symposium (METS)*, 2016.

[6] G. Barcelli and J.V. Ringwood. Constrained control of arrays of wave energy devices. *International Journal of Marine Energy*, 3:53–69, 2013.

[7] M.R. Belmont, J.M.K. Horwood, R.W.F. Thurley, and J. Baker. Filters for linear sea-wave prediction. *Ocean Engineering*, 33(17):2332–2351, 2006.

[8] R.D. Blevins. Applied fluid dynamics handbook. *New York, Van Nostrand Reinhold Co., 1984, 568 p.*, 1984.

[9] D. Bull and A. Dallman. Wave energy prize experimental sea state selection. In *ASME 2017 36th International Conference on Ocean, Offshore and Arctic Engineering*, pages V010T09A025–V010T09A025. American Society of Mechanical Engineers, 2017.

[10] C. Cecioni and G. Bellotti. Boundary conditions for modeling scattered wave field around floating bodies in elliptic wave models. *Applied Ocean Research*, 59:492–497, 2016.

[11] F.P. Chau and R.W. Yeung. Inertia, damping, and wave excitation of heaving coaxial cylinders. In *ASME 2012 31st International Conference on Ocean, Offshore and Arctic Engineering*, 2012. Rio de Janeiro, Brazil, July 1-6, OMAE2012-83987.

[12] B.F.M. Child and V. Venugopal. Optimal configurations of wave energy device arrays. *Ocean Engineering*, 37(16):1402–1417, 2010.

[13] A. Clément, P. McCullen, A. Falcão, A. Fiorentino, F. Gardner, K. Hammarlund, G. Lemonis, T. Lewis, K. Nielsen, S. Petroncini, and M.T. Pontes. Wave energy in europe: current status and perspectives. *Renewable and sustainable energy reviews*, 6(5):405–431, 2002.

[14] J.A. Cretel, G. Lightbody, G.P. Thomas, and A.W. Lewis. Maximisation of energy capture by a wave-energy point absorber using model predictive control. *IFAC Proceedings*, 44(1):3714–3721, 2011.

[15] J. Currie and D.I. Wilson. OPTI: Lowering the Barrier Between Open Source Optimizers and the Industrial MATLAB User. In Nick Sahinidis and Jose Pinto, editors, *Foundations of Computer-Aided Process Operations*, Savannah, Georgia, USA, 8–11 January 2012.

[16] A. De Andres, E. Medina-Lopez, D. Crooks, O. Roberts, and H. Jeffrey. On the reversed lcoe calculation: Design constraints for wave energy commercialization. *International journal of marine energy*, 18:88–108, 2017.

[17] B. Drew, A.R. Plummer, and M.N. Sahinkaya. A review of wave energy converter technology, 2009.

[18] H. Eidsmoen. Optimum control of a floating wave-energy converter with restricted amplitude. *Journal of Offshore Mechanics and Arctic Engineering.*, 118(2):96–101, 1996.

[19] Carnegie Clean Energy. *CTEO*, 2018.

[20] D.V. Evans. Some theoretical aspects of three-dimensional wave-energy absorbers. In *Proceedings of the first symposium on wave energy utilization, Chalmers University of Technology, Gothenburg, Sweden*, pages 77–106, 1979.

[21] D.V. Evans. Maximum wave-power absorption under motion constraints. *Applied Ocean Research*, 3(4):200–203, 1981.

[22] N. Faedo, S. Olaya, and J.V. Ringwood. Optimal control, mpc and mpc-like algorithms for wave energy systems: An overview. *IFAC Journal of Systems and Control*, 1:37–56, 2017.

[23] J. Falnes. Radiation impedance matrix and optimum power absorption for interacting oscillators in surface waves. *Applied Ocean Research*, 2(2):75–80, 1980.

[24] J. Falnes. *Ocean waves and oscillating systems: linear interactions including wave-energy extraction*. Cambridge university press, 2002.

[25] J. Falnes and K. Budal. Wave-power absorption by parallel rows of interacting oscillating bodies. *Applied Ocean Research*, 4(4):194–207, 1982.

[26] J. Falnes and J. Hals. Heaving buoys, point absorbers and arrays. *Phil. Trans. R. Soc. A*, 370(1959):246–277, 2012.

[27] E. Friis-Madsen, H.C. Soerensen, and I. Russell. "small is beautiful"-but will small wecs ever become commercial? In *The International Conference on Endodontics*, 2018. Cherbourg, France, June 12-14.

[28] F. Fusco and J.V. Ringwood. A study of the prediction requirements in real-time control of wave energy converters. *IEEE Transactions on Sustainable Energy*, 3(1):176–184, 2012.

[29] M. Göteman, J. Engström, M. Eriksson, and J. Isberg. Fast modeling of large wave energy farms using interaction distance cut-off. *Energies*, 8(12):13741–13757, 2015.

[30] J. Hals, J. Falnes, and T. Moan. A comparison of selected strategies for adaptive control of wave energy converters. *Journal of Offshore Mechanics and Arctic Engineering*, 133(3):031101, 2011.

[31] J. Hals, J. Falnes, and T. Moan. Constrained optimal control of a heaving buoy wave-energy converter. *Journal of Offshore Mechanics and Arctic Engineering*, 133(1):011401, 2011.

[32] M.D. Haskind. The exciting forces and wetting of ships in waves. *Izvestia Akademii Nauk SSSR, Otdelenie Tekhnicheskikh Nauk*, 7(307):65–79, 1957.

[33] M. Herceg, M. Kvasnica, C.N. Jones, and M. Morari. Multi-Parametric Toolbox 3.0. In *Proc. of the European Control Conference*, pages 502–510, Zürich, Switzerland, July 17–19 2013.

[34] P.T. Jacobson, G. Hagerman, and G. Scott. Mapping and assessment of the united states ocean wave energy resource. Technical report, Electric Power Research Institute, U.S., 2011.

[35] H. Kagemoto and D.K.P. Yue. Interactions among multiple three-dimensional bodies in water waves: an exact algebraic method. *Journal of Fluid Mechanics*, 166:189–209, 1986.

[36] M. Kashiwagi, K. Endo, and H. Yamaguchi. Wave drift forces and moments on two ships arranged side by side in waves. *Ocean Engineering*, 32(5-6):529–555, 2005.

[37] C.H. Lee and J.N. Newman. Wamit user manual. *WAMIT, Inc*, 2006.

[38] G. Li and M.R. Belmont. Model predictive control of sea wave energy converters–Part I: A convex approach for the case of a single device. *Renewable Energy*, 69:453–463, 2014.

[39] G. Li and M.R. Belmont. Model predictive control of sea wave energy converters–Part II: The case of an array of devices. *Renewable Energy*, 68:540–549, 2014.

[40] F. Madhi, M.E. Sinclair, and R.W. Yeung. The berkeley wedge: an asymmetrical energy-capturing floating breakwater of high performance. *Marine Systems & Ocean Technology, Journal of SOBENA*, 9(1):05–16, 2014.

[41] T. Matsui and T. Tamaki. Hydrodynamic interaction between groups of vertical axisymmetric bodies floating in waves. In *International Symposium on Hydrodynamics in Ocean Engineering*, pages 817–836, 1981.

[42] S.A. Mavrakos. Hydrodynamic coefficients for groups of interacting vertical axisymmetric bodies. *Ocean Engineering*, 18(5):485–515, 1991.

[43] S.A. Mavrakos and P. McIver. Comparison of methods for computing hydrodynamic characteristics of arrays of wave power devices. *Applied Ocean Research*, 19(5-6):283–291, 1997.

[44] D.Q. Mayne, J.B. Rawlings, C.V. Rao, and P.O. Scokaert. Constrained model predictive control: Stability and optimality. *Automatica*, 36(6):789–814, 2000.

[45] P. McIver. Some hydrodynamic aspects of arrays of wave-energy devices. *Applied Ocean Research*, 16(2):61–69, 1994.

[46] P. McIver. Wave interaction with arrays of structures. *Applied Ocean Research*, 24(3):121–126, 2002.

[47] P. McIver and D.V. Evans. Approximation of wave forces on cylinder arrays. *Applied Ocean Research*, 6(2):101–107, 1984.

[48] E.L. Morris, H.K. Zienkiewicz, and M.R. Belmont. Short term forecasting of the sea surface shape. *International shipbuilding progress*, 45(444):383–400, 1998.

[49] V.S. Neary, M. Previsic, R.A. Jepsen, M.J. Lawson, Y.H. Yu, A.E. Copping, A.A. Fontaine, K.C. Hallett, and D.K. Murray. Methodology for design and economic analysis of marine energy conversion (mec) technologies. (sand2014-9040). Technical report, Sandia National Laboratories. Albuquerque, NM, U.S., 2014.

[50] J.N. Newman. Exciting forces on fixed bodies in waves. *J. Ship Res.*, 6(4):10–17, 1962.

[51] J.N. Newman. Wave effects on multiple bodies. *Hydrodynamics in Ship and Ocean Engineering*, 3:3–26, 2001.

[52] The U.S. Department of Energy's Office of Energy Efficiency and Renewable Energy (EERE). Wave energy prize.

[53] M. Ohkusu. Hydrodynamic forces on multiple cylinders in waves. In *Proceedings of International Symposium on the Dynamics of Marine Vehicles and Structures in Waves*. Institute of Mechanical Engineers, 1974.

[54] S.H. Salter. Wave power. *Nature*, 249(5459):720–724, 1974.

[55] W. Scharmen, J. Zona, C. Fuentes, and A. LaBonte. Final technical report – wave energy prize. Technical report, The U.S. Department of Energy's Office of Energy Efficiency and Renewable Energy (EERE), U.S., 2017.

[56] A. Schwarzenegger. California ocean wave energy assessment. 2007.

[57] C. Sharp and B. DuPont. Wave energy converter array optimization: A genetic algorithm approach and minimum separation distance study. *Ocean Engineering*, 163:148–156, 2018.

[58] P. Siddorn and R.E. Taylor. Diffraction and independent radiation by an array of floating cylinders. *Ocean Engineering*, 35(13):1289–1303, 2008.

[59] M.J. Simon. Multiple scattering in arrays of axisymmetric wave-energy devices. part 1. a matrix method using a plane-wave approximation. *Journal of Fluid Mechanics*, 120:1–25, 1982.

[60] D. Son. *Performance evaluation and optimization of a dual coaxial-cylinder system as an ocean-wave energy converter*. PhD thesis, University of California at Berkeley, 2016.

[61] D. Son and R.W. Yeung. Optimizing ocean-wave energy extraction of a dual coaxial-cylinder wec using nonlinear model predictive control. *Applied Energy*, 187:746–757, 2017.

[62] D. Son and R.W. Yeung. Optimizing ocean-wave energy extraction of a dual coaxial-cylinder WEC using nonlinear model predictive control. *Applied Energy*, 187:746–757, 2017.

[63] D. Son and R.W. Yeung. Real-time implementation and validation of optimal damping control for a permanent-magnet linear generator in wave energy extraction. *Applied Energy*, 208:571–579, 2017.

[64] N. Tom and R.W. Yeung. Nonlinear model predictive control applied to a generic ocean-wave energy extractor. *Journal of Offshore Mechanics and Arctic Engineering*, 136(4):041901, 2014.

[65] N. Tom and R.W. Yeung. Experimental confirmation of nonlinear-model-predictive control applied offline to a permanent magnet linear generator for ocean-wave energy conversion. *IEEE Journal of Oceanic Engineering*, 41(2):281–295, 2016.

[66] A. Wächter and L.T. Biegler. On the implementation of an interior-point filter line-search algorithm for large-scale nonlinear programming. *Mathematical programming*, 106(1):25–57, 2006.

[67] G.N. Watson. *A treatise on the theory of Bessel functions*. Cambridge university press, 1995.

[68] J.V. Wehausen. The motion of floating bodies. *Annual Review of Fluid Mechanics*, 3(1):237–268, 1971.

[69] H.A. Wolgamot, P.H. Taylor, and R.E. Taylor. The interaction factor and directionality in wave energy arrays. *Ocean Engineering*, 47:65–73, 2012.

[70] Y. Ye and E. Tse. An extension of karmarkar's projective algorithm for convex quadratic programming. *Mathematical programming*, 44(1-3):157–179, 1989.

[71] R.W. Yeung. Added mass and damping of a vertical cylinder in finite-depth waters. *Applied Ocean Research*, 3(3):119–133, 1981.

[72] R.W. Yeung, A. Peiffer, N. Tom, and T. Matlak. Design, analysis, and evaluation of the uc-berkeley wave-energy extractor. *Journal of Offshore Mechanics and Arctic Engineering*, 134(2):021902, 2012.

[73] R.W. Yeung and S.H. Sphaier. Wave-interference effects on a truncated cylinder in a channel. *Journal of Engineering Mathematics*, 23(2):95–117, 1989.

[74] R.W. Yeung and L. Wang. Radiation and exciting forces of axisymmetric structures with a moonpool in waves. *Journal of Marine Science and Application*, 2018. Advance online publication. DOI: 10.1007/s11804-018-0043-3.

[75] O. Yılmaz and A. Incecik. Analytical solutions of the diffraction problem of a group of truncated vertical cylinders. *Ocean Engineering*, 25(6):385–394, 1998.

[76] Q. Zhong and R.W. Yeung. Wave-body interactions among an array of truncated vertical cylinders. In *ASME 2016 35th International Conference on Ocean, Offshore and Arctic Engineering*, 2016. Busan, South Korea, June 19-24, OMAE2016-55055.

[77] Q. Zhong and R.W. Yeung. An efficient convex formulation for model-predictive control on wave-energy converters. *Journal of Offshore Mechanics and Arctic Engineering*, 140(3):031901, 2017.

[78] Q. Zhong and R.W. Yeung. Performance of a wave-energy-converter array operating under model-predictive control based on a convex formulation. *IEEE Transactions on Sustainable Energy*, 2019. (under review).

[79] Q. Zhong and R.W. Yeung. Wave-body interactions among energy absorbers in a wave farm. *Applied Energy*, 233:1051–1064, 2019.